

Size reduction and polymer encapsulation of carbon black in gas-expanded solvents

by

Scott M. Paap

B.S., University of Wisconsin, Madison (2002)

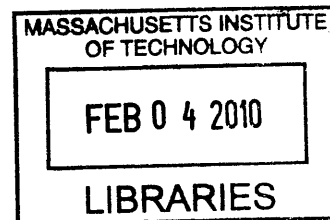
Submitted to the Department of Chemical Engineering
in partial fulfillment of the requirements for the degree of

Doctor of Philosophy

at the

MASSACHUSETTS INSTITUTE OF TECHNOLOGY

[February 2010]
September 2009



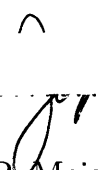
ARCHIVES

© Massachusetts Institute of Technology 2009. All rights reserved.

Author

Department of Chemical Engineering
15 September 2009

Certified by


Jefferson W. Tester
H. P. Meissner Professor of Chemical Engineering
Thesis Supervisor

Accepted by

William M. Deen
Carbon P. Dubbs Professor of Chemical Engineering
Chairman, Committee for Graduate Students

Size reduction and polymer encapsulation of carbon black in gas-expanded solvents

by

Scott M. Paap

Submitted to the Department of Chemical Engineering
on 15 September 2009, in partial fulfillment of the
requirements for the degree of
Doctor of Philosophy

Abstract

Ink jet printing is a demanding application that requires carefully formulated inks in order to quickly and reliably produce high-quality printed images. Although ink jet inks are currently produced via an aqueous process, supercritical fluids (SCF) and gas-expanded liquids (GXL) present alternative processing media for particle coating operations that may offer significant benefits with respect to the production of polymer-encapsulated pigment particles for these inks. The main thesis objective is the demonstration and analysis of a particle size reduction and encapsulation process which takes place in CO₂-expanded acetone and produces colloidal carbon black particles. These particles should be uniformly coated with functionalized hydrophobic resins such that they are easily redispersed in water or solvent to form stable nanoparticle dispersions suitable for use in ink jet inks.

A prototype size reduction and encapsulation system has been constructed based on a high-pressure stirred reaction vessel designed to operate at pressures up to 200 bar (3000 psi). The prototype vessel has a fluid volume of 1 liter with a multi-disc agitator capable of rotating at more than 3400 RPM. Pigment particles are initially milled in a solution of non-aqueous solvent and dissolved dispersing resin. Size reduction is achieved within the apparatus via the grinding action of 1.2 mm spherical ceramic media contacting the micron-size pigment particles. As milling progresses, high-pressure CO₂ is slowly introduced to the vessel; the CO₂ acts as an anti-solvent, lowering polymer solubility and driving adsorption of the dispersing resin onto the pigment particles as new surface area is exposed. After encapsulation is complete, the system is flushed with CO₂ and the product particles are retained as a dry powder in a high-pressure filter. The solvent-free particles are then recovered by venting the system to atmospheric pressure, and subsequently re-dispersed in water for analysis in inks.

The apparatus under investigation provides a new process approach to particle size reduction and coating that affords greater freedom in ink formulation, while offering a path to improved ink quality and possible cost savings in a highly competitive market. Specifically, the use of CO₂-expanded liquids enables the deposition of hydrophobic

polymers on the surface of particles for use in aqueous inks, thus significantly increasing the variety of polymers that are available for use in these systems. A representative model system of carbon black pigment and benzyl methacrylate/methacrylic acid (BzMA/MAA) copolymer dispersing resins of varying monomer compositions (BzMA/MAA mass ratio = 85/15, 80/20, and 75/25) has been studied in order to assess the feasibility of the high-pressure milling and encapsulation process for ink jet applications. These components have been successfully employed in high-pressure coating operations to produce encapsulated carbon black particles which were recovered as a dry, flowable powder. Dry product particles were redispersed in water to obtain stable aqueous dispersions with a number average particle size of 135-190 nm.

In order to guide the selection of appropriate process conditions for the encapsulation system, the high-pressure solid-liquid-vapor phase equilibrium of ternary CO₂-solvent-polymer systems has been probed experimentally and modeled with the PC-SAFT equation of state. Precipitation of BzMA/MAA copolymers generally required a larger overall CO₂ mole fraction – and thus a higher system pressure – for more dilute polymer solutions; however, a minimum in the precipitation pressure was observed for all polymer compositions and temperatures near a CO₂-free polymer mass fraction of 0.03. The ternary systems were characterized by a rapid reduction in polymer solubility over a relatively narrow range of pressure (between 200 psig and 400 psig, depending on the polymer and system temperature); the precipitation pressure increased with increasing temperature and BzMA mass fraction (per polymer mass unit). The PC-SAFT EOS was successfully employed to correlate the phase behavior data by adjusting only two binary interaction parameters; the average relative error associated with the predictions of precipitation pressure for each polymer was 3.7%.

Characterization of the encapsulation process also requires knowledge of the thermodynamics and kinetics of polymer adsorption onto particle surfaces from CO₂-expanded solvents. To this end, interactions with the particle surface have been investigated through the collection and correlation of experimental adsorption isotherm data. Adsorption of 85/15 and 75/25 BzMA/MAA polymers onto carbon black from CO₂-expanded acetone was measured at 35°C and pressures between 0 psig and 300 psig over a range of mixture compositions relevant to particle coating operations. Pressurization with CO₂ to pressures up to 200 psig caused a decrease in the amount of polymer adsorbed on particle surfaces, but further increases in pressure resulted in higher polymer loadings. In the case of 75/25 BzMA/MAA polymer, the polymer loading increased significantly between 200 psig and 300 psig as the solubility limit was approached or exceeded.

Our results are valuable not only in providing quantitative data to facilitate process optimization, but also in offering a more fundamental understanding of interactions among the pigment particles, the dispersant resin, and the gas-expanded liquid media. Such information is important to both process and product design.

Thesis Supervisor: Jefferson W. Tester

Title: H. P. Meissner Professor of Chemical Engineering

Acknowledgments

My experience in graduate school has been overwhelmingly positive, and I have many people to thank for making the good times much more memorable than the less-than-good. Jeff Tester has been an incredibly supportive advisor, and could always be counted on to put things in perspective when difficulties in the lab seemed to be insurmountable. Jeff's enthusiasm and energy are seemingly endless and his commitment to his students is exceptional. I also owe a debt of gratitude to Gwen Wilcox for holding the lab together and making sure that things actually got done.

I have benefitted from the expertise of an excellent thesis committee, who consistently provided valuable feedback and helped me keep sight of the broader thesis objectives whenever I was in danger of becoming mired in the details my project. Professor John Vander Sande's impressive knowledge of microscopy and sound advice regarding the general progress of my thesis were greatly appreciated during his time on my committee; Michael Wolfe of DuPont graciously shared his knowledge of ink jet ink formulation, and also provided assistance in analyzing many of the samples produced during the course of the thesis. Also at DuPont, Howard Zakheim and Erik Gommeren were instrumental in moving the project forward in its early stages.

In the lab, I was lucky to work with a great bunch of people in the Tester Group. I'd especially like to thank Kurt Frey for his work on the correlations in Chapter 4, and Chad Augustine for his help in the machine shop. Thanks also to Andy, Rocco, Hidda, Russ, Jason, Russell, and Heather for all of the good times both inside the lab and elsewhere. Greg, Don, Steph, Adam, Drew, and Bhargavi were a great help in the lab as undergraduate researchers, and certainly deserve much of the credit for the results of the thesis.

Elsewhere at MIT, I'd like to thank Peter Morley and everyone else at the MIT Machine Shop for all of their great work, Yong Zhang for his help with TEM, Blair Brettman for her help with DSC analysis, and Huan Zhang for his help with dynamic light scattering measurements.

I am very grateful for the friendships that I made during my time in graduate school, and I hope that our connections will last as we all go our separate ways. So to Curt, Sandeep, Dan, Rob, Ingrid and Foxy, Jie, Lily, Franklin, and everyone else: thanks for the fun. I would also like to thank Earl for being awesome. Thanks Earl.

To my family in Wisconsin and in Japan: thank you so much for your patience and support over the past six years. I didn't get to visit as much as I would have liked, but it always felt like home when I did. I am especially grateful to my parents for everything they've done for me, both before and during my time in graduate school. Finally, I want to thank my wonderful wife Yumi and amazing son James for always giving me a reason to smile, even when life in the basement lab was getting me down. Yumi, thank you so much for always being there for me, and for never – not even once – asking me when I was going to graduate.

Contents

1	Introduction and background	17
1.1	Ink jet technology	17
1.1.1	Industry overview	17
1.1.2	Ink jet inks	19
1.1.3	Pigmented ink production	20
1.2	Processing in high-pressure CO ₂ -based media	21
1.2.1	Carbon dioxide as an industrial solvent replacement	21
1.2.2	Gas-expanded solvents	24
1.2.3	Particle formation and encapsulation in CO ₂ -based media	24
2	Objectives and approach	35
2.1	Motivation	35
2.2	Thesis objectives	36
3	Model system	39
3.1	Pigment	40
3.2	Polymeric dispersant	40
3.2.1	Initial model polymer: Joncryl [®] resins	42
3.2.2	Benzyl methacrylate/methacrylic acid copolymers	42
3.3	Solvent	43
4	Measurement and correlation of the phase behavior of CO₂-acetone-polymer systems	47

4.1	Background	48
4.1.1	Previous studies of solid-fluid and solid-liquid-vapor equilibrium in CO ₂ -based media	48
4.1.2	Equation-of-state modeling of CO ₂ -solvent-polymer ternary phase behavior	49
4.2	Materials and methods	52
4.2.1	Experimental apparatus	52
4.2.2	Procedure	55
4.2.3	Data analysis	57
4.2.4	Correlation of polymer-CO ₂ -acetone solid-liquid-vapor equilibrium data with PC-SAFT EOS	59
4.3	Results and discussion	64
4.3.1	Experimental results	64
4.3.2	Modeling results	68
4.4	Conclusions	73
5	Adsorption of polymer onto carbon black particles from CO₂-expanded acetone	81
5.1	Background	82
5.1.1	Polymer adsorption from solution	82
5.1.2	Carbon black surface chemistry and adsorption characteristics	86
5.1.3	Previous studies of high-pressure adsorption from CO ₂	87
5.2	Materials and methods	88
5.2.1	Experimental Apparatus	88
5.2.2	Procedure	89
5.2.3	Data Analysis	92
5.3	Results and discussion	96
5.3.1	Atmospheric-pressure adsorption isotherms	96
5.3.2	High-pressure adsorption isotherms	99
5.4	Conclusions	103

6	Carbon black size reduction and polymer encapsulation in CO₂-expanded acetone	111
6.1	Background	112
6.1.1	Particle size reduction in liquid slurries	112
6.1.2	Previous studies of CO ₂ -based particle encapsulation	115
6.2	Materials and methods	117
6.2.1	Experimental apparatus	117
6.2.2	Procedure	123
6.2.3	Product characterization	126
6.3	Results and discussion	127
6.3.1	Performance of encapsulated particles in ink jet inks	129
6.3.2	TEM analysis	132
6.3.3	Process considerations	133
6.4	Conclusions	137
7	Conclusions and Recommendations	145
7.1	Phase behavior study	146
7.2	Investigation of polymer adsorption onto carbon black from CXLs . .	148
7.3	Particle size reduction and encapsulation in CXLs	152

List of Figures

1-1	A) TEM image of ink jet nozzle. B) Thermal ink jet configuration. . .	18
1-2	Pressure-temperature diagram for a pure component, including the supercritical state.	22
3-1	TEM image of a dispersed carbon black aggregate.	40
3-2	Styrene and acrylic moieties present in Joncryl [®] polymers.	42
3-3	Benzyl methacrylate and methacrylic acid moieties present in model polymers used for the current work.	43
3-4	Volume expansion with addition of CO ₂ as a function of system pressure for selected solvents	44
4-1	Schematic of the phase behavior measurement system.	53
4-2	Photograph of the phase behavior measurement system.	54
4-3	Schematic of the laser light scattering system for detection of polymer precipitation.	55
4-4	Representative UV absorption spectrum for 85/15 BzMA/MAA copolymer.	56
4-5	UV calibration curve for 85/15 BzMA/MAA in tetrahydrofuran. . . .	56
4-6	Representative temperature, pressure, and optical power data from a phase behavior measurement trial.	58
4-7	Representative pressure and optical power data from a single precipitation event in the course of a phase behavior measurement trial. . .	58
4-8	Solid-liquid-vapor equilibrium curves for systems containing CO ₂ , acetone, and Joncryl [®] polymers at 35°C.	59

4-9	Phase behavior data for 85/15 BzMA/MAA, 80/20 BzMA/MAA, and 75/25 BzMA/MAA copolymers in CO ₂ -expanded acetone.	65
4-10	Phase behavior data for BzMA/MAA copolymers in CO ₂ -expanded acetone at 25°C, 35°C, and 45°C.	66
4-11	Summary of phase behavior data for CO ₂ -acetone-polymer systems. .	67
4-12	Phase behavior data and PC-SAFT correlations for 85/15 BzMA/MAA, 80/20 BzMA/MAA, and 75/25 BzMA/MAA copolymers in CO ₂ -expanded acetone.	69
4-13	Precipitation pressure of 85/15 BzMA/MAA copolymer and calculated liquid phase CO ₂ mole fraction versus the liquid phase polymer mass fraction.	70
4-14	Precipitation pressure of BzMA/MAA copolymers versus the calculated liquid phase CO ₂ mole fraction.	71
4-15	Trends in binary interaction parameters with temperature and polymer composition.	72
5-1	Schematic of the high-pressure adsorption isotherm system.	90
5-2	Photograph of the high-pressure adsorption isotherm system.	90
5-3	Schematic of the custom-fabricated adapter used to provide ultrasonic agitation at high-pressure.	91
5-4	Volume expansion of CO ₂ -acetone liquid phase as a function of CO ₂ liquid mole fraction.	94
5-5	Comparison of saturated liquid density data and EOS correlations for the acetone-CO ₂ binary system at 35°C.	94
5-6	Comparison of saturated liquid mole fraction data and EOS correlations for the acetone-CO ₂ binary system at 35°C.	95
5-7	Adsorption of Joncryl [®] 678 polymer from water and methanol onto carbon black particles: Adsorption isotherms at 1 atm and 22°C. . . .	97
5-8	Adsorption of BzMA/MAA polymer from acetone onto carbon black particles: Adsorption isotherms at 1 atm and 22°C.	98

5-9	Adsorption of 85/15 BzMA/MAA polymer from CO ₂ -expanded acetone onto carbon black particles: Adsorption isotherms at elevated pressure and 35°C.	100
5-10	Adsorption of 75/25 BzMA/MAA polymer from CO ₂ -expanded acetone onto carbon black particles: Adsorption isotherms at elevated pressure and 35°C.	100
5-11	Trends in 85/15 BzMA/MAA polymer adsorption from CO ₂ -expanded acetone with changes in system pressure.	102
5-12	Normalized 85/15 BzMA/MAA polymer adsorption from CO ₂ -expanded acetone as a function of system pressure.	103
6-1	Schematic of a representative media mill for particle size reduction.	113
6-2	Schematic of the high-pressure particle encapsulation system.	117
6-3	Photograph of the high-pressure particle encapsulation system.	118
6-4	Schematic of the magnetic mixer and adapter for coupling to the encapsulation vessel cover.	119
6-5	Schematic of the high-speed disperser shaft for use in high-pressure encapsulation trials.	120
6-6	Schematic of the media milling impeller for use in high-pressure encapsulation trials.	121
6-7	Photographs of the media milling and HSD agitators.	122
6-8	Schematic of cooling loops for the high-pressure particle encapsulation system.	123
6-9	Illustration of the high-pressure media milling and encapsulation process.	125
6-10	Selected TEM images of uncoated carbon black and carbon-polymer composites.	133
6-11	Selected TEM images of polymer-encapsulated carbon black.	134
6-12	Plot of system temperature and pressure over the course of a representative high-pressure encapsulation trial.	135

List of Tables

1.1	Typical ink jet ink components	20
3.1	Selected properties of benzyl methacrylate/methacrylic acid random copolymers used in the current work.	43
3.2	Selected properties of acetone.	45
4.1	Pure-component PC-SAFT parameters for CO ₂ , acetone, poly(MAA) and poly(BzMA).	62
4.2	Final values of the copolymer pure component parameters used in PC-SAFT EOS correlations.	62
4.3	Final values of the CO ₂ -polymer and acetone-polymer binary interaction parameters, k_{ij} , used in PC-SAFT EOS correlations.	68
6.1	Summary of high-pressure encapsulation trials conducted using benzyl methacrylate/methacrylic acid random copolymers.	128
6.2	Summary of particle size measurement results for aqueous dispersions of BzMA/MAA-encapsulated carbon black product particles.	131

Chapter 1

Introduction and background

1.1 Ink jet technology

1.1.1 Industry overview

Ink jet printing is a non-impact process in which droplets of ink (typically 18-50 μm in diameter) are ejected through a nozzle and directed to a medium at a specified location to form an image. The technology was developed in the 1950s and 1960s, with the first commercial devices appearing in the late 1960s [Le, 1998]. The early generation ink jet printers were based on a process known as continuous ink jet, in which a steady stream of ink is broken up into uniform droplets. An electric charge is selectively applied to the ink droplets as they are ejected from the nozzle, and charged droplets are deflected to a gutter for recirculation while uncharged droplets are applied to the media.

In the 1970s development efforts focused on drop-on-demand technology for ink jet printing; as the name implies, these systems eject ink only when it is required for the image. The introduction of drop-on-demand technology offered a route to reduced complexity, improved reliability, and lower cost, and these systems soon came to compete with the dot-matrix printers that dominated the low-end printer market in the 1970s and early 1980s.

At present, nearly all commercial ink jet printers are based on one of two con-

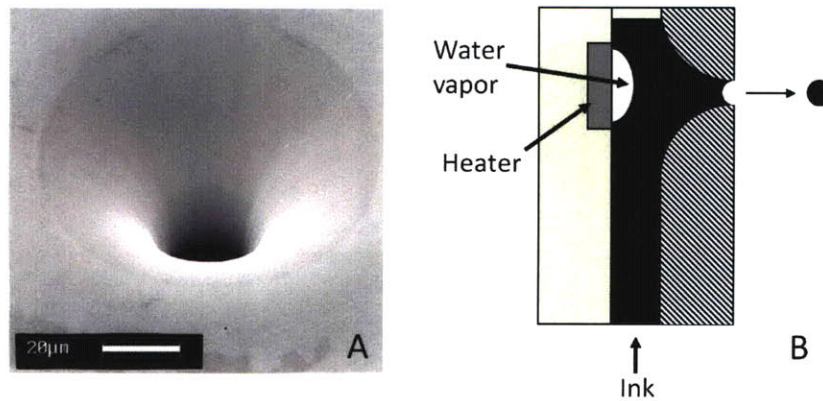


Figure 1-1: A) TEM image of ink jet nozzle (adapted from Le, 1998). B) Thermal ink jet configuration.

figurations, known as thermal and piezoelectric ink jet. In thermal ink jet systems - found in printers manufactured by Canon, HP, and Lexmark - ink is ejected from the print head upon the formation of a water vapor bubble on a small heater near the nozzle [Endo et al., 1979]. A schematic of a thermal ink jet printhead, as well as a TEM image of a printhead nozzle are pictured in Figure 1-1. Thermal ink jet manufacturers have benefited from advances in the semiconductor industry, allowing the low-cost production of disposable printheads with high nozzle density. Piezoelectric ink jet, pursued commercially most notably by Epson, utilizes a pressure wave generated by piezoelectric ceramics to force ink out of the printhead nozzles. In both of these configurations, ink is forced out of the nozzles by an acoustic pulse, and as the bubble collapses (or the piezo-ceramic returns to its original shape), a droplet breaks off and travels toward the media. Capillary action then draws the ink from the reservoir to refill the orifice. These phenomena occur at a frequency of 5-12kHz, and the refill time is on the order of 100-200 μ s.

Ink jet technology rapidly gained popularity among home and small business users beginning with the introduction of Hewlett-Packard's ThinkJet printer in 1984, and the total annual revenue in the ink jet ink industry has steadily climbed to its current

value of over \$60 billion, with more than half of this total derived from sales of ink [Darlin, 2006]. With continually improving image quality and a recent focus on large-format printers for textiles, industrial printing (packaging, posters, etc.), and printed electronics, ink jet is poised to expand from the low-end printer market to other sectors currently dominated by competing printing systems.

The interested reader is referred to the review by Le [1998] for a more detailed history and technology map of ink jet systems.

1.1.2 Ink jet inks

The nature of ink jet printing technology places a variety of demands on the inks used in ink jet devices. The ink must possess physical properties that are compatible with the droplet ejection process, the most important of these being viscosity and static and dynamic surface tension. Once the ink droplet strikes the printing media, it must penetrate into the bulk to avoid bleeding and smearing and to shorten drying time, but not so deeply as to be seen from the other side. Of course, the optical characteristics of the dried ink is extremely important; not only should the ink possess the desired light absorption spectra, but properties such as gloss, lightfastness, waterfastness, and rub resistance are also crucial. The liquid ink must also have a reasonably long shelf life, requiring ink stability with respect to time, temperature, and pH. As a final important requirement, health and safety issues such as toxicity and flammability must be addressed. The constraints described above require a surprisingly complex ink formulation that includes a variety of additives to modify the properties and improve the stability of the final product. A list of typical components of an ink jet ink is given in Table 1.1.

Pigmented inks versus dye-based inks

The color of an ink is provided either by a colloidal pigment or a dye. The main distinction between dyes and pigments is solubility: dyes are water-soluble molecules, while pigments are larger, insoluble particles (on the order of 70 to 100nm in diam-

Table 1.1: Typical ink jet ink components

Colorant (pigment or dye)
Carrier (water and/or solvent)
Polymer dispersant
Surfactant/wetting agent
Base
Biocide
Buffer
Anti-foaming agents
Binder
Humectant

eter for ink jet formulations). Although the first inks used in ink jet printers were dye solutions, pigment-based inks now dominate due to their superior lightfastness and color quality. However, the larger size of the pigment particles also presents a challenge, since dispersion instability can lead to clogging of the ink jet nozzles. Improved ink chemistry has allowed pigment-based inks to overcome early problems related to nozzle clogging; however, inks with smaller pigment particle sizes (20 to 50nm) and superior dispersion characteristics may be needed as the drive towards improved image resolution and increased printing speed continues, requiring smaller and more numerous printer nozzles.

1.1.3 Pigmented ink production

Pigmented ink jet ink dispersions are currently produced via the comminution of micron-size pigment particles or aggregates, typically in aqueous media. Large agglomerates are first broken up and dispersed in an aqueous solution containing polymeric dispersant molecules during a premix step. High-speed dispersers (HSD) are commonly used for this first step, employing shear stress and some attrition as the source of dispersion. Typical equipment used for further size reduction include media mills, microfluidizers, ball mills, and attritors. While undergoing size reduction (typically 75-90% of initial particle size) in the final grind, the pigment particles are simultaneously encapsulated with the dispersant resin dissolved in the aqueous

medium. In the final processing step, the pigment dispersion is filtered to remove any dust, undispersed pigment, or insoluble raw materials that may clog the printhead nozzles.

For a more detailed discussion of the various aspects of ink jet formulation and production, the reader is referred to the review by Wnek et al. in the Handbook of Imaging Materials [2002].

1.2 Processing in high-pressure CO₂-based media

1.2.1 Carbon dioxide as an industrial solvent replacement

Over the past several decades, carbon dioxide (CO₂) has received considerable attention as an alternative solvent for industrial applications. The search for alternative industrial solvents largely stems from concerns about the environmental, health, and safety implications of the use of traditional solvents, and CO₂ has been viewed as an excellent candidate due to the fact that it is a non-toxic, non-flammable, and non-corrosive material [Beckman, 2004].

Much of the recent attention directed towards carbon dioxide has focused on its use in the supercritical or near-critical state, for a variety of reasons. The supercritical state is indicated by the region in the upper right of the general pressure-temperature diagram shown in Figure 1-2; supercritical fluids (SCFs) have long been known to exhibit interesting and potentially useful properties [Hanney and Hogarth, 1879], most notably high compressibility, liquid-like density, and gas-like viscosity and diffusivity. The rapid change in fluid density near the critical point affords control over various physicochemical properties – such as solvation power, viscosity, and diffusivity – via changes in the system temperature and pressure. The lack of coexisting vapor and/or liquid phases also means that there are no phase interfaces or surface tension in the supercritical region, eliminating problems related to wetting. Because many SCFs are gases at ambient conditions, depressurization of a solution of less volatile solutes in a supercritical solvent results in the formation of multiple phases, and simple recovery

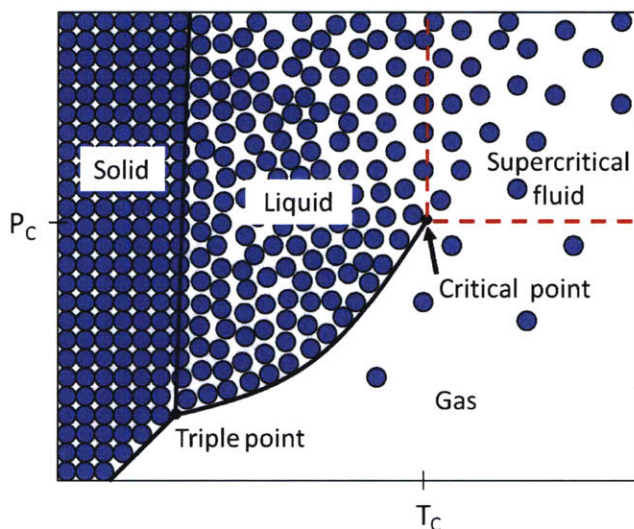


Figure 1-2: Pressure-temperature diagram for a pure component, including the supercritical state.

of the solvent in the gas phase.

In addition to these general properties of SCFs, CO₂ exhibits several desirable attributes that have led to increased interest in its application as an industrial solvent replacement. Its critical temperature and pressure of 31.3°C and 73.8 bar, respectively, make the supercritical region more accessible than that of other materials. In addition to the health and safety attributes mentioned above, CO₂ is also relatively inexpensive and readily available in commercial markets. Because of these characteristics, CO₂ has already found use in several important industrial processes. The pharmaceutical and food industries have shown particular interest in using supercritical carbon dioxide (scCO₂) as a substitute solvent due to its non-toxic nature. For example, this led to its wide-scale use as a replacement for methylene chloride in the extraction of caffeine from coffee [McHugh and Krukoni, 1994]. In the chemical industry, CO₂ already serves as a solvent for the polymerization of several important fluoro-carbon polymers [Du et al., 2009], and has been used as a solvent in Union Carbide's UniCarb coating process. The use of CO₂ in traditional chemical industries has the potential to grow rapidly in the coming years as environmental and health concerns mount with regard to traditional organic solvents used as processing and/or

reaction media [Beckman, 2004, Du et al., 2009].

Polymer solubility in high-pressure CO₂

One important limitation on the use of carbon dioxide in industrial processes is its relatively low solvation power. In fact, CO₂ is generally a poor solvent for polar, inorganic, or high molecular weight compounds – including polymers. Well-known exceptions include certain fluorinated polymers [Rindfleisch et al., 1996], poly(dimethylsiloxane) [Xiong and Kiran, 1995], and poly(ether-carbonate) copolymers [Sarbu et al., 2000]; however, in general polymer solubility is low and decreases with increasing molecular weight, increasing temperature (below 80°C), and decreasing pressure [McHugh and Krukoni, 1994].

The solubility of a polymer in CO₂ is governed by the relative magnitudes of the interactions between solvent-solvent, polymer-solvent, and polymer-polymer pairs, as well as the density of the polymer-CO₂ solution and the volume change upon mixing [Kirby and McHugh, 1999]. Combinatorial entropy effects resulting from the structure of the polymer are also important. The polarizability of CO₂ is relatively low, suggesting that dispersion interactions will be weak. On the other hand, while CO₂ has no dipole moment, it has a substantial quadrupole moment; although electrostatic forces arising from charge separation act over short distances, quadrupolar interactions dominate at low temperatures due to the fairly high density of supercritical CO₂ [Kirby and McHugh, 1999]. For this reason, CO₂ is a poor solvent for both nonpolar and very polar polymers. O’Neill and coworkers [1998] have suggested that polymer-polymer interactions govern solubility, and therefore polymer surface tension or cohesive energy density is the best indicator of solubility in CO₂. Kazarian and coworkers [1996] have observed specific interactions between CO₂ and electron-donating groups such as carbonyls; however, these interactions are only slightly stronger than dispersion interactions. As discussed above, certain polymers incorporating fluorinated side chains also exhibit enhanced solubility, although fluorination alone does not guarantee solubility. Some researchers have suggested that fluorinated side chains shield the polymer backbone from CO₂ interactions due to clustering or through the for-

mation of weak complexes [Kazarian et al., 1996]. Sarbu and co-workers [2000] have incorporated the observations described above into a set of guidelines to be used to design “CO₂-philic” copolymers. They recommend that one of the monomers provides high flexibility, high free volume, and low cohesive energy density, and that the other monomer contains groups which exhibit specific interactions with CO₂.

1.2.2 Gas-expanded solvents

The low solvating power of supercritical CO₂ may be overcome in many cases by adding an appropriate co-solvent. Liquid co-solvents such as acetone or methanol effectively increase the density of the SCF, thereby enhancing solubility. In addition, co-solvents which provide polar interactions, complex formation, or hydrogen bonding with the polymer can significantly improve solubility beyond simple density effects [Ekart et al., 1993]. Commonly used co-solvents for supercritical CO₂ systems include methanol, acetone, dimethylsulfoxide (DMSO), and toluene.

Conversely, compressible gases may be added to organic solvents to obtain gas-expanded liquids (GXL). Not surprisingly, these mixtures exhibit tunable properties between those of the pure liquid and the pure SCF, often retaining the high solvent strength of organic solvents as well as gas-like viscosity and low surface tension. Carbon dioxide-expanded liquids (CXLs) have been applied to separations processes, crystallization, particle formation, and chemical reactions; Jessop and Subramaniam discuss the advantages of GXLs and many of their applications in their recent review [2007].

1.2.3 Particle formation and encapsulation in CO₂-based media

Much of the recent research activity involving CO₂-based media has focused on methods of forming nanoparticles of one or more materials, taking advantage of the gas-like transport properties and tunable solvent character of supercritical fluids. Because of the desire to eliminate the use of harmful solvents, considerable effort has been di-

rected toward using scCO₂ and liquid CO₂ for pharmaceutical and drug delivery applications; researchers have also attempted to apply supercritical processing techniques to produce catalysts [Reverchon et al., 2003], cosmetics [Viswanathan and Gupta, 2003], pigments [Hong et al., 2000], and latexes [Liu and Yates, 2002], as well as novel micro- and nano-structured materials such as fibers [Mawson et al., 1995] and foams for a variety of applications [Tomasko et al., 2003].

The same processes that have been developed for particle formation have also been applied to particle encapsulation. The following sections review the main techniques being investigated for particle formation and encapsulation in supercritical CO₂, with a focus on encapsulation of nanoparticles with polymeric material. The reader is referred to the reviews by Reverchon [1999], Thiering and coworkers [2001], Jung and Perrut [2001], and Tomasko and coworkers [2003] for further discussion regarding particle design using CO₂ and CO₂-based mixtures.

Rapid expansion of a supercritical solution

The simplest technique for particle design using supercritical fluids is referred to as rapid expansion of a supercritical solution (RESS). Due to its simple, continuous, solvent-free operation, RESS is the preferred technique for coating materials which are soluble in scCO₂ at concentrations above 10⁻⁴ mole fraction [Shekunov et al., 2004]. For particle encapsulation applications, the coating material is first dissolved in scCO₂, the particles to be coated are added to the solution, and the resulting slurry is then expanded across a heated nozzle to a lower pressure. The solubility of the coating material decreases dramatically with pressure, leading to precipitation and encapsulation of the particles. Important process variables include temperature, pressure drop, nozzle geometry, and the structure of the coating material [Jung and Perrut, 2001, Thies et al., 2003]. The primary limitation of the RESS process is the poor solvent power of scCO₂ for many coating materials. Matsuyama and coworkers have developed a modified process – referred to as rapid expansion of a supercritical solution with an non-solvent (RESS-N) – in which ethanol is used as a co-solvent to enhance the solubility of the coating material [Matsuyama et al., 2003, 2001, Mishima

et al., 2000]. Although the addition of ethanol increases the solvent power of scCO₂, pure ethanol is not a solvent for any of the polymeric coating materials employed; if this were not the case, agglomeration of the product particles would be a concern, as it is in the antisolvent techniques discussed below [Shekunov et al., 2004]. The RESS-N process has been used to form microcapsules as small as 6 μm [Matsuyama et al., 2003]. In another modification of RESS, Shim expanded surfactant-stabilized suspensions of poly(2-ethylhexyl acrylate) in scCO₂ over a nozzle to produce uniform polymer films [Shim et al., 1999].

Processes employing CO₂ as an anti-solvent

Another class of processes utilizes SCFs as antisolvents, avoiding the difficulties encountered in the RESS process related to the poor solvent power of CO₂. The coating material is first dissolved in an appropriate solvent containing suspended particles, and one of two basic techniques is then employed to bring this suspension into contact with the supercritical antisolvent: the CO₂ can be injected into a tank containing the suspension, or the suspension can be fed into a vessel containing scCO₂. The naming of these antisolvent techniques is inconsistent in the literature, but in general gas antisolvent (GAS) systems refer to the former technique, while the terms precipitation with a compressed antisolvent (PCA), supercritical antisolvent (SAS) precipitation, aerosol solvent extraction system (ASES), and solution-enhanced dispersion by supercritical fluids (SEDS) describe variations of the latter. The acronyms GAS and PCA will be used below to refer to the two main classes of antisolvent processes. Although both the GAS and PCA techniques utilize CO₂ as an antisolvent, it has been suggested that they operate in different hydrodynamic regimes [Tomasko et al., 2003, Thiering et al., 2001]. In GAS systems, the solution containing suspended particles and dissolved coating material is expanded by the injection of compressed CO₂, causing supersaturation of the solution and precipitation of the coating material onto the particles. The process is operated in batch configuration, and expansion of the solution is followed by a washing step in which scCO₂ is pumped through the vessel to remove the remaining solvent. With regard to the GAS process, the rate of pressure

increase in the precipitation vessel is generally recognized as the most important process parameter [Reverchon, 1999]. However, Thiering and coworkers have examined the influence of operating temperature, solvent choice, rate of antisolvent addition, and solute concentration on the formation of protein particles, and found that the choice of solvent had the greatest impact [Thiering et al., 2000a,b]. Bertuccio and colleagues [1998] have developed a thermodynamic model of the GAS particle-formation process, and Muhrer and coworkers [2002] have extended this model to include nucleation and growth kinetics; the results of the latter model suggest that the conflicting conclusions of previous experimental studies can be explained by differences in the relative rates of primary and secondary nucleation. A model incorporating mass transfer effects has not yet been developed, although Elvassore and coworkers have modeled mass transport between a droplet of polymer-containing solvent and a miscible antisolvent [2004].

As discussed above, the PCA technique is essentially the reverse of the GAS technique: the suspension of particles and coating material is introduced into a vessel containing supercritical CO₂. A key difference in the PCA process is the fact that compressed CO₂ is often introduced along with the particle solution, allowing continuous or semi-continuous operation and providing desirable mass transfer effects in certain cases.

The mechanisms of mixing, supersaturation and precipitation during the spraying operation of the PCA process are not well understood, although several authors have attempted to model these phenomena to gain a better understanding of the fundamental processes involved [Lengsfeld et al., 2000, Jarmer et al., 2004, Werling and Debenedetti, 2000, Lora et al., 2000, Bristow et al., 2001]. Lengsfeld and colleagues [2000] determined that the length scale for the disappearance of surface tension ($\sim 1\mu\text{m}$) is less than that for jet breakup ($\sim 1\text{mm}$) during injection of methylene chloride into scCO₂, which implies that gas phase nucleation and growth rather than nucleation within discrete liquid drops is the relevant mechanism when the injected liquid is miscible with scCO₂. However, experimental data is still lacking, and the complex interplay between thermodynamics, mass transfer, nucleation and

growth kinetics, and jet hydrodynamics make this a challenging problem. Recently, Martin and Cocero [2004] have presented a model incorporating all of these aspects, and although it is not predictive, it may be useful for interpreting and correlating experimental results.

Although the precise mechanisms of the PCA process are not known with certainty, numerous empirical variations have been developed in order to improve the mass transfer upon introduction of the particle suspension and CO₂ into the pressurized vessel. For example, nozzles [Reverchon et al., 2003, Gao et al., 1998, Young et al., 1999, Wang et al., 2004], small internal diameter capillaries [Boutin et al., 2004], and vibrating orifices [Randolph et al., 1993] have been employed to inject the liquid solution, and coaxial nozzles for simultaneously injecting the liquid solution and CO₂ have been used to facilitate mixing [Mawson et al., 1997]. Power ultrasound has also been employed by several researchers. Randolph et al [1993] used a special nozzle to generate high-frequency sonic waves in the precipitation of poly(L-lactic acid) particles, Subramaniam and coworkers [Subramaniam et al., 1997] have patented a similar PCA technique using a specialized nozzle, and Chattopadhyay and Gupta [2002] have produced magnetically responsive composite particles of polymer and magnetite by impinging the liquid solution on an ultrasonic horn.

Because the PCA process mechanism remains largely uncharacterized, it is not surprising that there is some controversy as to the effects of process variables on product morphology. In fact, little agreement can be found in the literature, even with regard to the effects of pressure, temperature, and solute concentration [Reverchon, 1999]. More theoretical and experimental work is necessary to gain insight into the fundamental mechanics of PCA.

In addition to the RESS and antisolvent techniques described above, Seivers and coworkers have developed a CO₂-assisted nebulization process which can be used for water-soluble coating materials [2003], and Yue and coworkers [2004] have recently encapsulated particles of Dechlorane via *in situ* polymerization of poly(methyl methacrylate).

References

- E. J. Beckman. Supercritical and near-critical CO₂ in green chemical synthesis and processing. *Journal of Supercritical Fluids*, 28:121–191, 2004.
- A. Bertucco, M. Lora, and I. Kikic. Fractional crystallization by gas antisolvent technique: Theory and experiments. *AIChE Journal*, 44(10):2149–2158, 1998.
- O. Boutin, E. Badens, E. Carretier, and G. Charbit. Co-precipitation of a herbicide and biodegradable materials by the supercritical anti-solvent technique. *Journal of Supercritical Fluids*, 31(1):89–99, 2004.
- S. Bristow, B. Y. Shekunov, and P. York. Solubility analysis of drug compounds in supercritical carbon dioxide using static and dynamic extraction systems. *Industrial & Engineering Chemistry Research*, 40(7):1732–1739, 2001.
- P. Chattopadhyay and R. B. Gupta. Protein nanoparticles formation by supercritical antisolvent with enhanced mass transfer. *AIChE Journal*, 48(2):235–244, 2002.
- D. Darlin. New printer cartridge or a refill? either way, ink is getting cheaper, february 4, 2006. *New York Times*, 2006.
- L. Du, J. Y. Kelly, G. W. Roberts, and J. M. DeSimone. Fluoropolymer synthesis in supercritical carbon dioxide. *Journal of Supercritical Fluids*, 47(3):447–457, 2009.
- M. P. Ekart, K. L. Bennett, S. M. Ekart, G. S. Gurdial, C. L. Liotta, and C. A. Eckert. Cosolvent interactions in supercritical fluid solutions. *AIChE Journal*, 39(2):235–248, 1993.
- N. Elvassore, F. Cozzi, and A. Bertucco. Mass transport modeling in a gas antisolvent process. *Industrial & Engineering Chemistry Research*, 43(16):4935–4943, 2004.
- I. Endo, Y. Sato, S. Saito, T. Nakagiri, and S. Ohno. Liquid jet recording process and apparatus there for. *Great Britain Patent 2007162*, 1979.

- Y. Gao, T. K. Mulenda, Y. F. Shi, and W. K. Yuan. Fine particles preparation of Red Lake C Pigment by supercritical fluid. *Journal of Supercritical Fluids*, 13(1-3): 369–374, 1998.
- J. B. Hanney and J. Hogarth. On the solubility of solids in gases. *Proceedings of the Royal Society of London*, 29:324, 1879.
- L. Hong, J. Z. Guo, Y. Gao, and W. K. Yuan. Precipitation of microparticulate organic pigment powders by a supercritical antisolvent process. *Industrial & Engineering Chemistry Research*, 39(12):4882–4887, 2000.
- D. J. Jarmer, C. S. Lengsfeld, and T. W. Randolph. Nucleation and growth rates of poly(L-lactic acid) microparticles during precipitation with a compressed-fluid antisolvent. *Langmuir*, 20(17):7254–7264, 2004.
- P. G. Jessop and B. Subramaniam. Gas-expanded liquids. *Chemical Reviews*, 107: 2666–2694, 2007.
- J. Jung and M. Perrut. Particle design using supercritical fluids: Literature and patent survey. *Journal of Supercritical Fluids*, 20(3):179–219, 2001.
- S. G. Kazarian, M. F. Vincent, F. V. Bright, C. L. Liotta, and C. A. Eckert. Specific intermolecular interaction of carbon dioxide with polymers. *Journal of the American Chemical Society*, 118(7):1729–1736, 1996.
- C. F. Kirby and M. A. McHugh. Phase behavior of polymers in supercritical fluid solvents. *Chemical Reviews*, 99(2):565–602, 1999.
- H. P. Le. Progress and trends in ink-jet printing technology. *Journal of Imaging Science and Technology*, 42(1):49–62, 1998.
- C. S. Lengsfeld, J. P. Delplanque, V. H. Barocas, and T. W. Randolph. Mechanism governing microparticle morphology during precipitation by a compressed antisolvent: Atomization vs nucleation and growth. *Journal of Physical Chemistry B*, 104(12):2725–2735, 2000.

- H. Liu and M. Z. Yates. Development of a carbon dioxide-based microencapsulation technique for aqueous and ethanol-based latexes. *Langmuir*, 18(16):6066–6070, 2002.
- M. Lora, A. Bertucco, and I. Kikic. Simulation of the semicontinuous supercritical antisolvent recrystallization process. *Industrial & Engineering Chemistry Research*, 39(5):1487–1496, 2000.
- A. Martin and M. J. Cocero. Numerical modeling of jet hydrodynamics, mass transfer, and crystallization kinetics in the supercritical antisolvent (SAS) process. *Journal of Supercritical Fluids*, 32(1-3):203–219, 2004.
- K. Matsuyama, K. Mishima, T. Hirabaru, and K. Takahashi. Polymerization of glycidyl methacrylate in supercritical carbon dioxide. *Kobunshi Ronbunshu*, 58(10):552–556, 2001.
- K. Matsuyama, K. Mishima, K. Hayashi, and H. Matsuyama. Microencapsulation of TiO₂ nanoparticles with polymer by rapid expansion of supercritical solution. *Journal of Nanoparticle Research*, 5(1-2):87–95, 2003.
- S. Mawson, K. P. Johnston, J. R. Combes, and J. M. Desimone. Formation of poly(1,1,2,2-tetrahydroperfluorodecyl acrylate) submicron fibers and particles from supercritical carbon-dioxide solutions. *Macromolecules*, 28(9):3182–3191, 1995.
- S. Mawson, K. P. Johnston, D. E. Betts, J. B. McClain, and J. M. DeSimone. Stabilized polymer microparticles by precipitation with a compressed fluid antisolvent: 1. poly(fluoro acrylates). *Macromolecules*, 30(1):71–77, 1997.
- M. A. McHugh and V. J. Krukonis. *Supercritical Fluid Extraction Principles and Practice*. Butterworth, Stoneham, MA, 1994.
- K. Mishima, K. Matsuyama, D. Tanabe, S. Yamauchi, T. J. Young, and K. P. Johnston. Microencapsulation of proteins by rapid expansion of supercritical solution with a nonsolvent. *AIChE Journal*, 46(4):857–865, 2000.

- G. Muhrer, C. Lin, and M. Mazzotti. Modeling the gas antisolvent recrystallization process. *Industrial & Engineering Chemistry Research*, 41(15):3566–3579, 2002.
- M. L. O’Neill, Q. Cao, R. Fang, K. P. Johnston, S. P. Wilkinson, C. D. Smith, J. L. Kerschner, and S. H. Jureller. Solubility of homopolymers and copolymers in carbon dioxide. *Industrial & Engineering Chemistry Research*, 37(8):3067–3079, 1998.
- T. W. Randolph, A. D. Randolph, M. Mebes, and S. Yeung. Sub-micrometer-sized biodegradable particles of poly(L-lactic acid) via the gas antisolvent spray precipitation process. *Biotechnology Progress*, 9(4):429–435, 1993.
- E. Reverchon. Supercritical antisolvent precipitation of micro- and nano-particles. *Journal of Supercritical Fluids*, 15(1):1–21, 1999.
- E. Reverchon, G. Caputo, S. Corraera, and P. Cesti. Synthesis of titanium hydroxide nanoparticles in supercritical carbon dioxide on the pilot scale. *Journal of Supercritical Fluids*, 26(3):253–261, 2003.
- F. Rindfleisch, T. P. DiNoia, and M. A. McHugh. Solubility of polymers and copolymers in supercritical CO₂. *Journal of Physical Chemistry*, 100(38):15581–15587, 1996.
- T. Sarbu, T. Styranec, and E. J. Beckman. Non-fluorous polymers with very high solubility in supercritical CO₂ down to low pressures. *Nature*, 405(6783):165–168, 2000.
- B. Y. Shekunov, P. Chattopadhyay, and J. Seitzinger. Supercritical fluid processing techniques: comparing the products. *Respiratory Drug Delivery*, 9:289–296, 2004.
- J. J. Shim, M. Z. Yates, and K. P. Johnston. Polymer coatings by rapid expansion of suspensions in supercritical carbon dioxide. *Industrial & Engineering Chemistry Research*, 38(10):3655–3662, 1999.
- R. E. Sievers, E. T. S. Huang, J. A. Villa, G. Engling, and P. R. Brauer. Micronization of water-soluble or alcohol-soluble pharmaceuticals and model compounds with a low-temperature Bubble Dryer. *Journal of Supercritical Fluids*, 26(1):9–16, 2003.

- B. Subramaniam, S. Saim, R. Rajewski, and V. Stella. Methods for a particle precipitation and coating near-critical and supercritical antisolvents. *United States Patent 5,833,891*, 1997.
- R. Thiering, F. Dehghani, A. Dillow, and N. R. Foster. The influence of operating conditions on the dense gas precipitation of model proteins. *Journal of Chemical Technology and Biotechnology*, 75(1):29–41, 2000a.
- R. Thiering, F. Dehghani, A. Dillow, and N. R. Foster. Solvent effects on the controlled dense gas precipitation of model proteins. *Journal of Chemical Technology and Biotechnology*, 75(1):42–53, 2000b.
- R. Thiering, F. Dehghani, and N. R. Foster. Current issues relating to anti-solvent micronisation techniques and their extension to industrial scales. *Journal of Supercritical Fluids*, 21(2):159–177, 2001.
- C. Thies, I. R. Dos Santos, J. Richard, V. Vandeveld, H. Rolland, and J. P. Benoit. A supercritical fluid-based coating technology 1: Process considerations. *Journal of Microencapsulation*, 20(1):87–96, 2003.
- D. L. Tomasko, H. B. Li, D. H. Liu, X. M. Han, M. J. Wingert, L. J. Lee, and K. W. Koelling. A review of CO₂ applications in the processing of polymers. *Industrial & Engineering Chemistry Research*, 42(25):6431–6456, 2003.
- R. Viswanathan and R. B. Gupta. Formation of zinc oxide nanoparticles in supercritical water. *Journal of Supercritical Fluids*, 27(2):187–193, 2003.
- Y. L. Wang, R. N. Dave, and R. Pfeffer. Polymer coating/encapsulation of nanoparticles using a supercritical anti-solvent process. *Journal of Supercritical Fluids*, 28(1):85–99, 2004.
- J. O. Werling and P. G. Debenedetti. Numerical modeling of mass transfer in the supercritical antisolvent process: miscible conditions. *Journal of Supercritical Fluids*, 18(1):11–24, 2000.

- W. J. Wnek, M. A. Andreottola, P. F. Doll, and S. M. Kelly. Ink jet technology. In A. S. Diamond and D. S. Weiss, editors, *Handbook of Imaging Materials*, pages 531–602. Marcel Dekker, Inc., New York, 2nd edition, 2002.
- Y. Xiong and E. Kiran. Miscibility, density and viscosity of poly(dimethylsiloxane) in supercritical carbon-dioxide. *Polymer*, 36(25):4817–4826, 1995.
- T. J. Young, K. P. Johnston, K. Mishima, and H. Tanaka. Encapsulation of lysozyme in a biodegradable polymer by precipitation with a vapor-over-liquid antisolvent. *Journal of Pharmaceutical Sciences*, 88(6):640–650, 1999.
- B. Yue, J. Yang, Y. L. Wang, C. Y. Huang, R. Dave, and R. Pfeffer. Particle encapsulation with polymers via in situ polymerization in supercritical CO₂. *Powder Technology*, 146(1-2):32–45, 2004.

Chapter 2

Objectives and approach

2.1 Motivation

As discussed in Chapter 1, ink jet is a very demanding application that requires carefully formulated inks in order to quickly and reliably produce high-quality printed images. Although ink jet inks are currently produced via an aqueous process, SCFs and gas-expanded solvents present alternative processing media for particle coating operations that may offer significant benefits with respect to the production of polymer-encapsulated pigment particles for these inks.

Media milling technology using SCFs to produce particles with desirable properties has been developed by DuPont for pharmaceutical applications [Ford et al., 2002]; when combined with the gas antisolvent (GAS) particle encapsulation processes discussed in the previous chapter, this technology possesses several potentially important advantages over conventional water-based processes for the production of ink jet inks. For example, the low viscosity of the resulting slurry could lead to better dispersion and energy transfer, possibly improving particle size reduction and control from micro- to nano-particles. After the milling and encapsulation is complete, separation and elimination of CO₂ and any co-solvents is easily achievable in a single step, and the process would yield a dry flowable end-product. Perhaps most importantly, it would be possible to encapsulate pigment particles with hydrophobic resins which are not soluble in water and thus unavailable for use in the current process. A CO₂-

based process incorporating these hydrophobic resins would allow more efficient use of a wider range of dispersants with minimal losses – much lower than is possible with the current water-based process. An effort to develop such a process would provide new process approaches to particle size reduction and coating that would result in improved ink quality, greater freedom in ink formulation, and possible cost savings in a highly competitive market.

2.2 Thesis objectives

The main thesis objective is the demonstration and analysis of a particle size reduction and encapsulation process which takes place in CO₂-expanded acetone and produces colloidal carbon black particles which are uniformly coated with functionalized hydrophobic resins. The powder produced by the milling process should result in stable nanoparticle dispersions when mixed into either solvent or water, yielding pigment particle dispersions suitable for use in ink jet inks. The specific objectives and approach are as follows:

Selection of model system for study

A wide variety of pigments and dispersing resins are currently used in the production of commercial inks. In addition, the incorporation of high-pressure processing in gas-expanded solvents allows the use of a range of organic solvents during the encapsulation process. Thus, the first task was the selection of an appropriate model system for study. The desired system would be relevant to commercially viable inks, but would also be amenable to analysis that would lead to a deeper understanding of interactions among the pigment particles, the dispersant resin, and the gas-expanded liquid media. The considerations that led to the selection of the final model system are discussed in Chapter 3.

Phase behavior of CO₂-acetone-polymer systems

The selection of process conditions for encapsulation is guided by knowledge of the phase behavior of the polymer-solvent-CO₂ ternary systems which comprise the fluid phase. Solid-liquid-vapor equilibrium curves for these ternary systems were measured using an apparatus incorporating the detection of scattered laser light to determine the onset of polymer precipitation. Measurements were made at various values of the polymer weight fraction at three fixed temperatures; the equilibrium data gathered were then correlated using the PC-SAFT equation of state. The results of this study are presented in Chapter 4.

Adsorption of polymer onto carbon black particles from CO₂-expanded acetone

The conventional process to produce inks is governed by the adsorption equilibrium of the dispersing resin on the surface of the pigment particles. The high-pressure process under investigation can also be analyzed in terms of the adsorption equilibrium conditions; however, pressure is introduced as an additional parameter. An apparatus was designed and constructed for the experimental investigation of CO₂-solvent-polymer-particle interactions via high-pressure adsorption isotherms, and isotherm data was gathered for two polymers and correlated with the Langmuir equation. This investigation is summarized in Chapter 5.

Carbon black size reduction and polymer encapsulation in CO₂-expanded acetone

To meet the final thesis objective, a prototype high-pressure process was designed, constructed, and demonstrated for both size reduction and polymer encapsulation of pigment particles in gas-expanded solvent media. The process is based on the GAS process described in Chapter 1, and incorporates high-pressure milling techniques developed at DuPont. The results of the supporting tasks described above informed the selection of process operating conditions; the resulting product powders were

characterized via TEM analysis, and were also submitted to DuPont for evaluation in actual inks. The details of the development and validation of the high-pressure encapsulation process are included in Chapter 6.

References

W. N. Ford, E. H. J. C. Gommeren, and Q. Q. Zhao. High pressure media mill. *International Patent WO 02/094443 A2*, 2002.

Chapter 3

Model system

Ink jet inks are complex mixtures whose properties depend on the specific components chosen to formulate the ink, the relative amounts of these components, and the processing methods used to produce the final formulation. For the purposes of the thesis, we are concerned with the production of (dry) polymer-encapsulated pigment particles for use in aqueous inks. Thus, the focus will be on the pigment particles and the dispersant polymer that will be applied to the pigment particle surface; the various additives that are typically added to ink formulations to adjust their final properties and enhance stability (e.g. humectant, buffer, biocide, etc.) are outside the scope of the thesis and will not be discussed further. However, the solvent that serves as the processing medium for encapsulation (in combination with CO₂) will also strongly affect the process and product performance, and represents an additional component of the model system.

The model system chosen for study consists of carbon black (pigment), styrene/acrylic and benzyl methacrylate/methacrylic acid copolymers (dispersant resins), and acetone (solvent). The following sections describe the factors that led to the choice of this model system.

3.1 Pigment

The color of ink jet inks is imparted by either dyes or pigments; as discussed in Chapter 1, pigments have gradually come to replace dyes in many inks due to their superior lightfastness and tendency to remain at the surface of the medium after printing. However, the use of pigments requires that the individual particles are small and well-stabilized such that clogging of the printhead nozzles does not occur. A variety of pigments have been developed for cyan, magenta, and yellow inks [Herbst and Hunger, 1997, Abel, 1999, Patterson, 1967], but the most widely used and well-characterized pigment for ink jet is carbon black. Carbon black also possesses a tertiary structure in which primary particles on the order of 10-50nm form tightly bound aggregates that in turn form more loosely bound agglomerates; a TEM micrograph of a well-dispersed carbon black aggregate is shown in Figure 3-1. This structure is more amenable to size reduction than many of the organic pigments used for other colors, since aggregates on the order of 100 nm can be obtained by breaking apart the larger agglomerates. Carbon black was therefore an obvious choice as the model pigment for the current study.

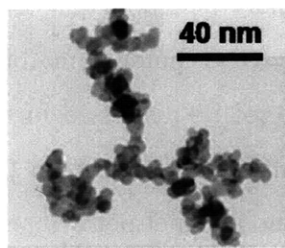


Figure 3-1: TEM image of a dispersed carbon black aggregate (source: Michael Wolfe, DuPont).

3.2 Polymeric dispersant

The dispersion of powders in liquids is a complex phenomena that is influenced by the properties of and interactions between the dispersed solid, the stabilizing agent (dispersant), and the fluid medium. In the absence of a stabilizing agent, colloidal

pigment particles in an aqueous dispersion will tend to coagulate due to interparticle Van der Waals forces [Israelachvili, 1992]. Thus, the polymeric dispersant applied to the particle surfaces plays a vital role in promoting the stability of the dispersion and preventing the formation of pigment aggregates which would increase the likelihood of sedimentation and nozzle clogging. This polymer coating also contributes to the adhesion of the pigment particles to paper during printing, and influences the quality of the final color of the ink. The dispersant resins must therefore be chosen carefully to produce high-quality, stable inks.

In a typical pigmented ink, dispersant molecules are fixed to particle surfaces by either adsorption or grafting, and these agents promote the dispersion of pigment by imparting electrostatic [Verwey, 1940] or steric [Napper, 1983] repulsive forces – or some combination of these – between the individual particles in the fluid medium. A detailed discussion of the mechanisms of colloidal dispersion is outside the scope of the thesis, but the reader is referred to the monographs by Parfitt [1981] and Stein [1996] for a comprehensive treatment of this subject.

In the specific case of aqueous carbon black pigment dispersions for inks, low molecular weight ($<10,000\text{g/mol}$) polymers containing aromatic rings or amines as well as carboxylic acid functionality are often utilized [Spinelli, 1998]. The aromatic rings and amine groups promote adsorption via specific acid-base interactions with oxygen-containing groups on the surface of the carbon black [Parfitt, 1981]; the carboxylic acid-containing moieties are neutralized in order to impart a charge on the particle, resulting in strong interparticle coulombic repulsion forces [Chang et al., 2003]. Branched and/or block copolymer structures can also be employed, in which certain segments of the polymer are hydrophobic and others are hydrophilic; the hydrophilic segments “dissolve” into the aqueous phase, extending away from the particle surface and providing steric stabilization to the dispersion. If these hydrophilic segments also contain acid groups, the dispersion will exhibit both stabilization mechanisms (ionic and steric) [Spinelli, 1998].

3.2.1 Initial model polymer: Joncryl[®] resins

Commercially available styrene-acrylic copolymer dispersing resins sold under the trade name Joncryl[®] (Joncryl[®] 678, Joncryl[®] 586, and Joncryl[®] 611) were chosen for investigation in preliminary studies. These resins have a branched structure and varying degrees of carboxylic acid functionality. Joncryl[®] 678 and Joncryl[®] 586 are water soluble, and suitable for use in the current water-based process to produce inks, while Joncryl[®] 611 is a hydrophobic dispersant typically used for solvent-based formulations. These resins were chosen based on the fact that they are representative of the dispersants currently used in commercial inks. Schematic representations the copolymer moieties found in the Joncryl[®] resins are shown in Figure 3-2.

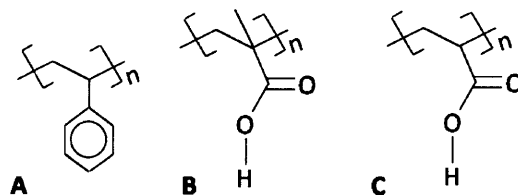


Figure 3-2: Styrene (A) and acrylic (B, C) moieties present in Joncryl[®] polymers.

3.2.2 Benzyl methacrylate/methacrylic acid copolymers

Upon completion of the initial process validation phase of the project, the Joncryl[®] dispersant resins were replaced with copolymers of benzyl methacrylate (BzMA) and methacrylic acid (MAA) synthesized at DuPont. See Figure 3-3 for schematic representations of these moieties. The BzMA/MAA polymers feature a well-defined random linear structure and uniform molecular weight (~ 5500 g/mol) that is more appropriate for fundamental studies of the interactions between these polymers, the fluid phase, and the pigment particle surfaces. Three resins with varying ratios of BzMA and MAA moieties (BzMA/MAA = 85/15, 80/20, 75/25) were used in all subsequent investigations. These ratios were selected such that the acid functional groups would be numerous enough to aid in the dispersion of encapsulated particles,

but not so numerous as to significantly increase the solubility of the polymers in water. Important properties of the polymers are given in Table 3.1.

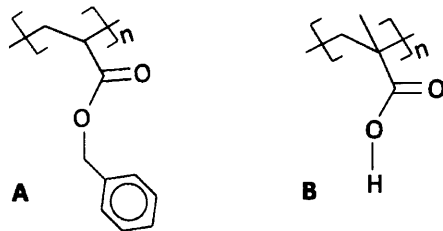


Figure 3-3: Benzyl methacrylate (A) and methacrylic acid (B) moieties present in model polymers used for the current work.

Table 3.1: Selected properties of benzyl methacrylate/methacrylic acid random copolymers used in the current work.

BzMA/MAA mass ratio	Acid value (meq/g)	M _n	
		M _n	M _w /M _n
85/15	1.76	5451	1.13
80/20	2.35	5895	1.14
75/25	2.89	5686	1.13

3.3 Solvent

Although the solvent used in the particle encapsulation process under investigation will not be present in the final inks, it represents an integral component of the model system. Because the GAS process applied to particle encapsulation is governed by the phase behavior of the fluid phase and adsorption of polymer from the fluid phase onto the particle surfaces, the choice of solvent to a large extent dictates the process operating conditions and encapsulation efficiency. The polymer dispersant must be soluble in the solvent, but not so soluble that a large degree of CO₂-driven volume expansion – and high operating pressure – is required to reduce the polymer solubility sufficiently to achieve encapsulation. The extent of volume expansion with CO₂ addition will also affect the operating pressure, and should be taken into consideration.

A plot of volume expansion with CO₂ versus pressure for several solvents is shown in Figure 3-4, where volume expansion is calculated from the original CO₂-free liquid volume, V_i , and the final CO₂-expanded liquid volume, V_f , as:

$$\Delta V = \frac{V_f(T, P, x_{CO_2}) - V_i(T, P^0)}{V_i(T, P^0)} \quad (3.1)$$

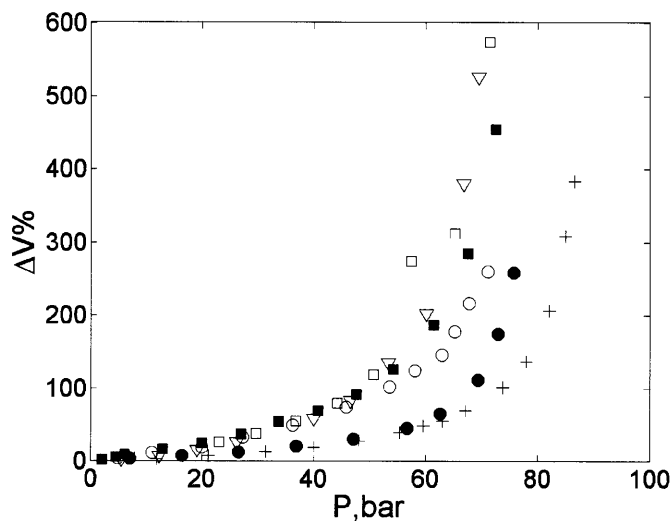


Figure 3-4: Volume expansion with addition of CO₂ as a function of system pressure for selected solvents: ○, acetone, 323K, ▽, dichloromethane, 313K, ●, 2-Propanol, 313K, □, tetrahydrofuran, 313K, +, toluene, 323K, ■, acetonitrile, 313K. Data taken from Lazzaroni et al. [2005].

In addition to favorable polymer-solvent and CO₂-solvent binary phase behavior, the liquid must exhibit no strong interactions with the surface of the pigment particles that would interfere with the adsorption of the dispersant. Practical considerations such as cost, health and safety issues, and vapor pressure also influence the selection of a solvent. Acetone was chosen as the solvent for the model system based on these factors. Acetone-CO₂ phase behavior has been well-studied in the literature [Chiu et al., 2008, Jin and Subramaniam, 2004, Liu and Kiran, 2007, Day et al., 1996], and it is known to expand readily upon pressurization with CO₂. It is an adequate solvent for the polymers of interest for this study, is relatively inexpensive, and has no chronic health effects. Table 3.2 enumerates several key properties of acetone.

Table 3.2: Selected properties of acetone.

Molecular Formula	C ₃ H ₆ O
Molecular Weight	58.08 g/mol
Density (20°C)	0.79 g/cm ³
Dipole moment	2.88
Boiling point	56.53°C
Critical point	234.95°C, 4.70 MPa
Viscosity (20°C)	0.32 cP

References

- A.G. Abel. Pigments for paint. In R. Lambourne and T.A. Strivens, editors, *Paint and Surface Coatings - Theory and Practice*. Woodhead Publishing, 2nd edition, 1999.
- C. J. Chang, S. J. Chang, S. Tsou, S. I. Chen, F. M. Wu, and M. W. Hsu. Effects of polymeric dispersants and surfactants on the dispersing stability and high-speed-jetting properties of aqueous-pigment-based ink-jet inks. *Journal of Polymer Science Part B-Polymer Physics*, 41(16):1909–1920, 2003.
- H. Y. Chiu, M. J. Lee, and H. M. Lin. Vapor-liquid phase boundaries of binary mixtures of carbon dioxide with ethanol and acetone. *Journal of Chemical and Engineering Data*, 53:2393–2402, 2008.
- C. Y. Day, C. J. Chang, and C. Y. Chen. Phase equilibrium of ethanol plus CO₂ and acetone plus CO₂ at elevated pressures. *Journal of Chemical and Engineering Data*, 41(4):839–843, 1996.
- W. Herbst and K. Hunger. *Industrial Organic Pigments*. VCH, Weinheim, 1997.
- J. Israelachvili. *Intermolecular and Surface Forces*. Academic Press, New York, 1992.
- H. Jin and B. Subramaniam. Homogeneous catalytic hydroformylation of 1-octene in CO₂-expanded solvent media. *Chemical Engineering Science*, 59(22-23):4887–4893, 2004.

- M. J. Lazzaroni, D. Bush, J. S. Brown, and C. A. Eckert. High-pressure vapor-liquid equilibria of some carbon dioxide plus organic binary systems. *Journal of Chemical and Engineering Data*, 50(1):60–65, 2005.
- K. Liu and E. Kiran. Viscosity, density and excess volume of acetone plus carbon dioxide mixtures at high pressures. *Industrial & Engineering Chemistry Research*, 46(16):5453–5462, 2007.
- D. H. Napper. *Polymeric Stabilisation of Colloidal Dispersions*. Academic Press, London, 1983.
- G. D. Parfitt. *Dispersion of Powders in Liquids*. Applied Science Publishers, London, 3rd edition, 1981.
- D. Patterson. *Pigments: An Introduction to their Physical Chemistry*. Elsevier Publishing Co., London, 1st edition, 1967.
- H. J. Spinelli. Polymeric dispersants in ink jet technology. *Advanced Materials*, 10(15):1215–+, 1998.
- H. N. Stein. *The Preparation of Dispersions in Liquids*. CRC Press, New York, 1996.
- E. J. W. Verwey. Electrical double layer and stability of emulsions. *Trans Far Soc*, 36:192, 1940.

Chapter 4

Measurement and correlation of the phase behavior of CO₂-acetone-polymer systems

The selection of suitable process conditions for particle encapsulation in CO₂-expanded solvents requires knowledge of the phase behavior of the polymer-solvent-CO₂ ternary systems which comprise the fluid phase. The goal of the encapsulation process is to reduce the size of the carbon black particles while simultaneously depositing a dispersant polymer on the surface of these same particles. Ideally, polymer molecules should be available in the fluid medium for deposition onto the particles as new surfaces become available during the comminution process, requiring a certain degree of polymer solubility in the liquid phase. Conversely, if the polymer solubility in the liquid is too high, the polymer molecules will tend to remain in solution rather than encapsulate the particles. Although the use of a CXL enables tuning of the solvation power with changes in pressure such that it is possible to efficiently coat the particles with polymer, the actual implementation of such a process depends upon the availability of information regarding the solubility limits of the polymers of interest in the CXL over a range of pressures.

In order to fully realize the benefits of using CO₂-expanded acetone for particle coating operations, the solid-liquid-vapor equilibrium of the model dispersant poly-

mers in these media was investigated experimentally and subsequently correlated with the PC-SAFT equation of state. The following chapter is concerned with details of this investigation.

4.1 Background

4.1.1 Previous studies of solid-fluid and solid-liquid-vapor equilibrium in CO₂-based media

A review of the literature related to the collection of phase behavior data for CO₂-based systems reveals that much of the early work focused on the use of pure scCO₂ as a solvent for extractions and organic synthesis [Dohrn and Brunner, 1995]. As the limited solvation strength of CO₂ became apparent, more researchers began to investigate the benefits of adding cosolvents to scCO₂ in order to explore new applications. In the case of both pure sCO₂ and cosolvent-modified sCO₂, the preferred approach for determining the solubility of a solute is the cloud point method [McHugh and Krukonic, 1994]. A typical experiment is carried out in a variable-volume vessel equipped with windows for visual access; the solute (and any cosolvent) are first added to the vessel, and the system is pressurized with CO₂ at a constant temperature until a single phase is obtained. The volume of the vessel is then increased isothermally, and the point at which the solute first precipitates from solution – referred to as the cloud point – is determined visually. Christov and Dohrn [2002] have published a comprehensive review of SCF phase equilibrium data which includes many such cloud point measurements.

The addition of a second phase introduces an additional degree of freedom to GXL systems, and thus the cloud point measurements as described above cannot be used to completely determine the state of a binary or ternary system. Rather, analytical techniques must be employed to measure the composition of one or more phases within the system. Experimental investigations of high-pressure solid-liquid-vapor equilibrium in binary or ternary mixtures are much less common in the literature

than studies of SCF-solid equilibrium [Shariati and Peters, 2002]. The data that do exist are often motivated by interest in the GAS process for micronization or fractionation of compounds for such applications as pharmaceuticals [Gallagher et al., 1994] and explosives [Gallagher et al., 1992]. In one of the earliest studies, Chang and Randolph [1990] measured the solubility of β -carotene in CO₂-expanded toluene and acetaminophen in CO₂-expanded butanol by precipitating and filtering particles from a saturated solution. Dixon and Johnston [1991] have investigated systems consisting of naphthalene and/or phenanthrene in CO₂-expanded toluene as a model for fractional crystallization with a gas antisolvent, employing an apparatus that allows sampling of a saturated liquid phase at a constant temperature and pressure. Shariati and Peters [2002] devised a synthetic method to measure solid-liquid-vapor equilibrium curves for salicylic acid in CO₂-expanded 1-propanol, in which the equilibrium points were obtained from the intersections of vapor-liquid and solid-liquid isopleths. Liu and coworkers have measured the solubility of ortho and para isomers of hydroxybenzoic acid [2000a] and aminobenzoic acid [2000b] in ethyl acetate and ethanol, respectively, for GAS fractionation applications; the apparatus and method used for these experiments is similar to that proposed by Dixon and Johnston [1991].

To date, there have been very few experimental studies involving polymer solubility in CO₂-expanded solvents. Clearly, there is a need for fundamental phase behavior data in order to fully realize the benefits of GXLs for polymer processing applications.

4.1.2 Equation-of-state modeling of CO₂-solvent-polymer ternary phase behavior

Cubic equations of state such as the Peng-Robinson (PR) and Soave-Redlich-Kwong (SRK) equations have been successfully employed to correlate equilibrium data from CO₂-solvent binary systems [Jha and Madras, 2005] as well as SCF and GXL systems containing small-molecule solutes [Bertakis et al., 2007, Crampon et al., 1999, Chang and Randolph, 1990]. Good agreement with experimental phase composition data can

generally be achieved by varying a single binary interaction parameter for each pair of components in a system. To overcome shortcomings with regard to the predictions of molar volume, modifications to the general cubic equations of state in the form of volume translation terms have also been proposed [Frey et al., 2007].

Although appropriate for use with systems containing small molecules, cubic equations of state have been shown to be ineffective for correlating phase behavior of SCF-polymer (and GXL-polymer) systems due to molecular size differences between solute and solvent species [Fermeglia et al., 1997, Muller and Gubbins, 2001]. Traditional Flory-Huggins theory – normally applied to polymer solutions – does not account for the high compressibility of these systems and is therefore also not appropriate.

The most commonly used equations of state for modeling the behavior of high-pressure mixtures containing polymers are based on the Statistical Associating Fluid Theory (SAFT) developed by Chapman et al. [1989]. Within the framework of SAFT, molecules are represented as covalently bonded chains of spherical segments with the ability to form associative complexes at specific sites on the molecular segments. Since the introduction of the SAFT equation of state two decades ago, numerous variations on the basic form have been introduced [Tan et al., 2008]; one of the most popular implementations for systems containing polymers is the Perturbed-Chain (PC) SAFT equation developed by Gross and Sadowski [2001].

PC-SAFT Equation of State

Like the original SAFT EOS, the PC-SAFT EOS is given as a perturbation expansion of the residual Helmholtz free energy,

$$\tilde{a}^{res} = (\tilde{a}^{hs} + \tilde{a}^{chain}) + \tilde{a}^{disp} + \tilde{a}^{assoc} \quad (4.1)$$

with contributions from hard-sphere repulsion between molecular segments (\tilde{a}^{hs}), connectivity of chains of segments (\tilde{a}^{chain}), attractive dispersion forces (\tilde{a}^{disp}), and associative interactions between segments (\tilde{a}^{assoc}). The difference between the SAFT EOS and the PC-SAFT EOS essentially arises from the choice of reference fluid in

the perturbation expansion. The SAFT EOS specifies a hard-sphere fluid with dispersion interactions as the reference fluid, effectively grouping the dispersion term in Equation 4.1 with the hard sphere term; in the case of PC-SAFT, the reference is taken to be the hard chains of connected segments – the hard-sphere and chain terms in Equation 4.1 – with no attractive interactions. The formulation of the EOS in terms of the Helmholtz free energy allows the calculation of all other thermodynamic properties via derivatives of this quantity [Tester and Modell, 1996].

The interactions between pairs of spherical segments are assumed to follow a modified square-well potential

$$u(r) = \begin{cases} \infty & r < (\sigma - s_1) \\ 3\epsilon & (\sigma - s_1) \leq r < \sigma \\ -\epsilon & \sigma \leq r < \lambda\sigma \\ 0 & r \geq \lambda\sigma \end{cases} \quad (4.2)$$

where $u(r)$ is the pair potential, r is the radial distance between two segments, σ is the temperature-independent segment diameter, ϵ is the depth of the potential well, λ is the reduced well width, and $s_1/\sigma = 0.12$. In the case of non-associating molecules, only three pure-component parameters are necessary to implement the EOS: σ , ϵ , and the number of segments per chain m . For use with mixtures, the PC-SAFT EOS requires a binary interaction parameter k_{ij} for each component pair. This parameter is used in the following mixing rules:

$$\sigma_{ij} = \frac{1}{2}(\sigma_i + \sigma_j) \quad (4.3)$$

$$\epsilon_{ij} = \sqrt{\epsilon_i \epsilon_j} (1 - k_{ij}) \quad (4.4)$$

Additional perturbation terms for Equation 4.1 have been proposed to account for dipolar and quadrupolar interactions [Karakatsani and Economou, 2006], and researchers have applied the PC-SAFT EOS to systems containing homopolymers [Tumakaka et al., 2002], copolymers [Gross et al., 2003], electrolytes [Cameretti et al.,

2005], and aqueous amino acids and polypeptides [Fuchs et al., 2006]. The PC-SAFT EOS has proven to be a useful tool for correlating the phase behavior of polymers in compressible fluid media based on a small amount of data [Tumakaka et al., 2007, Kleiner et al., 2006, Gornert and Sadowski, 2008], and is one of the few practical options for modeling these systems.

The complete implementation of the PC-SAFT EOS is presented in Gross and Sadowski [2001] and will not be reproduced here. Müller and Gubbins [2001] have published a thorough review of the SAFT formalism, including a simplified heuristic argument for its derivation.

4.2 Materials and methods

In the context of the current thesis work, it is desirable to investigate the phase behavior of the polymer-acetone-CO₂ systems that will comprise the fluid phase during particle encapsulation operations. An experimental apparatus that allows the collection of solid-liquid-vapor equilibrium data was designed and constructed based on the previous work outlined above. The experimental method described in the following sections essentially allows for the precipitation of polymer particles from a saturated solution under controlled conditions, much like a typical GAS process for particle formation [Gallagher et al., 1989]. This apparatus yields information that significantly enhances understanding of the particle coating process, and use of the PC-SAFT EOS to correlate the results effectively reduces the amount of data necessary to make informed decisions with regard to process operating conditions.

4.2.1 Experimental apparatus

The experimental apparatus that was used to gather phase behavior data is depicted schematically in Figure 4-1; a photograph of the system is shown in Figure 4-2. The main component of the system is a high-pressure view cell equipped with sapphire windows for visual access. The view cell, supplied by Thar Technologies (P/N 05422-3), has an internal volume of 50 ml, and a maximum working pressure of 6,000 psi

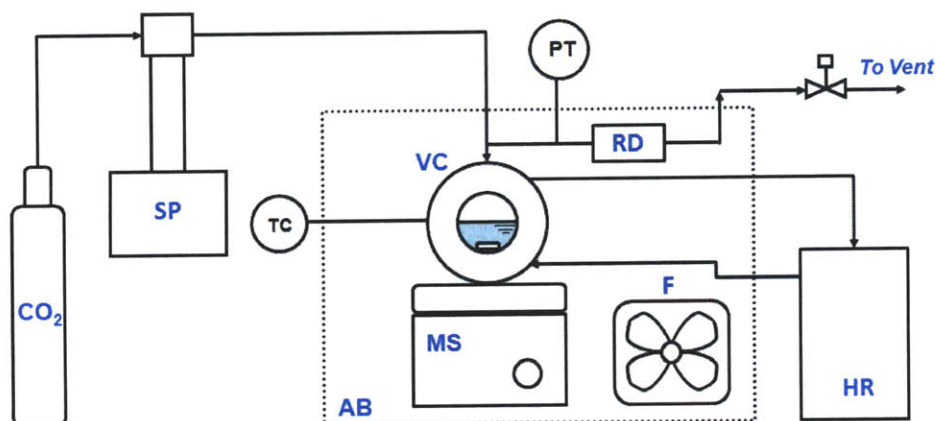


Figure 4-1: Schematic of the phase behavior measurement system. System components: carbon dioxide supply (CO₂), syringe pump (SP), view cell (VC), magnetic stirrer (MS), air bath (AB), fan (F), heated recirculator (HR), rupture disc (RD) thermocouple (TC), pressure transducer (PT).

at 150°C. Teflon-encapsulated viton o-rings (McMaster Carr, P/N 93445K218) were employed to make the seal between the view cell body and the sapphire windows. The view cell is suspended above a magnetic stir plate such that agitation within the view cell may be provided by a magnetic stir bar. Carbon dioxide is supplied to the system using a high-pressure syringe pump (Teledyne-Isco, Model 500D) equipped with air-actuated inlet and outlet valves (P/N 681247089).

System temperature is regulated via recirculation of water through copper tubing by a recirculating heater (VWR, Model 1160S); the copper tubing is wrapped around the view cell to provide direct contact and improved heat transfer. A polycarbonate enclosure around the system serves as both an air bath as well as a physical barrier to contain any projectiles resulting from catastrophic failure of process components; a fan within the air bath provides circulation to improve temperature uniformity. System temperature and pressure are monitored by thermocouples (type T, Omega Engineering, P/N GTMQSS-062U-6, tolerance $\pm 1\text{K}$) and a pressure transducer (Omega Engineering, P/N PX303-2KG5V, accuracy $\pm 7.5\text{psi}$), respectively; the output from the thermocouples and pressure transducer are recorded on a personal computer using LabVIEW data acquisition software. Temperature within the view cell is controlled

to within 0.2°C by manually adjusting the temperature of the bath of the recirculating heater.

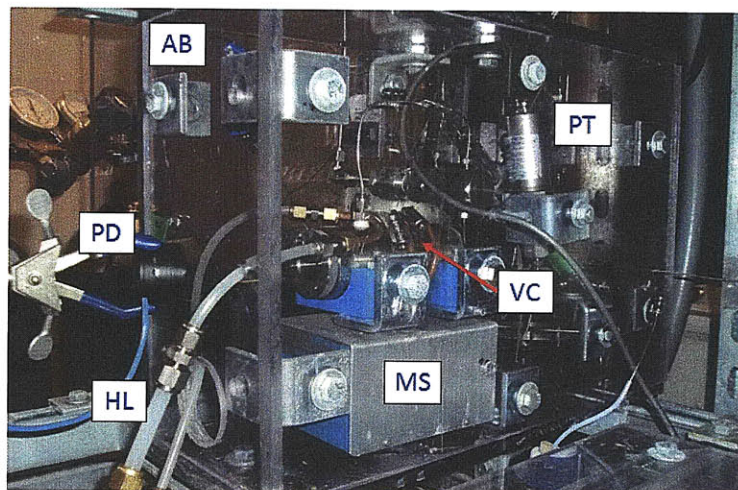


Figure 4-2: Photograph of the phase behavior measurement system. System components: view cell (VC), magnetic stirrer (MS), air bath (AB), heating loop (HL), pressure transducer (PT), photodiode detector (PD).

Laser light scattering for detection of polymer precipitation

The precipitation of polymer particles from the CO₂-expanded acetone is detected using a low-angle laser light scattering apparatus, depicted schematically in Figure 4-3. In this configuration a 5 mW laser beam ($\lambda = 660$ nm) is transmitted through the liquid phase within view cell, and light scattered by polymer particles or aggregates present in the solution strikes a photodiode detector (Newport, Model 818-SL) positioned 8 cm from the view cell at an angle of approximately 15 degrees from the laser beam. The photodiode detector is connected to a power meter (Newport, Model 835) which outputs a voltage signal proportional to the intensity of the scattered light to a personal computer; LabVIEW software is used to monitor and record the light intensity data. According to Rayleigh-Gans-Debye (RGD) theory, the intensity of scattered light is proportional to the particle volume and consequently the sixth power of the particle diameter for particles whose radius is less than one-fourth the wavelength of the scattered light [Kratohvil, 1987]. Thus, as solubility of poly-

mer molecules in the CXL decreases and polymer aggregates begin to form, significant light scattering will occur before particles are detectable by simple visual observation.

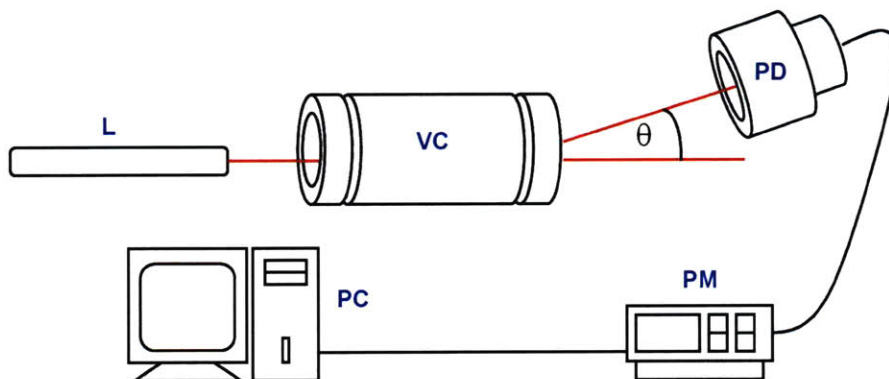


Figure 4-3: Schematic of the laser light scattering system for detection of polymer precipitation. System components: laser (L), view cell (VC), photodiode detector (PD), power meter (PM), data acquisition computer (PC).

4.2.2 Procedure

The BzMA/MAA polymers investigated in the current study were synthesized by Harry Spinelli at DuPont and delivered as concentrated ($\sim 50\text{wt}\%$) solutions in tetrahydrofuran (THF). To prepare polymer solutions in acetone, the THF was first evaporated from samples of each original solution in a vacuum oven. The solid THF-free polymers were then redissolved in acetone (Malinkrodt, mass fraction >0.995) to yield stock solutions for further dilution. The Joncryl[®] polymers were received as solids chips, and used as received to formulate solutions in acetone. Instrument-grade liquified CO_2 was purchased from Airgas.

For the preparation of all polymer solutions, the polymer weight fraction was determined by UV absorption using a Cary 50 spectrophotometer; UV absorption analysis was carried out in spectroscopy-grade THF (EMD, mass fraction >0.9999) after evaporation of acetone from each sample. A sample UV absorption spectrum showing the multip peaked absorption band at 259 nm due to the benzyl chromophore [Morcelletsauvage et al., 1982] in the BzMA moieties is shown in Figure 4-4, and the calibration curve for 85/15 BzMA/MAA at a wavelength of 259 nm is given in Figure

4-5. For the solution compositions of interest to the current study, the polymer weight fraction determined by UV spectroscopy was accurate to within 3% or better.

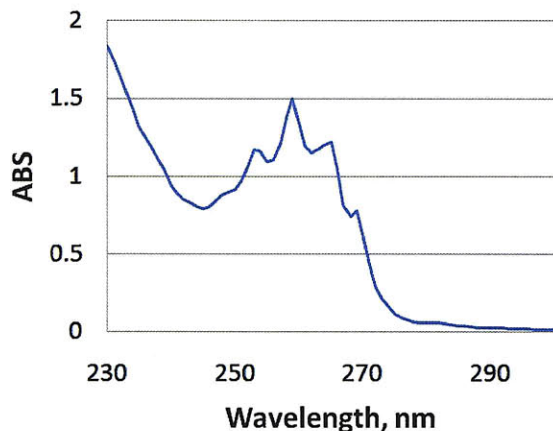


Figure 4-4: Representative UV absorption spectrum for 85/15 BzMA/MAA copolymer.

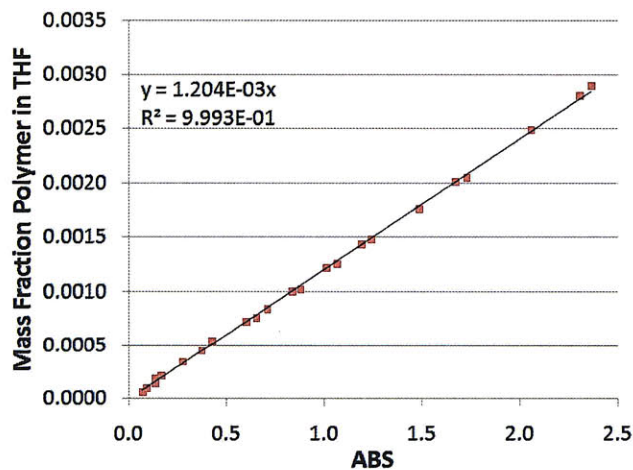


Figure 4-5: UV calibration curve for 85/15 BzMA/MAA in tetrahydrofuran.

In a typical phase behavior experiment, a polymer solution of known composition was first loaded into the view cell and the total mass of the solution determined gravimetrically to within 0.02 g ($\pm 0.1\%$ of a typical sample). The view cell was then placed inside the air bath and connected to the CO₂ delivery system. The headspace above the liquid phase was flushed with low-pressure CO₂ to remove air before selected trials, but conducting measurements without this step did not affect

the reproducibility of the results. The temperature within the air bath was raised to 25°C initially, and the addition of CO₂ began after the temperature had stabilized. During this stage of the trial, the syringe pump was operated in pressure gradient mode such that the pressure within the view cell increased at a constant rate (normally 1-2psi/min). As CO₂ was added to the system, the intensity of scattered light was monitored in order to detect the point at which the reading increased above the baseline value, signaling the onset of precipitation. The lights in the room were turned off to increase the sensitivity of the scattered light measurements.

Upon further addition of CO₂, the solution quickly became turbid due to the presence of a large number of polymer particles. The syringe pump continued to run for another 10-20 minutes after precipitation occurred, at which point the settings were changed such that the pressure decreased at a rate equivalent to the previous rate of increase (1-2 psi/min). Again the intensity of light was monitored in order to detect the point at which the reading returned to its previous baseline value. After the signal from the optical power meter had stabilized, the same procedure was repeated at 35°C and 45°C.

4.2.3 Data analysis

Temperature, pressure, and scattered light intensity data from a typical phase behavior experimental trial are plotted as a function of time in Figure 4-6, and the pressure and light intensity data for a single precipitation event are plotted in Figure 4-7; the shaded areas in Figure 4-6 represent regions of solid-liquid-vapor equilibrium, in which the solutions are very turbid and little light reaches the photodiode detector.

The trend of scattered light intensity with changes in pressure near the S-L-V region is seen more easily in Figure 4-7 (the noise in the data upon depressurization is caused by the formation of bubbles as CO₂ leaves the liquid phase). The MATLAB Wavelet Toolbox was used to determine the point at which the signal from the optical power meter rose above the baseline value, but the results of this analysis agreed very well with those obtained by simple visual inspection of the data. The pressure at which polymer precipitation occurred was determined to within an uncertainty of

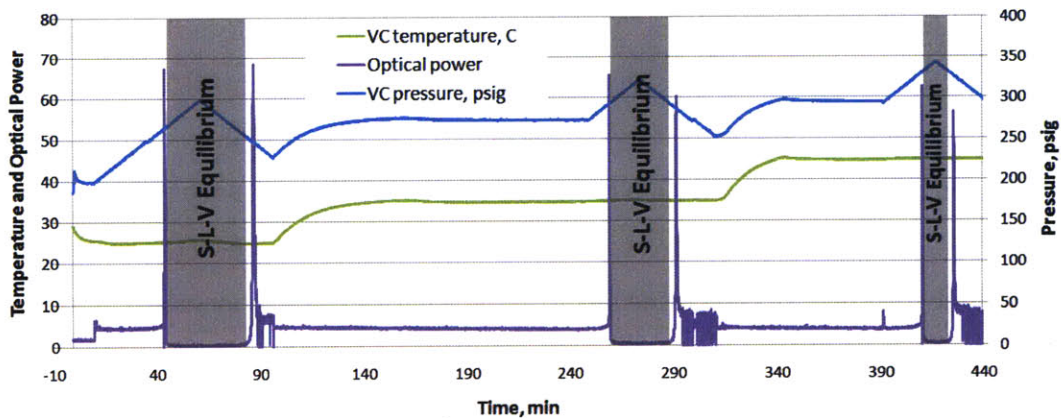


Figure 4-6: Representative temperature, pressure, and optical power data from a phase behavior measurement trial.

10 psi, which is only slightly greater than the uncertainty in the values of pressure measured by pressure transducers in the system (± 7.5 psi). The rapid transition from clear to turbid solution aided in the accurate determination of the precipitation pressure, and can be attributed to the low polydispersity of the polymers under investigation (Table 3.1); Kirby and McHugh [1999] have reported that accurate cloud point measurements may be obtained as long as polydispersity is below ~ 3.0 .

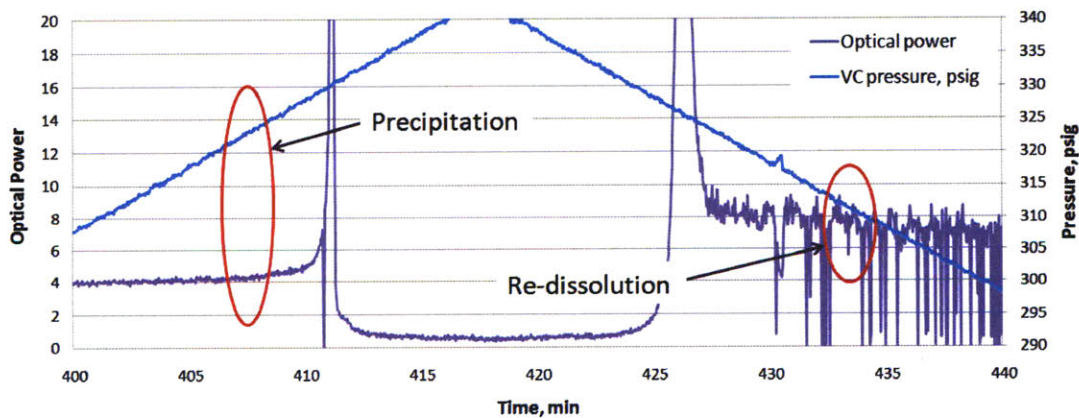


Figure 4-7: Representative pressure and optical power data from a single precipitation event in the course of a phase behavior measurement trial.

As an illustration of the improvement in accuracy afforded by the light-scattering detection system, precipitation data collected previously from systems containing

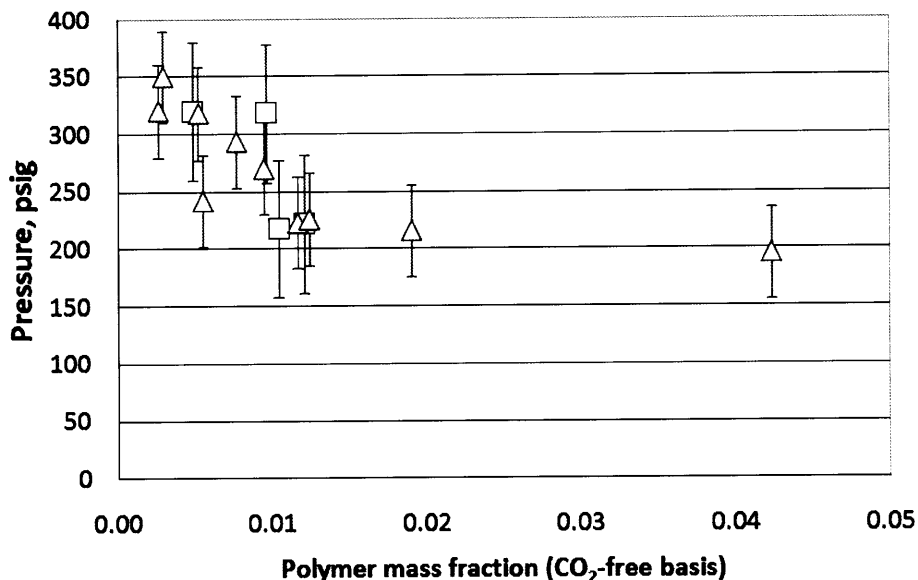


Figure 4-8: Solid-liquid-vapor equilibrium curves for systems containing CO₂, acetone, and Joncryl[®] polymers at 35°C. Δ, Joncryl[®] 586; □, Joncryl[®] 611.

Joncryl[®] 611 and Joncryl[®] 586 are plotted in Figure 4-8; the pressure at which polymer precipitated from the CO₂-expanded liquid phase based on visual observation of the solution is plotted as a function of the initial polymer weight fraction in CO₂-free solution. Because the solutions are dilute in polymer, they do not immediately become turbid as polymer molecules begin to aggregate and precipitate. Thus, the transition is not easily observed, and uncertainties exceeding 10% of the system pressure are common. The error bars in Figure 4-8 represent the uncertainty in this determination of the precipitation pressure.

4.2.4 Correlation of polymer-CO₂-acetone solid-liquid-vapor equilibrium data with PC-SAFT EOS

A thermodynamic model of the GAS process for precipitation of solute particles from GXLs has been developed and implemented, following the general approach of Kikic et al. [1997]; the model assumes isothermal operation and well-mixed vapor and liquid phases, such that the system is considered to be at equilibrium at all times and an

energy balance is not required. Lin et al [2003] have shown that this is a reasonable assumption under the agitation conditions and CO₂ addition rate of a typical GAS process. The vapor pressure of the solute (polymer) is also neglected, and the solid phase is assumed to be pure.

Given the above assumptions, phase equilibrium in a system composed of polymer (component 1), acetone (component 2), and CO₂ (component 3) is governed by the following isofugacity constraints:

$$f_1^s = x_1 \bar{\phi}_1^l P \quad (4.5)$$

$$x_2 \bar{\phi}_2^l P = y_2 \bar{\phi}_2^v P \quad (4.6)$$

$$x_3 \bar{\phi}_3^l P = y_3 \bar{\phi}_3^v P \quad (4.7)$$

where $\bar{\phi}_i^j$ is the fugacity coefficient of component i in phase j , P is the pressure, and x and y are the liquid and vapor mole fractions, respectively. In the case of a pure crystalline material, the solid fugacity f_1^s can be related to the fugacity of a hypothetical pure subcooled liquid phase $f_1^{l,0}$ according to [Prausnitz et al., 1986]

$$f_1^s(T, P^0) = f_1^{l,0}(T, P^0) \exp \left[\frac{\Delta h_1^f}{RT_1^f} \left(1 - \frac{T_1^f}{T} \right) \right] \quad (4.8)$$

where T is the system temperature, Δh^f is the heat of fusion, T^f is the melting temperature, and R is the gas constant. Equation 4.8 is strictly valid at the triple point of the solute; it may be applied at other temperatures if the difference between the liquid and solid phase heat capacities is negligible. For applications at elevated pressure, the addition of the Poynting correction is necessary:

$$\begin{aligned} f_1^s(T, P) &= f_1^s(T, P^0) \exp \int_{P^0}^P \frac{v_1^s}{RT} dP \\ &= f_1^{l,0}(T, P^0) \exp \left[\frac{\Delta h_1^f}{RT_1^f} \left(1 - \frac{T_1^f}{T} \right) + \frac{(P - P^0)v_1^s}{RT} \right] \end{aligned} \quad (4.9)$$

assuming the molar volume of the solid v_1^s is constant with pressure. The treatment of

systems containing solid polymers introduces an additional parameter, the degree of crystallinity c . For 100% crystalline polymers, $c = 1$, while for amorphous polymers $c = 0$. Harismiadis and Tassios [1996] have noted that the following relationship is valid:

$$\ln \frac{f_1^s}{f_1^{l,0}} = cu \left(\ln \frac{f_1^s}{f_1^{l,0}} \right)_{c=1} \quad (4.10)$$

where u is the degree of polymerization, and the subscript $c = 1$ indicates that the quantity in parentheses is evaluated at 100% crystallinity.

PC-SAFT parameters

The PC-SAFT EOS is used to calculate the fugacity coefficients of all species in the liquid and vapor phases. The use of this EOS requires three pure-component parameters for each species, as well as a binary interaction parameter k_{ij} for each component pair. The copolymer parameters are calculated from the homopolymer segment parameters as

$$\epsilon_P = \sum_A^{N_{seg}} X_A \epsilon_A \quad (4.11)$$

$$\sigma_P = \sum_A^{N_{seg}} X_A \sigma_A \quad (4.12)$$

$$m_P = M \sum_A^{N_{seg}} X_A r_A \quad (4.13)$$

where the subscripts P and A indicate the copolymer and homopolymer segment parameters, respectively, N_{seg} is the number of distinct segment types present in the copolymer, X_A is the segment mass fraction of segment type A in the copolymer, M is the number average molecular weight of the copolymer, and r_A is the ratio m_A/M determined from homopolymer data.

The pure-component parameters for CO₂, acetone, and methacrylic acid polymer segments have been published previously, and are listed in Table 4.1. The pure component parameters for poly(benzyl methacrylate) segments were calculated via the group contributions method proposed by Tihic et al. [2008]; the results are also

listed in Table 4.1. The final values of the copolymer pure component parameters obtained from Equations 4.11, 4.12, and 4.13 are listed in Table 4.2.

Table 4.1: Pure-component PC-SAFT parameters for CO₂, acetone, poly(MAA) and poly(BzMA).

Component	σ	ϵ/k	m or m/M	Reference
CO ₂	2.7852	169.211	2.0729	Gross and Sadowski [2001]
Acetone	3.2557	253.406	2.77409	Kouskoumvekaki et al. [2004]
poly(MAA)	3.70	249.5	0.024	Kleiner et al. [2006]
poly(BzMA)	3.78	304.5	0.02	Tihic et al. [2008]

Table 4.2: Final values of the copolymer pure component parameters used in PC-SAFT EOS correlations.

Polymer	M (g/mol)	σ	ϵ/k	m
85/15 BzMA/MAA	5451	3.77	296.3	112.3
80/20 BzMA/MAA	5895	3.76	293.5	122.6
75/25 BzMA/MAA	5686	3.76	290.8	119.4

The binary interaction parameter for CO₂-acetone was regressed from published data [Adrian and Maurer, 1997, Chiu et al., 2008, Bamberger and Maurer, 2000] for the binary system at temperatures relevant to the current study; the final value used in correlations was $k_{ij} = 0.01$. The remaining interaction parameters were varied to improve the fit of the correlations to experimental data, as described below in Section 4.3.2.

Algorithm for flash calculations

The isofugacity constraints described above were employed in conjunction with material balance equations in order to calculate the equilibrium pressure at which precipitation of polymer occurs for a given initial solution concentration. Iterative three-phase isothermal flash calculations were performed using a modified Rachford-Rice procedure outlined by Michelsen and Mollerup [2007]. For a system with F phases and C

species, this involves the formulation of the mass balance in terms of the overall mole fraction of each species i , z_i , and the mole fraction of each phase j , β_j :

$$\sum_{j=1}^F \beta_j y_i^j = z_i \quad i = 1, 2, \dots, C \quad (4.14)$$

The method consists of three nested iterations, starting with guesses for the fugacity coefficients, overall CO₂ mole fraction, and system pressure. The values of the system temperature, volume, and polymer-to-acetone mole ratio are chosen to match those of the experimental system and remain constant throughout the calculations. In the first (innermost) iteration, Newton's method is used to find the phase fractions β_j which minimize the following objective function (the modified Rachford-Rice equation):

$$Q(\beta) = \beta_s - z_1 \ln \sum_{k=1}^F \frac{\beta_k}{\bar{\phi}_1^k} + \sum_{j=1(\neq s)}^F \beta_j - \sum_{i=2}^C z_i \ln \sum_{k=1}^F \frac{\beta_k}{\bar{\phi}_i^k} \quad (4.15)$$

subject to the constraints $\beta_j \geq 0$. For each iteration of β the PC-SAFT EOS is used to calculate new values of $\bar{\phi}_i^j$. The procedure allows for "deletion" of the solid phase if β_s drops below zero during the iterations, such that the convergence may be reached with either two or three phases. The formation of the solid phase requires that $\beta_s = 0$; the pressure is varied in the next set of iterations until this condition is satisfied.

In the final (outermost) set of iterations, the total mole fraction of CO₂, z_3 is varied such that the system volume calculated using the PC-SAFT EOS based on the current guesses for pressure and phase mole fractions matches the actual value. This entire procedure is then repeated at each new set of values for the system temperature and polymer-to-acetone mole ratio to construct solid-liquid-vapor equilibrium curves.

4.3 Results and discussion

4.3.1 Experimental results

The GAS precipitation trials described in Section 4.2.2 were carried out at temperatures of 25°C, 35°C, and 45°C for each of the three BzMA/MAA copolymers (85/15, 80/20, and 75/25 BzMA/MAA mass ratios) in CO₂-expanded acetone. Each trial yielded three values of pressure at which precipitation occurred (one precipitation event at each temperature), corresponding to fixed masses of polymer and acetone within the view cell. A range of initial polymer mass fraction spanning more than two decades was explored: the mass fraction of the most dilute solution was 0.0007, and that of the most concentrated solution was 0.14. As the weight fraction of polymer in the acetone solution was increased beyond 20wt%, it was impossible to obtain solid-liquid-vapor equilibrium data due to the fact that the stir bar was unable to provide adequate mixing; similar limitations have been observed in the literature [Kirby and McHugh, 1999].

The solid-liquid-vapor curves for systems containing BzMA/MAA polymers in CO₂-expanded acetone at the three temperatures investigated are plotted in Figure 4-9; the data are plotted as the value of the pressure at which precipitation occurred versus the original mass fraction of polymer in acetone on a CO₂-free basis. In general, the precipitation pressure increases as the original polymer mass fraction decreases, although a minimum in precipitation pressure is observed at mass fractions near 0.03. The precipitation pressure is expected to decrease as the polymer mass fraction is increased beyond 0.15, eventually reaching atmospheric pressure at the solubility limit of polymer in pure acetone.

Inspection of Figure 4-9 reveals a clear trend of increasing precipitation pressure at higher temperatures. Although the general shape of the curves traced by the data is similar for each polymer and at each temperature, an increase in temperature of 10°C causes the pressure at which precipitation occurs to rise between 25 and 75 psi (approximately 10-20%). Similar behavior was observed in previous studies of GAS precipitation of smaller organic solutes from CO₂-expanded solvents

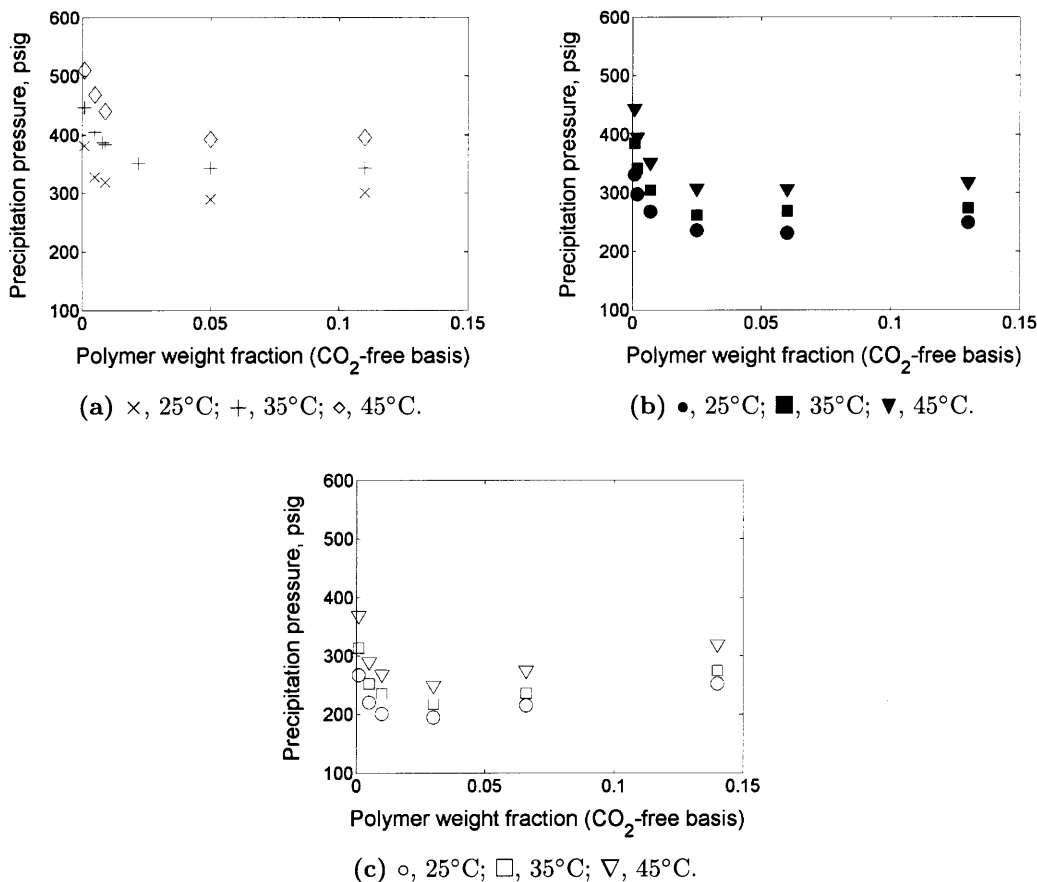
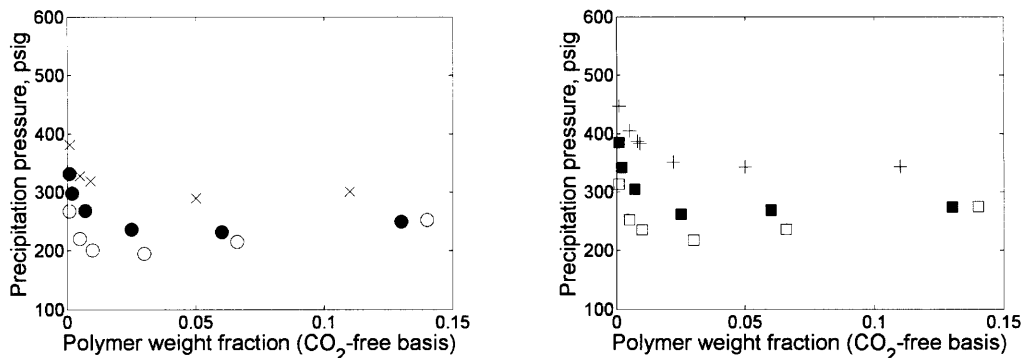


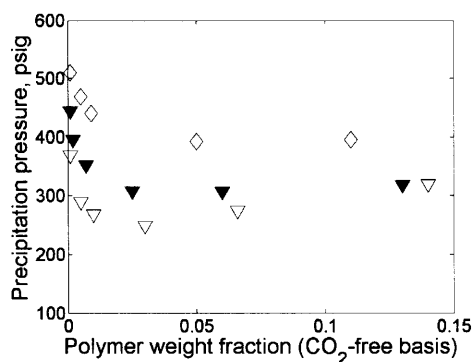
Figure 4-9: Phase behavior data for (a) 85/15 BzMA/MAA, (b) 80/20 BzMA/MAA, (c) 75/25 BzMA/MAA copolymers in CO₂-expanded acetone.

[Shariati and Peters, 2002, Liu et al., 2000a]. The trends with temperature can be explained by considering the effects of temperature on polymer-acetone, acetone-CO₂, and CO₂-polymer interactions. In general, polymer solubility in acetone increases with temperature in the absence of CO₂. This trend is reinforced by the fact that at constant pressure, the CO₂ mole fraction in the liquid phase decreases as temperature increases, resulting in improved solvation of the polymer. As discussed in Section 1.2.1, a slight increase in solubility of the polymer in CO₂ may be expected with increasing temperature, but this effect is small compared to those related to the polymer-solvent and solvent-CO₂ interactions.

Similar trends with respect to polymer composition can be seen by examining



(a) × , 85/15 BzMA/MAA, •, 80/20 BzMA/MAA, o, 75/25 BzMA/MAA. (b) +, 85/15 BzMA/MAA, ■, 80/20 BzMA/MAA, □, 75/25 BzMA/MAA.



(c) ◇, 85/15 BzMA/MAA, ▼, 80/20 BzMA/MAA, ▽, 75/25 BzMA/MAA.

Figure 4-10: Phase behavior data for BzMA/MAA copolymers in CO₂-expanded acetone at (a) 25°C, (b) 35°C, (c) 45°C.

Figure 4-10. At all temperatures, the precipitation pressure decreases with increasing mass fraction of poly(methyl methacrylate) moieties. This is not surprising, since acetone is known to be a poor solvent for poly(methacrylic acid) homopolymers due to the polymer's strong tendency to form hydrogen-bonds [Ho et al., 1991].

All phase behavior data collected for systems containing BzMA/MAA copolymers are shown on a semi-log plot in Figure 4-11, revealing the relative importance of changes in temperature and polymer composition. The effect of increasing the temperature 10°C is approximately equal to that of decreasing the MAA mass fraction by five percent.

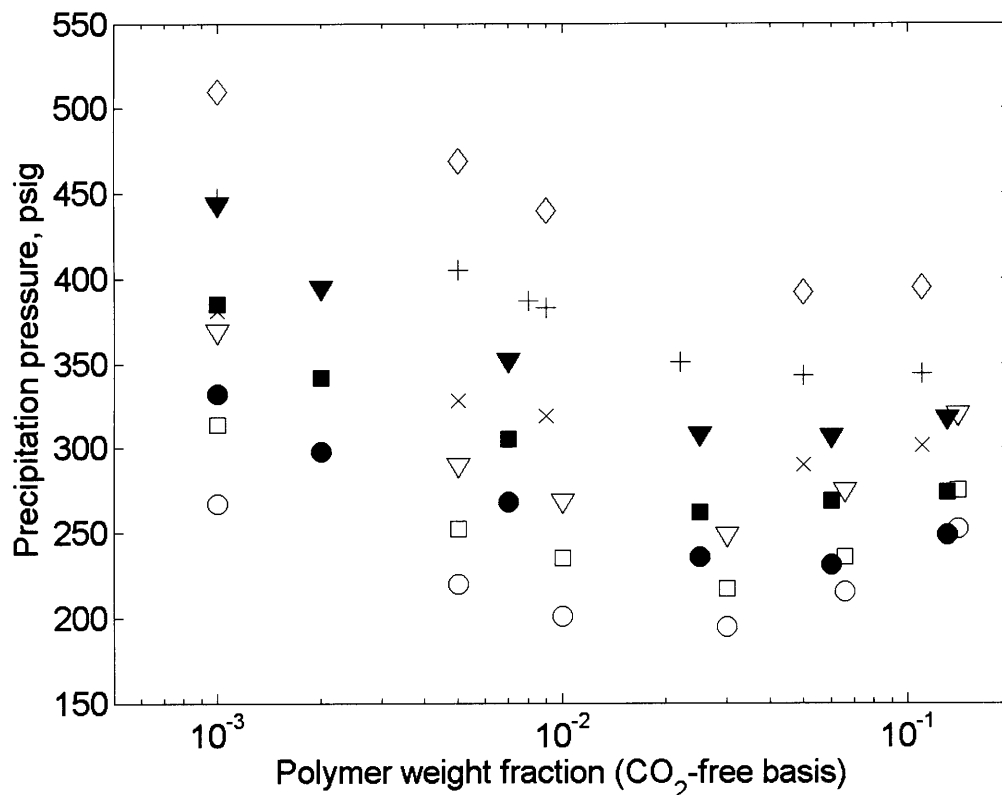


Figure 4-11: Summary of phase behavior data for CO₂-acetone-polymer systems. ○, 75/25 BzMA/MAA, 25°C; □, 75/25 BzMA/MAA, 35°C; ▽, 75/25 BzMA/MAA, 45°C; ●, 80/20 BzMA/MAA, 25°C; ■, 80/20 BzMA/MAA, 35°C; ▼, 80/20 BzMA/MAA, 45°C; ×, 85/15 BzMA/MAA, 25°C; +, 85/15 BzMA/MAA, 35°C; ◇, 85/15 BzMA/MAA, 45°C.

At this point it is prudent to revisit an important assumption that was made during the collection and analysis of phase behavior data. Specifically, it was assumed that a negligible amount of solvent was present in the vapor phase during all phase behavior trials, allowing the use of a synthetic experimental method that did not require the removal of high-pressure samples. The results of the modeling efforts described above using the PC-SAFT EOS indicate that for a typical experiment the vapor phase consists of approximately 1 mol% acetone, and the total vapor phase mole fraction (β_v) is approximately 0.1. Thus, approximately 0.01 mol% of all acetone within the view cell is expected to be in the vapor phase. The PC-SAFT is generally

accurate to within several percent in the prediction of phase distributions of small molecules, but even in the case of large errors in the estimation of y_2 and β_v the original assumption appears to be reasonable.

4.3.2 Modeling results

The PC-SAFT EOS was used to correlate the phase behavior data collected at each temperature for all polymers, employing the procedure outlined in Section 4.2.4. The CO₂-polymer and acetone-polymer binary interaction parameters were adjusted manually to obtain the best fit of the data; the final values of the temperature-dependent CO₂-polymer and acetone-polymer parameters are listed in Table 4.3. The contribution to the residual Helmholtz free energy in Equation 4.1 due to association interaction (\tilde{a}^{assoc}) was neglected in all calculations. With regard to the solid fugacity relationship introduced in Equations 4.9 and 4.10, an analysis of the BzMA/MAA polymers using dynamic scanning calorimetry (DSC) indicated that they can be considered amorphous. Thus, the crystallinity, c , in Equation 4.10 was set to zero and the solid polymer fugacity was taken to be equal to the subcooled liquid fugacity.

Table 4.3: Final values of the CO₂-polymer and acetone-polymer binary interaction parameters, k_{ij} , used in PC-SAFT EOS correlations.

Binary interaction	Temperature	BzMA/MAA	BzMA/MAA	BzMA/MAA
		85/15, k_{ij}	80/20, k_{ij}	75/25, k_{ij}
CO ₂ -copolymer	25°C	0.0278	0.0281	0.0292
Acetone-copolymer	25°C	0.0901	0.0929	0.0960
CO ₂ -copolymer	35°C	0.0295	0.0302	0.0315
Acetone-copolymer	35°C	0.0935	0.0967	0.0992
CO ₂ -copolymer	45°C	0.0312	0.0318	0.0335
Acetone-copolymer	45°C	0.0969	0.0995	0.1031

The modeling results are plotted along with the experimental data for each polymer in Figure 4-12. The PC-SAFT EOS predicts the correct trends in precipitation pressure with respect to temperature and polymer composition, and adjustments to the polymer-acetone and polymer-CO₂ interaction parameters enables a qualitative

representation of the pressure minimum exhibited by the experimental data. The pressure at which precipitation occurs was correlated to within an average relative error of 3.7% for all polymers.

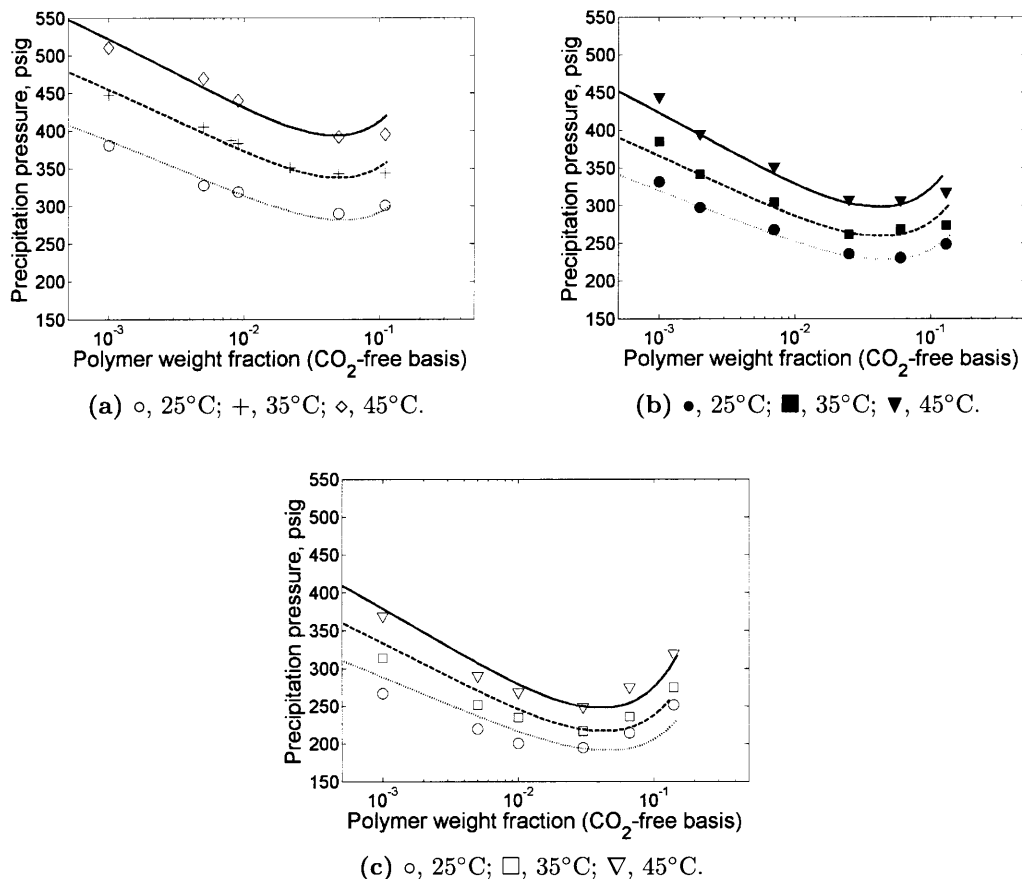


Figure 4-12: Phase behavior data and PC-SAFT correlations for (a) 85/15 BzMA/MAA, (b) 80/20 BzMA/MAA, (c) 75/25 BzMA/MAA copolymers in CO₂-expanded acetone. Lines represent correlations with the PC-SAFT EOS.

The precipitation pressure of 85/15 BzMA/MAA copolymer and the corresponding liquid-phase CO₂ mole fraction are plotted versus the CO₂-free liquid-phase polymer mass fraction in Figure 4-13; both the precipitation pressure and the CO₂ mole fraction values were calculated using the PC-SAFT EOS. Inspection of Figure 4-13 indicates that the minimum in precipitation pressure at each temperature coincides with a minimum in the liquid-phase CO₂ mole fraction. Similar behavior was observed for the 75/25 and 80/20 BzMA/MAA copolymers as well. At values of the CO₂-free

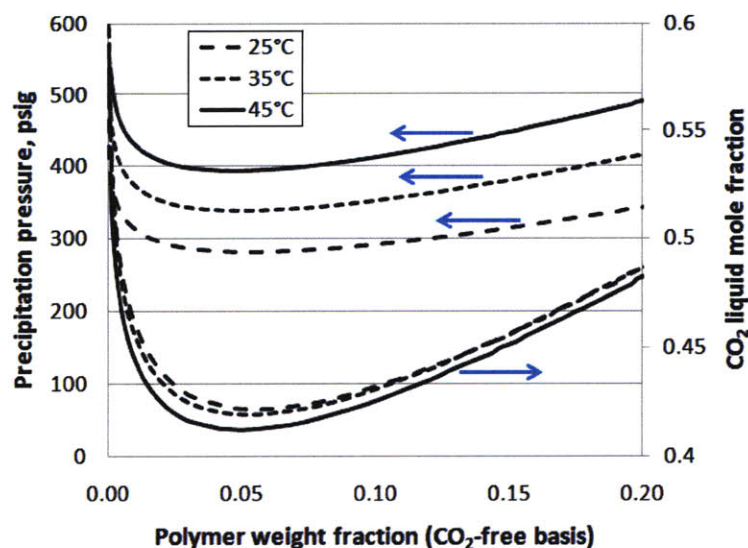


Figure 4-13: Precipitation pressure of 85/15 BzMA/MAA copolymer and liquid phase CO_2 mole fraction versus the liquid phase polymer mass fraction. Both values calculated using the PC-SAFT EOS.

liquid-phase polymer mass fraction greater than 0.20, both curves are expected to reach a local maximum and begin to decrease to zero at the atmospheric-pressure solubility limit of the polymer at each temperature. The presence of a local minimum and a (hypothesized) local maximum in the curves indicates that CO_2 may provide some degree of cosolvency over a certain composition range. The correlation of this experimentally observed behavior was only possible with careful adjustment of the values of the CO_2 -copolymer and acetone-copolymer interaction parameters.

The similarity of trends in precipitation pressure and CO_2 mole fraction in Figure 4-13 can be explained by the fact that over much of the range of polymer concentrations studied in the current investigation (dilute in polymer), the polymer precipitation pressure traces the CO_2 -acetone binary saturation curve very closely. This can be seen in the plot of the calculated precipitation pressure as a function of the calculated liquid-phase CO_2 mole fraction shown in Figure 4-14. The CO_2 -acetone saturation curve at 35°C is also plotted for reference. Because most of the systems were very dilute in polymer, and because the polymer molecular weight was large compared with acetone and CO_2 , the polymer *mole* fraction in the liquid phase was

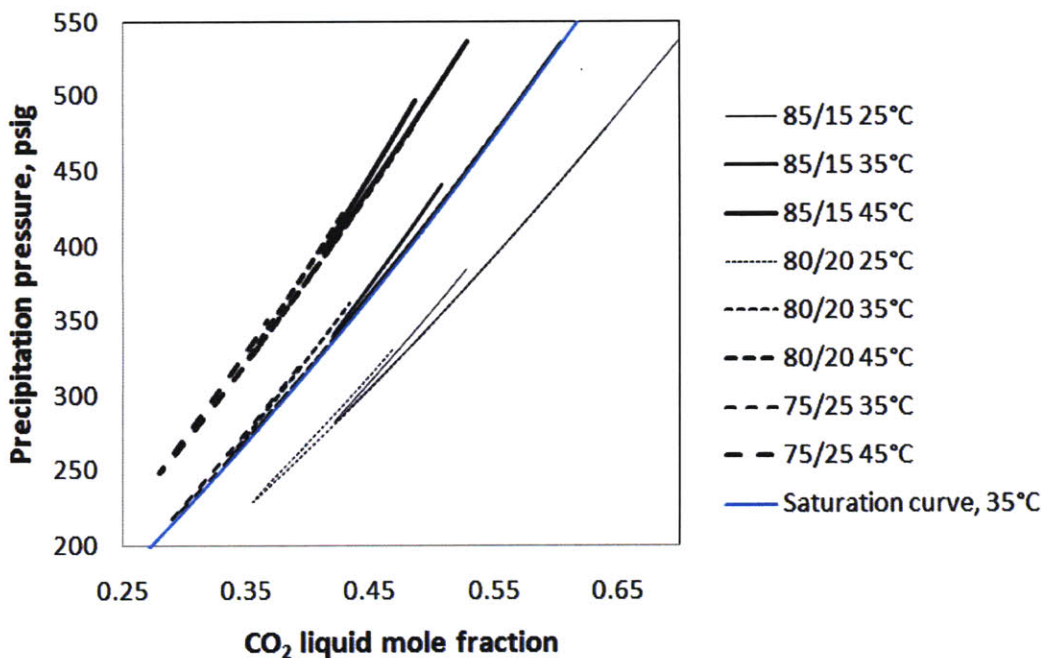


Figure 4-14: Precipitation pressure of BzMA/MAA copolymers versus the liquid phase CO_2 mole fraction calculated using the PC-SAFT EOS.

negligible for most experiments and the CO_2 and acetone mole fractions were relatively unaffected. Thus, as CO_2 was added during the course of an experimental trial, the pressure increased along the CO_2 -acetone saturation curve until precipitation occurred. Only at higher polymer mass fractions did the values of the CO_2 and acetone liquid-phase mole fractions deviate significantly from those of a binary system at the same pressure. It was in this composition range that the values of pressure at which precipitation occurred began to rise again; as mentioned in the previous paragraph, these curves are expected to reverse direction once again at even higher polymer content and eventually trend towards 0 psig at 0 CO_2 mole fraction, corresponding to the solubility limit at atmospheric pressure.

A satisfactory fit of the experimental data was possible with relatively small values of the two interaction parameters. The values of the polymer-acetone and polymer- CO_2 interaction parameters are plotted versus temperature in Figure 4-15. Inspection of this plot reveals a generally linear trend with temperature for each parameter at

a given polymer composition, with k_{ij} increasing as the temperature is raised. It is important to remember that the interaction parameters simply represent deviations from the assumed form of the mixing rules as given in Equation 4.4 (with k_{ij} set to zero); in the case of the PC-SAFT EOS mixing rules, the energy parameter ϵ for a binary pair is taken to be the geometric average of the ϵ values of the pure components, and the interaction parameter enables adjustment of this (arbitrary) choice. Accurate representation of the interactions between the copolymer and CO₂ require a larger value of k_{ij} than for those between the copolymer and acetone; the value of both interaction parameters also increases with the mass fraction of methacrylic acid moieties within the polymer.

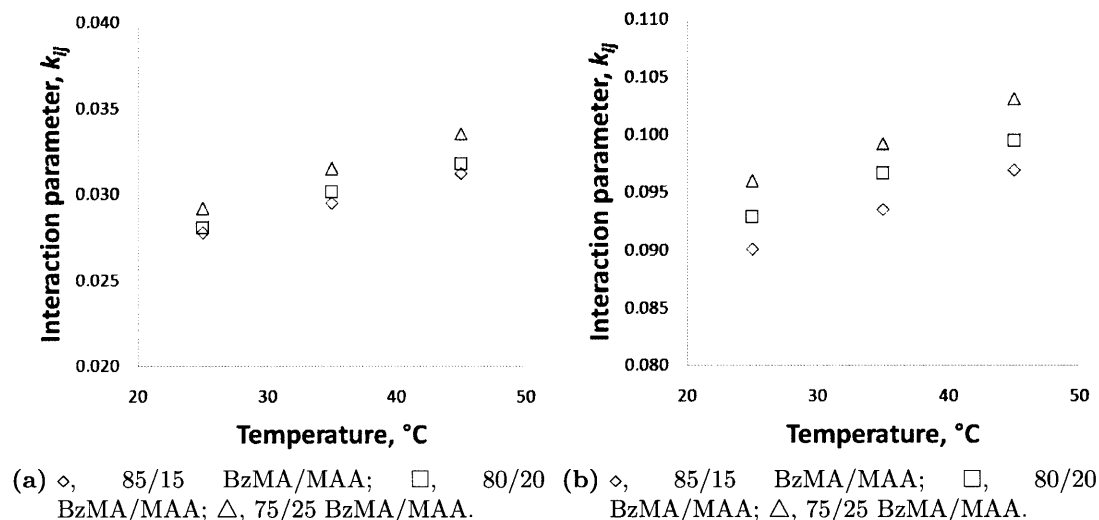


Figure 4-15: Trends in (a) solvent-polymer and (b) CO₂-polymer binary interaction parameters with temperature and polymer composition.

The binary interaction parameters are employed in modifications to the pure component energy parameter, ϵ/k , according to the relationships previously given in Equations 4.4 and 4.11. Thus the sensitivity of the fit of the data to the values of ϵ/k is low. However, it is instructive to examine the relative effects of the remaining pure component parameters on the quality of the correlation provided by the PC-SAFT EOS. The interaction distance parameter, σ , is the most sensitive of the pure component parameters, although its value is reasonable well established in the

literature ($\sigma \approx 3.7$ for most poly methacrylates). The segment size parameter, m , has the strongest influence on the quality of the fit of the data. In particular, the location of the minimum in precipitation pressure is strongly affected by the value of this parameter, with larger values of m causing the minimum to move to lower polymer mass fractions. Because the polymers under investigation are not monodisperse ($M_w/M_n \approx 1.13$), adjustments to the parameter m also account for uncertainties in the molecular weight of the precipitating polymer.

As discussed in Section 4.2.4, the pure component parameters for BzMA polymer segments were calculated from a group contributions method; the fit of experimental data is expected to improve if these parameters are instead regressed from experimental phase behavior data. Beyond adjustments to the pure component and binary interaction parameters, another possible route to improving the correlations is via the introduction of additional perturbation terms to the PC-SAFT EOS. The implementation of the association term \tilde{a}^{assoc} – neglected for the current study – would enable more accurate modeling of the associations among and between acetone molecules and MAA polymer segments, and the incorporation of a term proposed by Karakatsani and Economou [2006] would take into account the quadrupolar interactions exhibited by CO₂ molecules. Of course, the incorporation of these terms also introduces additional adjustable parameters. An adjustable binary interaction parameter may also be introduced to account for segment-segment interactions in the calculation of copolymer segment parameters [Gross et al., 2003].

4.4 Conclusions

The phase behavior of ternary CO₂-acetone-polymer systems has been probed experimentally and modeled with the PC-SAFT equation of state in order to guide the selection of appropriate operating conditions for a GAS-based particle encapsulation process. Precipitation of BzMA/MAA copolymers generally required a larger overall CO₂ mole fraction – and thus a higher system pressure – for more dilute polymer solutions; however, a minimum in the precipitation pressure was observed for all poly-

mer compositions and temperatures near a CO₂-free polymer mass fraction of 0.03. The precipitation pressure increased with increasing temperature and BzMA mass fraction (per polymer mass unit). The ternary systems were characterized by a rapid reduction in polymer solubility over a relatively narrow range of pressure (between 200 psig and 400 psig, depending on the polymer and system temperature)

The PC-SAFT EOS was successfully employed to correlate the phase behavior data by adjusting only two binary interaction parameters. Both qualitative and quantitative agreement between the experimental and calculated values of the precipitation pressure was achieved. The average relative error associated with the predictions of precipitation pressure for each polymer was 3.7% over the range of temperature and composition explored in the experimental study, demonstrating that accurate correlations of phase behavior data over a wide range of conditions relevant to GAS processing can be obtained with a relatively small amount of data.

The information obtained from the phase behavior study is directly applicable to the optimization of a GAS-based particle encapsulation process, and offers a deeper understanding of the fundamental interactions between the system components which govern the solvation power of the fluid phase with respect to the polymers of interest.

References

- T. Adrian and G. Maurer. Solubility of carbon dioxide in acetone and propionic acid at temperatures between 298 K and 333 K. *Journal of Chemical and Engineering Data*, 42(4):668–672, 1997.
- A. Bamberger and G. Maurer. High-pressure (vapor + liquid) equilibria in (carbon dioxide + acetone or 2-propanol) at temperatures from 293 K to 333 K. *Journal of Chemical Thermodynamics*, 32:685–7000, 2000.
- E. Bertakis, I. Lemonis, S. Katsoufis, E. Voutsas, R. Dohrn, K. Magoulas, and D. Tassios. Measurement and thermodynamic modeling of solid-liquid-gas equilibrium of some organic compounds in the presence of CO₂. *Journal of Supercritical Fluids*, 41(2):238–245, 2007.
- L. G. Cameretti, G. Sadowski, and J. M. Mollerup. Modeling of aqueous electrolyte solutions with perturbed-chain statistical associated fluid theory. *Industrial and Engineering Chemistry Research*, 44:3355, 2005.
- C. J. Chang and A. D. Randolph. Solvent expansion and solute solubility predictions in gas-expanded liquids. *AIChE Journal*, 36(6):939–942, 1990.
- W. G. Chapman, K. E. Gubbins, G. Jackson, and M. Radosz. SAFT - equation-of-state solution model for associating fluids. *Fluid Phase Equilibria*, 52:31–38, 1989.
- H. Y. Chiu, M. J. Lee, and H. M. Lin. Vapor-liquid phase boundaries of binary mixtures of carbon dioxide with ethanol and acetone. *Journal of Chemical and Engineering Data*, 53(10):2393–2402, 2008.
- M. Christov and R. Dohrn. High-pressure fluid phase equilibria - experimental methods and systems investigated (1994-1999). *Fluid Phase Equilibria*, 202(1):153–218, 2002.

- C. Crampon, G. Charbit, and E. Neau. High-pressure apparatus for phase equilibria studies: solubility of fatty acid esters in supercritical CO₂. *Journal of Supercritical Fluids*, 16(1):11–20, 1999.
- D. J. Dixon and K. P. Johnston. Molecular thermodynamics of solubilities in gas antisolvent crystallization. *AIChE Journal*, 37(10):1441–1449, 1991.
- R. Dohrn and G. Brunner. High-pressure fluid-phase equilibria - experimental methods and systems investigated (1988-1993). *Fluid Phase Equilibria*, 106(1-2):213–282, 1995.
- M. Fermeglia, A. Bertucco, and D. Patrizio. Thermodynamic properties of pure hydrofluorocarbons by a perturbed hard sphere chain equation of state. *Chemical Engineering Science*, 52(9):1517–1527, 1997.
- K. Frey, C. Augustine, R. P. Ciccolini, S. Paap, M. Modell, and J. Tester. Volume translation in equations of state as a means of accurate property estimation. *Fluid Phase Equilibria*, 260(2):316–325, 2007.
- D. Fuchs, J. Fischer, F. Tumakaka, and G. Sadowski. Solubility of amino acids: Influence of the pH value and the addition of alcoholic cosolvents on aqueous solubility. *Industrial and Engineering Chemistry Research*, 45:6578, 2006.
- P. M. Gallagher, M. P. Coffey, V. J. Krukonis, and N. Klasutis. Gas antisolvent recrystallization - new process to recrystallize compounds insoluble in supercritical fluids. *ACS Symposium Series*, 406:334–354, 1989.
- P. M. Gallagher, M. P. Coffey, and V. J. Krukonis. Gas anti-solvent recrystallization of rdx: formation of ultra-fine particles of a difficult-to-comminute explosive. *Journal of Supercritical Fluids*, 5:130, 1992.
- P. M. Gallagher, M. P. Coffey, and V. J. Krukonis. Application of supercritical fluids in recrystallization: nucleation and gas antisolvent techniques. *Drug Delivery*, 4: 287, 1994.

- M. Gornert and G. Sadowski. Phase-equilibrium measurement and modeling of the PMMA/MMA/carbon dioxide ternary system. *Journal of Supercritical Fluids*, 46: 218–225, 2008.
- J. Gross and G. Sadowski. Perturbed-chain SAFT: An equation of state based on a perturbation theory for chain molecules. *Industrial & Engineering Chemistry Research*, 40(4):1244–1260, 2001.
- J. Gross, O. Spuhl, F. Tumakaka, and G. Sadowski. Modeling copolymer systems using the perturbed-chain SAFT equation of state. *Industrial & Engineering Chemistry Research*, 42(6):1266–1274, 2003.
- V. I. Harismiadis and D. P. Tassios. Solid-liquid-liquid equilibria in polymer solutions. *Industrial & Engineering Chemistry Research*, 35(12):4667–4681, 1996.
- B. C. Ho, W. K. Chin, and Y. D. Lee. Solubility parameters of polymethacrylonitrile, poly(methacrylic acid) and methacrylonitrile/methacrylic acid copolymer. *Journal of Applied Polymer Science*, 42(1):99–106, 1991.
- S. K. Jha and G. Madras. Correlations for binary phase equilibria in high-pressure carbon dioxide. *Fluid Phase Equilibria*, 238:174–179, 2005.
- E. K. Karakatsani and I. G. Economou. Perturbed chain-statistical associating fluid theory extended to dipolar and quadrupolar molecular fluids. *Journal of Physical Chemistry B*, 110(18):9252–9261, 2006.
- I. Kikic, M. Lora, and A. Bertucco. A thermodynamic analysis of three-phase equilibria in binary and ternary systems for applications in rapid expansion of a supercritical solution (ress), particles from gas-saturated solutions (pgss), and supercritical antisolvent (sas). *Industrial & Engineering Chemistry Research*, 36(12):5507–5515, 1997.
- C. F. Kirby and M. A. McHugh. Phase behavior of polymers in supercritical fluid solvents. *Chemical Reviews*, 99(2):565–602, 1999.

- M. Kleiner, F. Tumakaka, G. Sadowski, H. Latz, and M. Buback. Phase equilibria in polydisperse and associating copolymer solutions: Poly (ethene-co-(meth)acrylic acid)-monomer mixtures. *Fluid Phase Equilibria*, 241(1-2):113–123, 2006.
- I. A. Kouskoumvekaki, N. von Solms, M. L. Michelsen, and G. M. Kontogeorgis. Application of the perturbed chain SAFT equation of state to complex polymer systems using simplified mixing rules. *Fluid Phase Equilibria*, 215(1):71–78, 2004.
- P. Kratochvil. *Classical light scattering from polymer solutions*. Elsevier, New York, 1987.
- C. Lin, G. Muhrer, and M. Mazzotti. Vapor-liquid mass transfer during solvent recrystallization: Modeling and experiments. *Industrial and Engineering Chemistry Research*, 42(1):2171–2182, 2003.
- Z. Liu, D. Li, G. Yang, and B. Han. Solubility of hydroxybenzoic acid isomers in ethyl acetate expanded with CO₂. *Journal of Supercritical Fluids*, 18:111–119, 2000a.
- Z. Liu, G. Yang, L. Ge, and B. Han. Solubility of o- and p-aminobenzoic acid in ethanol plus carbon dioxide at 308.15 K to 318.15 K and 15 bar to 85 bar. *Journal of Chemical and Engineering Data*, 45(6):1179–1181, 2000b.
- M. A. McHugh and V. J. Krukonis. *Supercritical Fluid Extraction Principles and Practice*. Butterworth, Stoneham, MA, 1994.
- M. L. Michelsen and J. M. Mollerup. *Thermodynamic Models: Fundamentals and Computational Aspects*. Tie-Line Publications, Denmark, 2007.
- J. Morcelletsauvage, M. Morcellet, and C. Loucheux. Polymethacrylic acid-derivatives: 2. Spectroscopic study of the compact conformation to coil transition. *Makromolekulare Chemie-Macromolecular Chemistry and Physics*, 183(4):821–829, 1982.
- E. Muller and K. E. Gubbins. Molecular-based equations of state for associating fluids: A review of SAFT and related approaches. *Industrial and Engineering Chemistry Research*, 40:2193–2211, 2001.

- J. M. Prausnitz, R. N. Lichtenthaler, and E. G. de Asevedo. *Molecular thermodynamics of fluid-phase equilibria*. Prentice-Hall, Englewood Cliffs, NJ, 1986.
- A. Shariati and C. J. Peters. Measurements and modeling of the phase behavior of ternary systems of interest for the gas process: I. The system carbon dioxide + 1-propanol + salicylic acid. *Journal of Supercritical Fluids*, 23:195–208, 2002.
- S. P. Tan, H. Adidharma, and M. Radosz. Recent advances and applications of statistical associating fluid theory. *Industrial & Engineering Chemistry Research*, 47(21):8063–8082, 2008.
- J. W. Tester and M. Modell. *Thermodynamics and its Applications*. Prentice Hall, Upper Saddle River, NJ, 3rd edition, 1996.
- A. Tihic, G. M. Kontogeorgis, N. von Solms, and M. L. Michelsen. A predictive group-contribution simplified PC-SAFT equation of state: Application to polymer systems. *Industrial and Engineering Chemistry Research*, 47:5092–5101, 2008.
- F. Tumakaka, J. Gross, and G. Sadowski. Modeling of polymer phase equilibria using Perturbed-Chain SAFT. *Fluid Phase Equilibria*, 194:541–551, 2002.
- F. Tumakaka, G. Sadowski, H. Latz, and M. Buback. Cloud-point pressure curves of ethylene-based terpolymers in fluid ethene and in ethene-comonomer-mixtures - experimental study and modeling via PC-SAFT. *Journal of Supercritical Fluids*, 41(3):461–471, 2007.

Chapter 5

Adsorption of polymer onto carbon black particles from CO₂-expanded acetone

As in the conventional (low-pressure) process to produce inks, particle encapsulation in CXLs is achieved via the adsorption of dissolved polymer molecules onto particle surfaces. The polymer-acetone-CO₂ phase behavior study described in Chapter 4 represents an important step toward a fundamental understanding of the GAS-based encapsulation of pigment nanoparticles with polymer, but knowledge of the fluid phase behavior alone will not allow complete characterization of the encapsulation process; interactions with the particle surface must be included in order to provide a comprehensive framework for analysis. In particular, it is desirable to obtain information regarding the degree and nature of polymer adsorption at equilibrium for a variety of conditions that are relevant to the particle coating process.

With this in mind, an experimental investigation of the adsorption behavior of systems containing carbon black and polymer in both pure solvent and CO₂-expanded solvent was carried out, and the resulting adsorption data was correlated using the Langmuir isotherm equation. The details of this investigation are presented in the following chapter.

5.1 Background

5.1.1 Polymer adsorption from solution

The adsorption of polymers from solution is a phenomenon that plays a crucial role in the dispersion of pigment particles for commercial inks and paints. As discussed in Chapter 1, adsorption of polymeric dispersants onto the surfaces of pigments is a means of imparting electrostatic and/or steric interparticle repulsive interactions in order to promote the stability of the final dispersions. Electrostatic forces are typically generated by adsorption of ions or polyelectrolytes (surfactants or polymers) onto particle surfaces [Doroszkowski, 1999]. Block or graft copolymers are preferred in the case of steric stabilization [Wnek et al., 2002], such that hydrophobic segments adsorb strongly to the particle surface while hydrophilic segments extend into the liquid phase of aqueous inks and provide entropic repulsive forces. Structured polymers with acid functional groups are able to employ both stabilization mechanisms [Spinelli, 1998].

Regardless of the specific mechanism by which interparticle repulsive interactions are generated, the stability of the resulting dispersion is highly dependent on the strength of polymer adhesion to the particle surface. The interactions between polymer “anchor” groups and the particle surface must be strong enough to prevent desorption or redistribution of the polymer molecules upon the approach of another particle, as either of these events will result in particle flocculation [Napper, 1983]. Thus, it is desirable to select polymers containing functional groups that exhibit favorable interactions with the particle surface.

The effect of solvent on adsorption

The extent and strength of adsorption is not only governed by interactions between the adsorbate (polymer) and adsorbent (particle); the nature of the solvent can also have a significant impact on the behavior of the system. Strong interactions between the solvent and the particle surface can result in competitive adsorption of solvent molecules, while strong solvent-polymer interactions enhance the solubility of the polymer in the liquid phase and thus reduce the driving force for adsorption [Lipatov

and Sergeeva, 1974]. For these reasons, it is advantageous to employ a “neutral” solvent that is able to adequately dissolve the dispersant polymer without interacting strongly with either the polymer molecules or the particle surfaces. This discussion also provides additional motivation for the use of an antisolvent such as CO₂ in order to tune the adsorption of polymers via changes in solvent strength. The use of antisolvents has been shown to increase adsorption for certain systems [Kolthoff et al., 1951, Jean and Yeh, 2001, Lin et al., 2002]; however, it is important to note that specific interactions between the antisolvent and the particle surface could result in a *decrease* in adsorption, and should be avoided.

The effect of temperature on adsorption

Adsorption of polymers is typically endothermic, indicating that an increase in temperature will result in increased adsorption. While this is generally true, there are some cases in which an increase in temperature causes a decrease in adsorption [Gilliland and Gutoff, 1960]. Such a situation could arise if an increase in temperature results in a significant increase in solvent strength with respect to the polymer. If the increase in polymer solubility is large enough to overcome the entropic driving force for adsorption that would be expected for an endothermic process, a net desorption would be observed. If adsorption isotherms (see below) are measured at more than one temperature, the value of the enthalpy of adsorption can be estimated using the Clausius-Clapeyron equation at very dilute conditions [Koral et al., 1958]:

$$\frac{\Delta H}{R} = \frac{H_S - H_L}{R} = \frac{d \ln c}{d(1/T)} \quad (5.1)$$

where H_S and H_L are the partial molar enthalpies of the adsorbed and dissolved polymer, respectively, and C is the concentration of polymer in the fluid phase at a given polymer loading.

Kinetics of adsorption

In most systems, the kinetics of polymer adsorption are dominated by the diffusion of the polymer molecules to the particle surface [Lipatov and Sergeeva, 1974]. In the case of adsorption onto smooth, flat surfaces, equilibrium may be reached in a matter of seconds. However, adsorption onto porous substrates may take much longer to reach equilibrium – on the order of hours or even days – as macromolecule diffusion in pores is a relatively slow process. Although carbon black primary particles are not in themselves porous, the tertiary structure of many carbon blacks may significantly hinder the penetration of the polymer molecules to the innermost particle surfaces.

Adsorption isotherms

The general considerations outlined above are useful when formulating a dispersion, but in practice experimental data is generally required to gain a deeper understanding of the interactions between system components. A common experimental technique for this purpose is the construction of adsorption isotherms, in which the extent of adsorption (typically given as the mass of polymer adsorbed per mass of adsorbent) is plotted as a function of equilibrium polymer concentration (or mass fraction) in the liquid phase. The collection of adsorption isotherm data at ambient pressure is straightforward: known amounts of adsorbent and polymer solution are placed in glass jars along with glass grinding beads, and the mixtures are agitated for 24 hours or more to ensure that equilibrium has been reached. Sedimentation of the particles is then induced either gravimetrically or by centrifugation, and aliquots of the particle-free supernatant are removed for analysis in order to determine the polymer content of the continuous phase [Doroszkowski and Lambourne, 1978].

The Langmuir isotherm equation

Experimental adsorption data is often correlated using one of several semi-empirical equations. Perhaps the most commonly used correlation is the Langmuir equation

[Langmuir, 1916]:

$$\frac{n}{n_m} = \frac{C/K}{1 + C/K} \quad (5.2)$$

where C is the concentration of polymer in the fluid phase at equilibrium, n is the mass of adsorbed polymer per mass of particles at equilibrium, and K and n_m are adjustable parameters. The Langmuir isotherm was originally developed to describe the adsorption of gases onto solid substrates, based on a proposed kinetic mechanism in which gas molecules A combine with adsorption sites S with forward and reverse rate constants of k and k^{-1} , respectively:



At equilibrium, we have

$$K = \frac{\theta}{(1 - \theta)P} \quad (5.4)$$

where $K = k/k^{-1}$ and θ is the surface coverage of the adsorbed molecules. This relationship may then be rearranged to obtain Equation 5.2, in which θ is replaced with n/n_m and P is replaced with C for use with liquid solutions. The derivation of the Langmuir equation is based on the following assumptions:

- All adsorption sites are equivalent.
- All adsorption occurs through the same mechanism.
- Adsorbed molecules do not interact with each other.
- A monolayer of adsorbed molecules is formed at the adsorption limit.

Although the first three assumptions listed above are rarely valid for systems involving polymer adsorption, the Langmuir equation often provides an adequate empirical fit of experimental data, and is therefore a useful correlating tool for the evaluation of particle-solvent-polymer interactions. It can also be used to obtain an estimate of the free energy of adsorption, ΔG_{ads} , from

$$K = \exp \frac{-\Delta G_{ads}}{RT} \quad (5.5)$$

The value of ΔG_{ads} obtained from polymer adsorption isotherms should be used with caution, since polymers adsorb at multiple sites on the particle surface depending on their conformation; however, the parameter K can be viewed as an approximate measure of adsorption strength. Thus, the parameters K and n_m – which represents the maximum extent of adsorption – offer valuable insight into the adsorption behavior of polymer-stabilized particle dispersions.

For a more detailed discussion of the various aspects of polymer adsorption, the reader is referred to the texts by Fler et al. [1993] and Lipatov and Sergeeva [1974].

5.1.2 Carbon black surface chemistry and adsorption characteristics

A substantial body of literature exists concerning the adsorption of molecules onto carbonaceous materials. The extensive use of carbon black as a pigment has motivated many studies related to the adsorption of polymers and surfactants from both organic [Pugh and Fowkes, 1984, Nsib et al., 2006] and aqueous solutions [Parfitt and Picton, 1968, Ridaoui et al., 2006]. A common theme in these adsorption investigations is a focus on the structure and surface properties of the carbon material. The adsorption capacity of carbon black can largely be attributed to the high surface area of these materials (between 200-500 m²/g); however, the extent to which this surface area can be utilized for adsorption is governed by the surface chemistry of the particles.

Oxygen and hydrogen are the major surface constituents of carbon black, and their abundance and state is determined by the production and post-treatment conditions [Donnet and Voet, 1993]. Regardless of the production method, all carbon blacks possess highly heterogeneous surfaces that contain some distribution of acidic and basic functional groups. The nature of these functional groups have been probed using titration, calorimetry, Fourier transform infrared spectroscopy (FTIR), X-ray photoelectron spectroscopy (XPS), and electron spin resonance (ESR) [Boehm, 1994, Pena et al., 2000]. Acidic surface oxides are thought to be of carboxylic, lactonic or phenolic character, while basic oxides are likely carbonyls or chromenes. These

functional groups are bonded to the particle surfaces at the edges of ordered graphene layers that comprise 90-99% of the carbon black primary particles. It has also been suggested that electron-rich regions within graphene layers near the particle surfaces can act as Lewis base sites [Lopez-Ramon et al., 1999].

An understanding of the distribution of surface functional groups is important in interpreting the adsorption behavior of carbon black. This is particularly true for systems containing organic solvents, in which the adsorption of polymers is often governed by acid-base interactions between polymer segments and surface groups [Napper, 1983]. Most carbon blacks used as pigments are dominated by acidic surface oxides, which interact favorably with basic styrene or benzyl groups present in the polymeric dispersants commonly employed in commercial inks.

5.1.3 Previous studies of high-pressure adsorption from CO₂

As interest in SCFs has grown over the past two decades, adsorption from scCO₂ and near-critical CO₂ has been investigated in the context of supercritical chromatography [Lubbert et al., 2007], regeneration of adsorbents [Tan and Liou, 1990], soil remediation [Macnaughton and Foster, 1995, Goto et al., 2005], and recovery of extraction products [Shojibara et al., 1995, Lucas et al., 2004]. Most of these studies involve adsorption of organic molecules onto activated carbon or chromatography media from either pure scCO₂ or cosolvent-modified scCO₂, and dynamic adsorption experiments based on packed chromatography columns are typically employed to gather adsorption data. Brunner and Johannsen [2006] have recently provided an excellent review of the state-of-the art in scCO₂ adsorption experiment and modeling.

One of the few investigations of polymer adsorption from scCO₂ was conducted by Cho et al. [2005], who deposited poly(styrene-*b*-dimethylsiloxane) block copolymers onto polystyrene substrates. Polymer adsorption was controlled by tuning the solvent strength of CO₂ with changes in temperature and pressure, and monolayer block copolymer films were obtained. Members of the same research group have also investigated the adsorption of metallic precursors from scCO₂ onto a variety of substrates for the production of supported metallic nanoparticles [Zhang and Erkey,

2005, Zhang et al., 2005a,b, Zhang and Erkey, 2006]. In a subsequent study, a model of the kinetics of adsorption from CO₂ onto a porous media was developed [Zhang et al., 2008], illustrating the benefits of the gas-like transport properties of scCO₂ in achieving rapid equilibrium.

5.2 Materials and methods

The goal of the adsorption study is to obtain and correlate data related to the effect of CO₂ addition on adsorption of polymer molecules from acetone onto the surface of carbon black particles. To this end, an experimental apparatus was designed and constructed that would provide high-pressure adsorption data via sampling of a particle-free supernatant. Adsorption data was collected at 35°C for 85/15 BzMA/MAA and 75/25 BzMA/MAA copolymers at 100psig, 200psig, and 300psig; adsorption isotherm data were also collected for systems consisting of carbon black, BzMA-MAA polymer, and acetone at atmospheric pressure.

5.2.1 Experimental Apparatus

A schematic representation of the apparatus for collection of high-pressure adsorption data is depicted in Figure 5-1; a photograph of the system is shown in Figure 5-2. Mixtures of carbon black, polymer, acetone, and CO₂ are contained within a Jerguson sight gauge (Model 11-T-20), allowing visual access at pressures up to 2000 psig at 38°C. Agitation within the sight gauge is provided by a 3/8" ultrasonic horn (Sonics & Materials, P/N A06963PRB) introduced to the bottom of the vessel through a custom-designed adapter [Ciccolini, 2008] fabricated by the MIT Machine Shop (Figure 5-3). The ultrasonic horn is powered by a Branson Sonifier[®] S-450A analog ultrasonic processor and converter. The liquid phase within the system is circulated through an external loop by a gear pump (Micropump, Model GAHV21.J8.A) to improve mixing and enable sampling of the liquid phase at high pressure. Liquid samples are isolated for removal using a 6-port HPLC switching valve (Valco, Model 6UW) and 2 ml sampling loop (Valco, P/N SL2KUW). A 40 μm T-type filter (Swagelok,

P/N SS-2TF-40) removes any large carbon black particles from the recirculated fluid before they are able to reach the gear pump and HPLC valve.

The temperature is monitored at four locations within the system with type T thermocouples (Omega Engineering, P/N GTMQSS-062U-6, tolerance $\pm 1\text{K}$): at the center of the sight gauge, within the ultrasonic horn adapter, and immediately following the HPLC valve and the gear pump in the recirculation loop. System temperature is maintained to within 0.2°C via the use of insulated heat tape (Omega Engineering, Model FGH051-040) powered by variable autotransformers (VWR, P/N 62546-364). Thermocouple output was recorded on a personal computer using LabVIEW data acquisition software, and temperature was regulated by manually adjusting the voltage output of the variable autotransformers. System pressure was measured using an analog pressure gauge (Swagelok, P/N PGI-100C-PG2000-LAOX) with an uncertainty of $\pm 10\text{psi}$. A forward-pressure line regulator (Scott Specialty Gases, Model 51-2713B) connected to a 300ml high-pressure CO_2 reservoir (Swagelok, P/N 304L-HDF4-300) was employed to maintain the pressure within the sight gauge at a constant value.

5.2.2 Procedure

Polymer solutions used in the adsorption study were formulated as described in Section 4.2.2. Carbon black particles were purchased from Evonik and used as received. The carbon black – sold under the trade name NIPex[®] 180 IQ – has an average primary particle size of 15 nm and a BET surface area of approximately $260\text{ m}^2/\text{g}$. NIPex[®] 180 is an acidic, highly structured carbon black specifically developed for use in pigmented inks.

Atmospheric-pressure adsorption isotherms

To construct adsorption isotherms at atmospheric pressure, a series of dispersions containing known amounts (determined gravimetrically to within $\pm 0.01\text{g}$) of carbon black, polymer, and solvent were formulated at various polymer:particle mass ratios. The dispersions were shaken vigorously by hand, then placed on a sample rotator

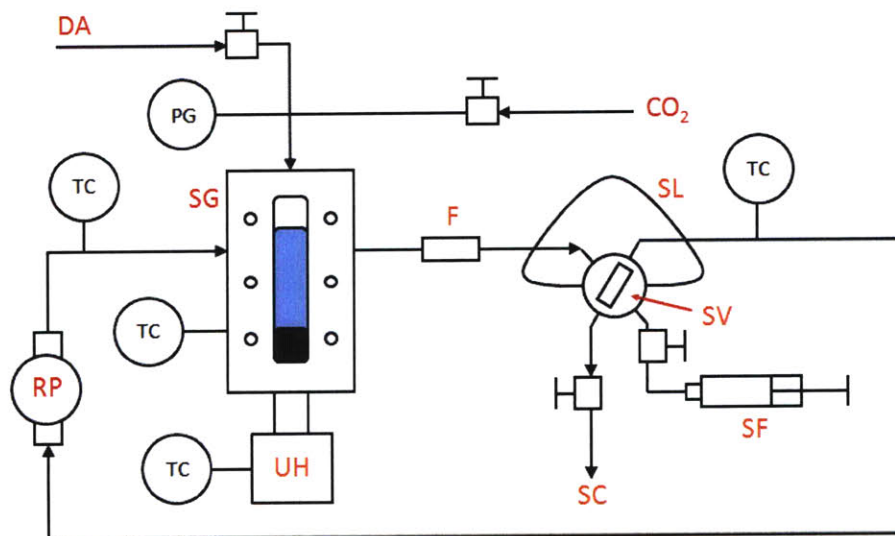


Figure 5-1: Schematic of the high-pressure adsorption isotherm system. System components: carbon dioxide supply (CO_2), dispersion addition (DA), sight gauge (SG), filter (F), switching valve (SV), sample loop (SL), solvent flush (SF), solvent collection (SC), ultrasonic horn (UH), recirculation pump (RP), thermocouple (TC), pressure gauge (PG).

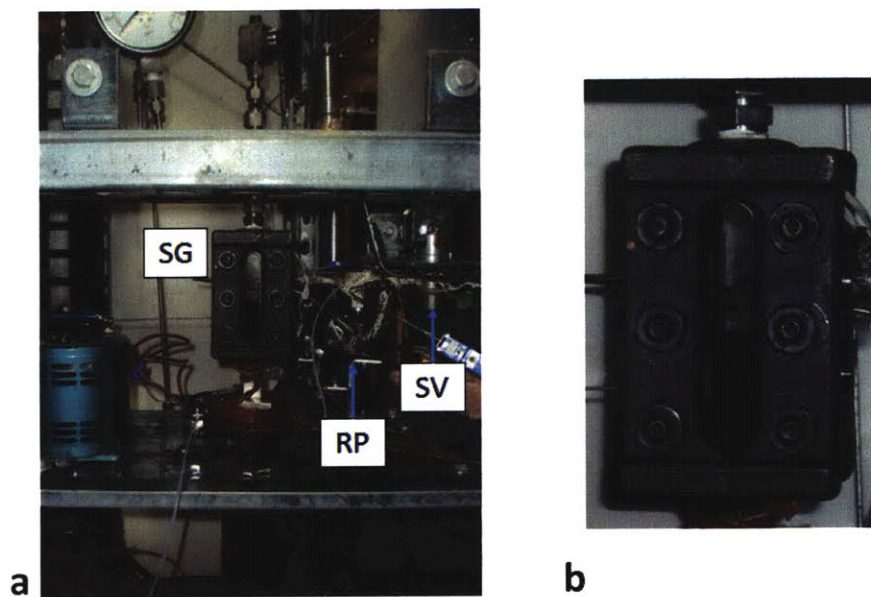


Figure 5-2: Photographs of the high-pressure adsorption isotherm system (a) and sight gauge (b). Major system components: sight gauge (SG), switching valve (SV), recirculation pump (RP)

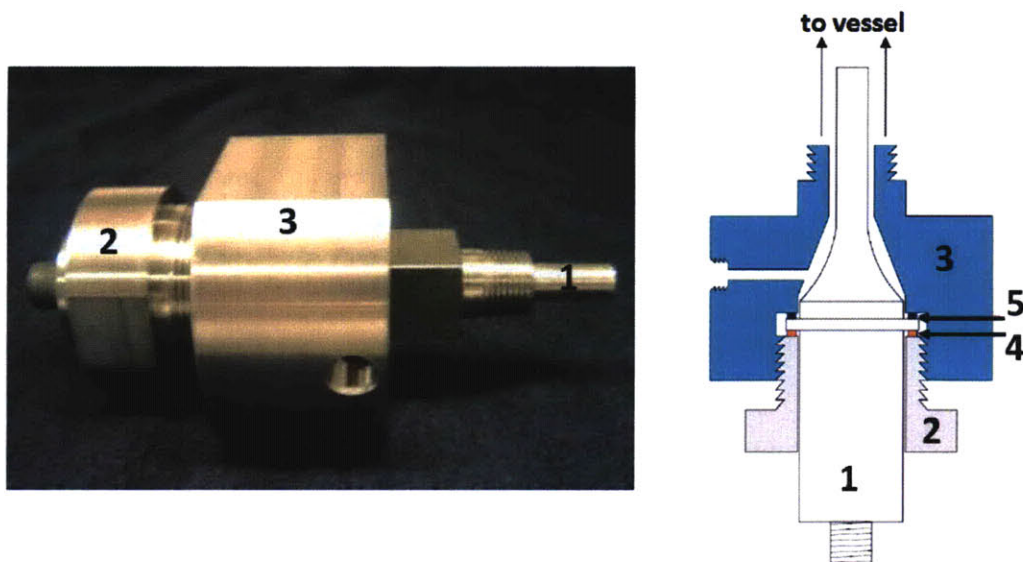


Figure 5-3: Schematic of the custom-fabricated adapter used to provide ultrasonic agitation at high-pressure (adapted from Ciccolini [2008]). System components: (1) ultrasonic horn, (2) gland, (3) adapter body, (4) copper gasket, (5) teflon-encapsulated o-ring (McMaster Carr, P/N 93445K218). Adapter gland (2) was tightened to 50 ft-lb torque to maintain a seal up to 1000 psig.

(Glas-Col, P/N 099A-CR4012) for at least 24 hours; glass grinding beads (Quakenbush Ceramedia 700) were added to the samples to facilitate deagglomeration of carbon black aggregates during agitation. After the agitation step the particles were allowed to settle gravimetrically, and an aliquot of the clear supernatant was removed from each sample and analyzed using UV spectroscopy to determine the concentration of polymer in the liquid phase (for aqueous systems, it was necessary to centrifuge and/or filter the dispersion to obtain a particle-free liquid sample). The amount of polymer adsorbed on the particle surfaces was then calculated by subtraction from the total polymer mass in the system.

High-pressure adsorption isotherms

High-pressure adsorption measurement trials were each conducted over a period of several days. Before each trial, the apparatus was flushed with CO₂ several times to remove residual air and acetone. A dispersion of pigment particles in a solution of

dissolved polymer and solvent was then added to the sight gauge through a funnel such that the total mass was known to within an uncertainty of $\pm 0.1\text{g}$ ($\sim 0.2\%$). The temperature was raised to 35°C , and carbon dioxide was subsequently added via the forward-pressure regulator until the system pressure reached 100 psig. The system was then agitated using power ultrasound to ensure that large agglomerates were broken up in order to maximize the amount of particle surface area available for adsorption and facilitate the diffusion of polymer molecules to the particle surfaces. The mixtures were typically sonicated for approximately five minutes at a duty cycle of 30% and output control setting of 3 on the ultrasonic processor after each pressure adjustment.

The system was maintained at 100 psig for at least 24 hours, with periodic ultrasonic agitation. After the particles had settled to the bottom of the sight gauge, the liquid phase was circulated through the external loop until a constant temperature was attained throughout the system. At this point, several samples were removed via the HPLC switching valve. The sample loop was flushed with acetone after each sample was removed, and the polymer content of the liquid phase was determined using UV spectroscopy. The composition of the liquid phase was then calculated (see Section 5.2.3) in order to determine the final point on the adsorption isotherm. This procedure was repeated at 200 psig and 300 psig for all trials, and also at 0 psig for selected trials. After samples had been collected at each pressure, the sight gauge was emptied and cleaned before a new trial was conducted at a different particle:polymer mass ratio.

5.2.3 Data Analysis

The experimental trials described above yielded measurements of the mass of polymer collected in the sample loop at each set of experimental conditions (T , P , and overall composition). In order to calculate the total amount of polymer in the fluid phase – and thus by subtraction the total amount of polymer adsorbed on the carbon black particles – an accurate estimate of the liquid molar volume, v^L , and acetone mole fraction, x_2 , is required. If these two quantities are known, the CO_2 -free mass

fraction of polymer in the liquid phase, w_1^L , can be calculated from:

$$w_1^L = \frac{m_1^{SL}}{m_1^{SL} + m_2^{SL}} = \frac{m_1^{SL}}{m_1^{SL} + (V^{SL}x_2M_2)/v^L} \quad (5.6)$$

where m_1^{SL} and m_2^{SL} are the mass of polymer and acetone in the sample loop, respectively, V^{SL} is the volume of the sample loop, and M_2 is the molecular weight of acetone. It was assumed that the polymer did not significantly affect the liquid phase composition or density, since the equilibrium polymer mass fraction rarely exceeded 2% (on a CO₂-free basis) during the adsorption trials. As was the case for the phase behavior trials described in Chapter 4, the amount of acetone in the vapor phase was also assumed to be negligible (see Section 4.3.2 for a discussion of the validity of this assumption).

The saturated liquid properties of CO₂-expanded acetone have been investigated by several researchers [Lazzaroni et al., 2005, Stievano and Elvassore, 2005, Day et al., 1999], and these studies provide a starting point for the estimation of v^L and x_2 in Equation 5.6. Most of the published data are not at 35°C; however, Besanehtak et al. [2002] have shown that volume expansion of the liquid phase in GXL systems is a function of CO₂ mole fraction within the saturated liquid phase, independent of temperature. To illustrate this phenomena, a plot of previously published volume expansion data versus the liquid phase CO₂ mole fraction for CO₂-acetone binary mixtures at several temperatures is shown in Figure 5-4.

Based upon the excellent agreement between data sets in Figure 5-4, the data at 35°C from Day et al. [1999] were assumed to be sufficiently accurate for use in comparisons to predictions with various equations of state. Figure 5-5 shows a plot of the corresponding density data as a function of system pressure, along with a data point at atmospheric pressure [Hafez and Hartland, 1976] and the density predictions obtained from the Peng-Robinson (PR) EOS, the Soave-Redlich-Kwong (SRK) EOS, the SRK EOS with a density-modified translation (DMT) [Frey et al., 2009], the PC-SAFT EOS, and the modified Rackett equation [Spencer and Danner, 1972] at 35°C (binary interaction parameters, k_{ij} , were set to zero for all correlations). The modified

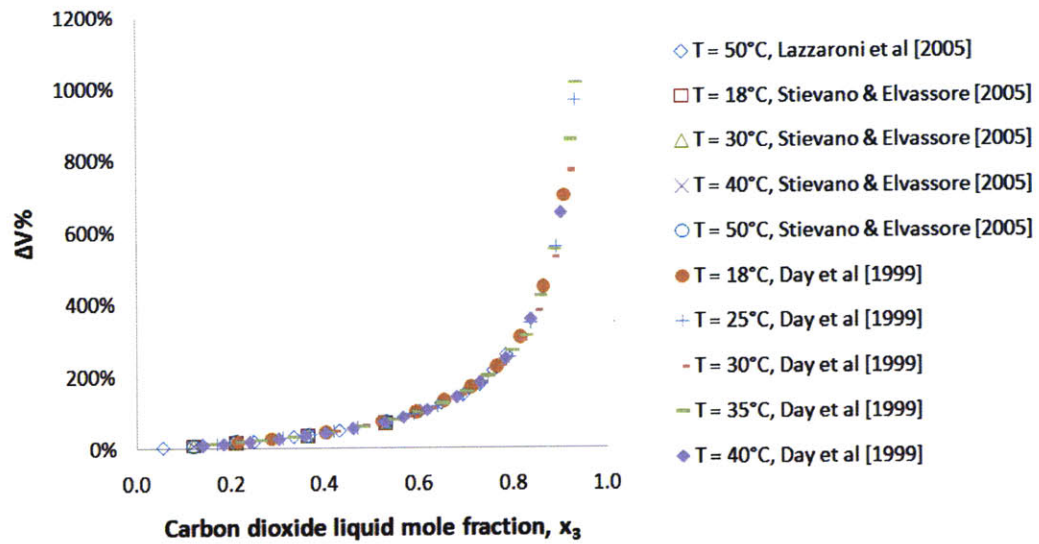


Figure 5-4: Volume expansion of CO₂-acetone liquid phase as a function of CO₂ liquid mole fraction.

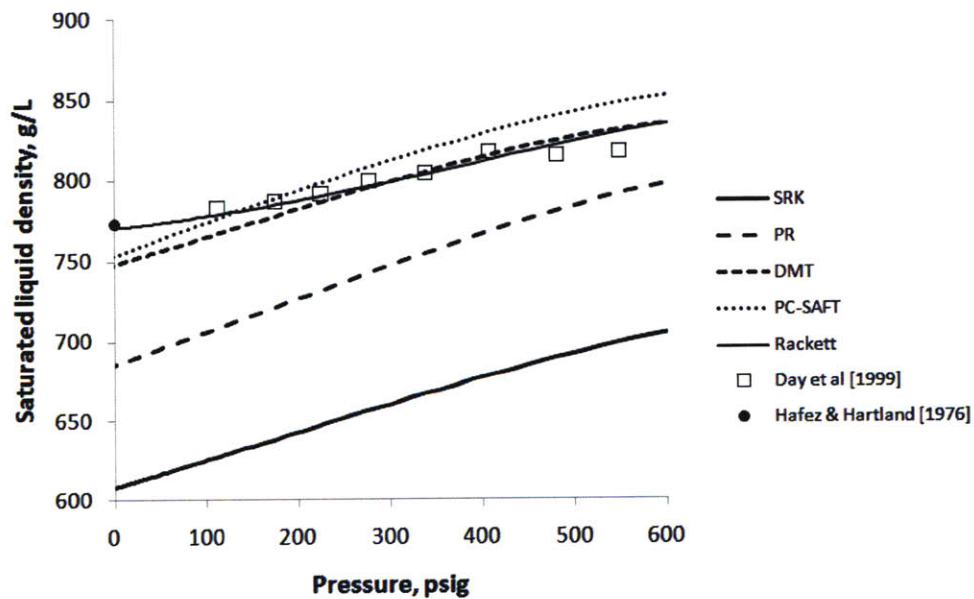


Figure 5-5: Comparison of saturated liquid density data and EOS correlations for the acetone-CO₂ binary system at 35°C. SRK: Soave-Redlich-Kwong EOS, PR: Peng-Robinson EOS, DMT: SRK EOS with density-modified volume translation. Interaction parameters set to zero for all correlations.

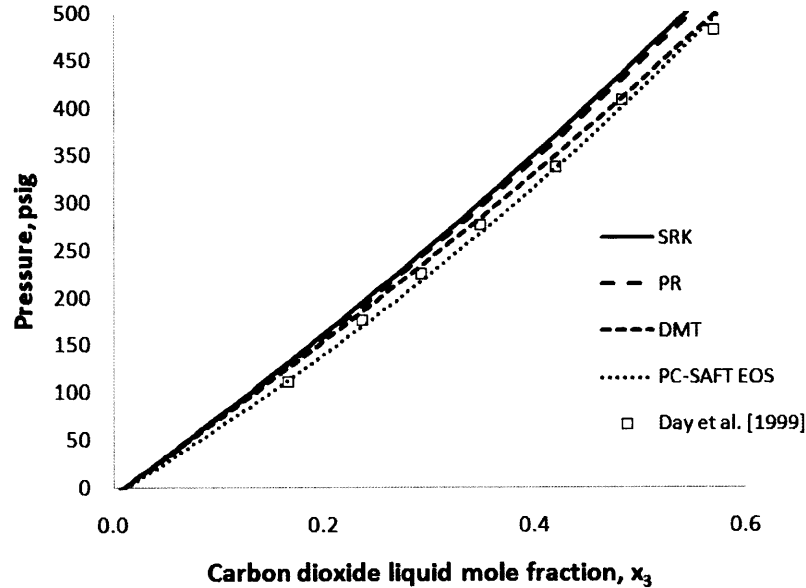


Figure 5-6: Comparison of saturated liquid mole fraction data and EOS correlations for the acetone-CO₂ binary system at 35°C. SRK: Soave-Redlich-Kwong EOS, PR: Peng-Robinson EOS, DMT: SRK EOS with density-modified volume translation. Interaction parameters set to zero for all correlations.

Rackett equation was developed specifically for the prediction of liquid molar volume data based on the critical constants and a single component-specific parameter, and provided the best fit of the data in the range of pressures that was relevant to the adsorption study. The average absolute deviation (AAD) of the predictions obtained using the Rackett equation was 0.54% when compared to the data shown in Figure 5-5.

A plot of experimental and predicted vapor-liquid phase boundaries for the CO₂-acetone binary system can be seen in Figure 5-6. In the case of phase composition, the PC-SAFT EOS afforded the closest approximation to experimental data, with AAD = 2.1% for liquid phase CO₂ mole fractions at pressures below 500 psig. Thus, the Rackett equation was used to estimate v^L , and the PC-SAFT EOS was used to predict x_2 in all further calculations.

The calculation of polymer mass fraction in the liquid phase also requires an accurate measurement of the sample loop volume in Equation 5.6. The sample loop

volume was determined by loading a dilute polymer solution of known concentration into the adsorption apparatus at room temperature, and then removing a liquid sample for analysis using the HPLC valve and sample loop. The mass of polymer in the sample loop determined using UV spectroscopy was then used to calculate the volume of the sample loop based on the previously measured solution concentration. Several trials were conducted at various dilutions to avoid any effects associated with adsorption of polymer onto surfaces within the apparatus. The resulting value of the sample loop volume was $V^{SL} = 2.06 \pm 0.2$ ml.

5.3 Results and discussion

5.3.1 Atmospheric-pressure adsorption isotherms

Adsorption isotherms were constructed for systems containing Joncryl[®] and BzMA/MAA polymers in a variety of solvents at atmospheric pressure and 22°C. Figure 5-7 displays two such isotherms characterizing the adsorption of Joncryl[®] 678 onto carbon black from both water and methanol. Based on the data in Figure 5-7, at pigment-to-dispersant mass ratios (P:D between 2 and 5) and pigment loadings (~20 wt%) representative of commercial inks, approximately 0.2 to 0.4 g of polymer per gram of pigment is expected to adsorb onto the particle surface. In addition, the liquid phase will contain between 0.4 wt% and 2.6 wt% polymer (representing 7% to 19% of the total polymer content); this excess polymer does not serve to stabilize the pigment dispersion, and reduces formulation flexibility by increasing ink viscosity.

The removal of “free” dispersant polymer in the liquid phase of aqueous inks is an important goal of the current work. However, it is clear from inspection of Figure 5-7 that the use of methanol alone will not provide such a reduction. Similar Joncryl[®] 678 adsorption behavior was observed in other organic solvents (acetone, n-butanol, 2-n-butoxyethanol) as well, with polymer adsorption reaching a plateau below 0.25 g per gram of carbon black in all cases. This behavior is not unexpected, since organic solvents such as the ones employed in this study are known to be good

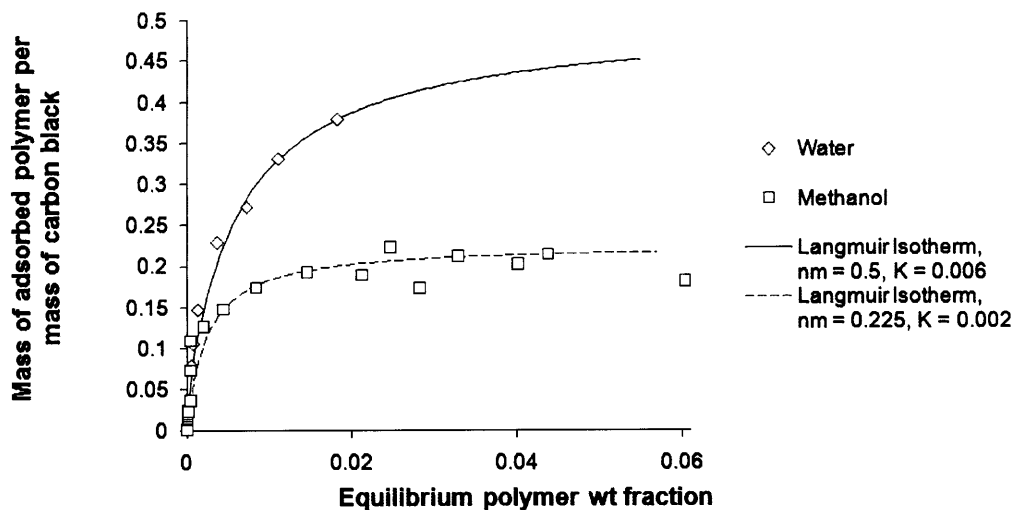


Figure 5-7: Adsorption of Joncryl[®] 678 polymer from water and methanol onto carbon black particles: Adsorption isotherms at 1 atm and 22°C.

solvents for acrylic polymers; adsorption from a poorer solvent – such as water – is generally greater than from a good solvent [Jean and Yeh, 2001], characterized by an increase in the parameter n_m and/or a decrease in the parameter K from Equation 5.2. The strong polymer-solvent interactions in a good solvent tend to dominate the polymer-particle interactions, and solvation is favored over adsorption.

Joncryl[®] 678 is a water-soluble (>15 wt%) polymer, and provides useful insight into the adsorption behavior of commercially available aqueous inks. However, hydrophilic polymers such as this are not appropriate for use with CO₂-based processing methods, as they would tend to desorb from the particle surfaces after addition to water in the final ink formulation. The model BzMA/MAA polymers are only sparingly soluble in water (<0.5 wt%) even when the methacrylic acid functional groups have been completely neutralized with base, serving as a model system that is more relevant to the process under investigation. Hydrophobic polymers such as these will remain at the particle surface when employed in water-based inks, and the GAS-based particle encapsulation process provides a route for depositing these polymers on the particle surface before they are added to the aqueous carrier.

Adsorption data for all three BzMA/MAA polymers in systems containing acetone

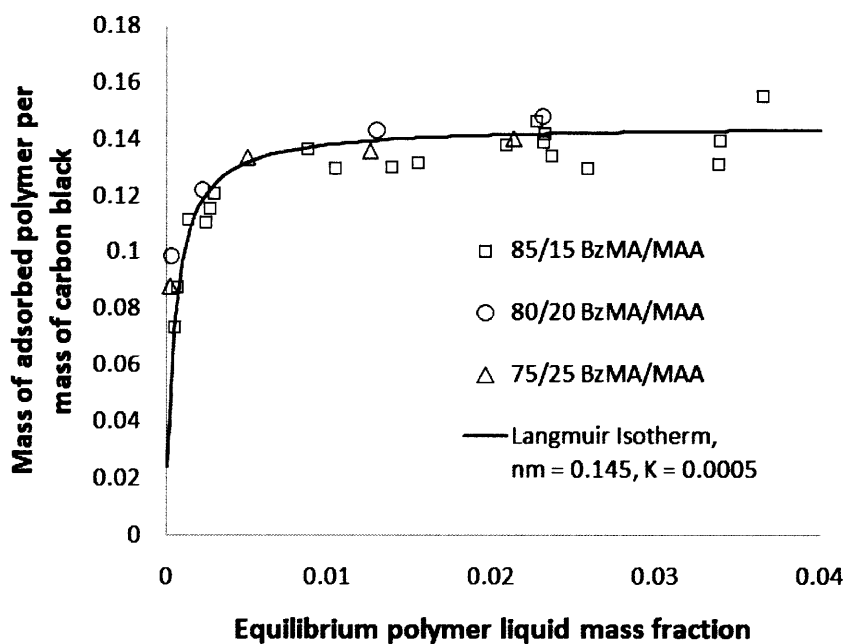


Figure 5-8: Adsorption of BzMA/MAA polymer from acetone onto carbon black particles: Adsorption isotherms at 1 atm and 22°C.

and carbon black are plotted in Figure 5-8. Inspection of Figure 5-8 indicates that the Langmuir Isotherm equation provides a reasonable fit of the atmospheric-pressure experimental data, suggesting that the polymers indeed adsorb from solution to form a monolayer at high liquid-phase concentrations. The values of equilibrium polymer mass fraction in the plot were directly determined to within an uncertainty of $\pm 4\%$, and the values of the polymer loading were calculated from an overall mass balance with an uncertainty of $\pm 7\%$ due to propagation of error. Again, adsorption from acetone is quite modest in comparison to the adsorption of Joncryl[®] 678 from water. Also, the adsorption isotherms for the three BzMA/MAA polymers are essentially indistinguishable given the uncertainty of the data. This behavior can be understood by examining the polymer-solvent and polymer-particle interactions in these systems: although the 85/15 BzMA/MAA polymer has the highest solubility in acetone (see Chapter 4), it contains more benzyl groups that provide specific acid-base interactions with the particle surface. Based on the data, the magnitudes of these two opposing

effects are similar.

The effects of agitation and equilibration time were also explored during the atmospheric-pressure adsorption trials. Mixtures were typically agitated for 24 hours on a lab rotator in a jar containing glass grinding media, as discussed in Section 5.2.2. However, several samples were not agitated at all after the initial shaking by hand (with no grinding media). Other samples were left – either agitated or unagitated – for 48 hours or more before supernatant samples were removed. In all cases, the resulting data were in agreement with the “standard” method described previously, and it was assumed that this procedure was sufficient to ensure that the samples had reached equilibrium before aliquots were removed.

5.3.2 High-pressure adsorption isotherms

Summaries of the high-pressure adsorption data collected for systems containing 85/15 BzMA/MAA polymer and 75/25 BzMA/MAA polymer are shown in Figures 5-9 and 5-10, respectively. The values of equilibrium polymer mass fraction in the liquid (on a CO₂-free basis) were calculated to within an uncertainty of $\pm 10\%$ based on measurements of the total polymer mass in the sample loop and estimates of the acetone mole fraction and overall liquid phase density (see Section 5.2.3); the values of the polymer loading were calculated from an overall mass balance with an uncertainty of $\pm 13\%$ due to propagation of error.

In the case of 85/15 BzMA/MAA polymer, the addition of CO₂ to the system appears to have relatively little effect on the adsorption of polymer for the pressure range investigated (0 to 300 psig). Conversely, a significant increase in 75/25 BzMA/MAA polymer adsorption is observed between 200 psig and 300 psig. This difference can be explained by the solubility characteristics of these polymers: as the pressure is raised to 300 psig, the equilibrium 75/25 BzMA/MAA polymer mass fraction in the liquid phase begins to approach – and in some cases exceed – the solubility limit in CO₂-expanded acetone. As the solubility limit is approached, the sudden decrease in solubility causes a rapid increase in polymer loading on the particle surfaces. On the other hand, 85/15 BzMA/MAA polymer is soluble in CO₂-expanded acetone up to

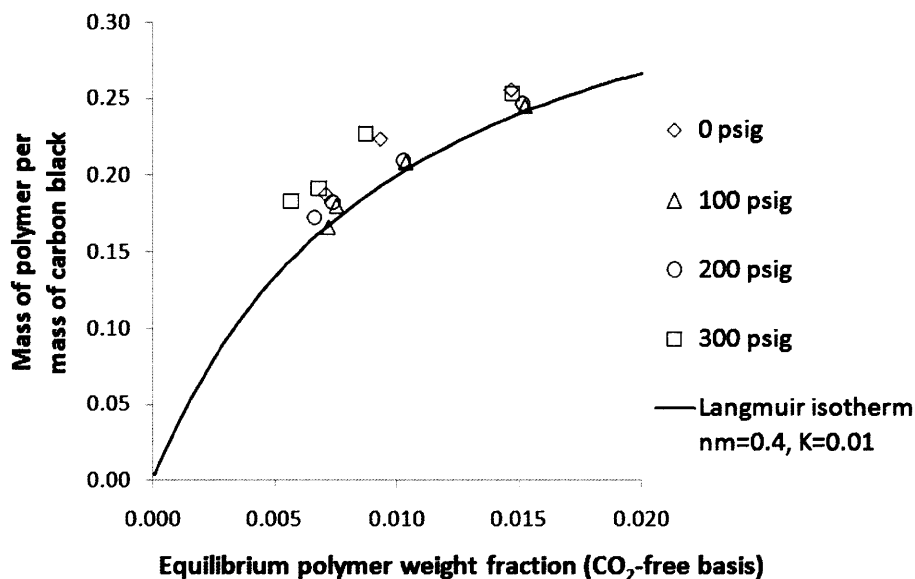


Figure 5-9: Adsorption of 85/15 BzMA/MAA polymer from CO₂-expanded acetone onto carbon black particles: Adsorption isotherms at elevated pressure and 35°C.

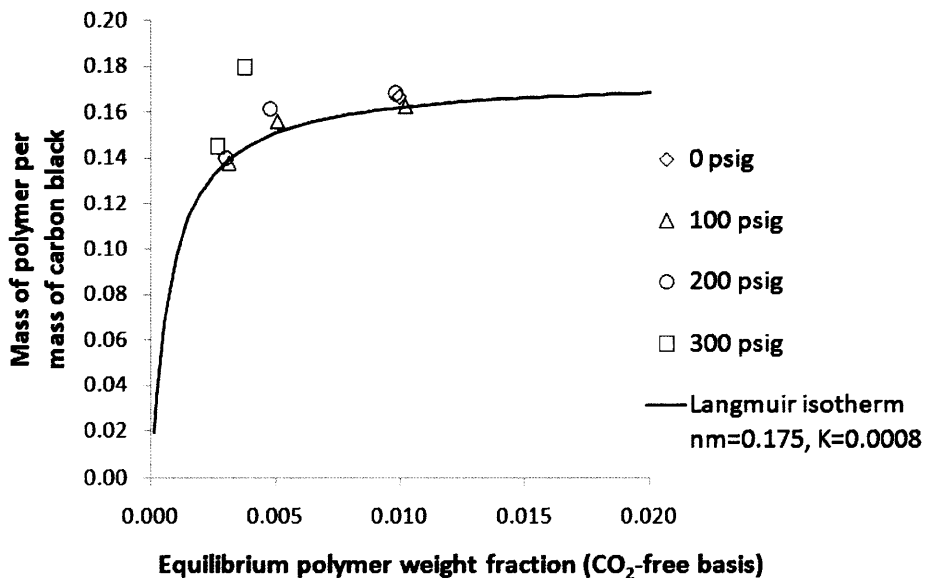


Figure 5-10: Adsorption of 75/25 BzMA/MAA polymer from CO₂-expanded acetone onto carbon black particles: Adsorption isotherms at elevated pressure and 35°C.

pressures exceeding 350 psig over the entire range of mass fractions relevant to the adsorption study.

The data at each value of pressure in Figures 5-9 and 5-10 exhibit Langmuir-type behavior, with the exception of the 75/25 BzMA/MAA data taken at 300 psig. The addition of CO₂ does appear to shift the isotherms (in effect changing the parameters n_m and K in Equation 5.2); however, the regression of meaningfully different parameters for isotherms at each pressure is impossible due to the scatter of the data. There are several potential causes for error in the values of the equilibrium polymer mass fraction. One potential source of error was the presence of a small amount of carbon black particles in a number of the liquid samples withdrawn from the sample loop. This may have led to a small increase in the polymer mass determined by UV spectroscopy, as any polymer adsorbed onto the particle surfaces would likely desorb when the sample was diluted with THF for UV analysis. A 40 μm filter was in place before the HPLC valve in the recirculation loop, but this filter was only intended to prevent damage to the gear pump and clogging of the HPLC valve due to larger particle agglomerates. Test trials were carried out using smaller filter pore sizes (as small as 0.5 μm), but this had a negative impact on the recirculation of liquid through the sample loop. As recirculation is slowed by a filter or by a blockage of particles, the temperature uniformity within the sample loop is affected, which is another potential source of error (since temperature is an important parameter in the correlations used to estimate liquid density and composition). The speed of the gear pump may be increased to a certain degree to compensate for blockage, but as the speed is increased above approximately half of the maximum value, the heat generated in the pump head is enough to cause cavitation and drastically reduce the liquid flow rate. Thus, the 40 μm filter was found to strike an adequate balance between filtration of carbon black and liquid recirculation rate at reasonable pump speeds.

Although the absolute values of the data shown in Figures 5-9 and 5-10 are subject to some uncertainty, a clear and reproducible trend was observed with changes in pressure among the data collected at each polymer:particle mass ratio. Specifically, the addition of CO₂ was found to initially cause desorption of the polymer from the

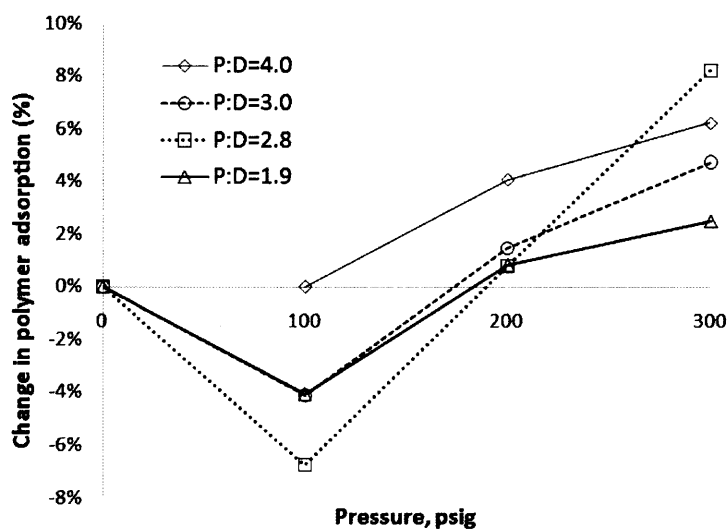


Figure 5-11: Trends in 85/15 BzMA/MAA polymer adsorption from CO₂-expanded acetone with changes in system pressure.

particle surface, with polymer loading at 100 psig consistently lower than that at atmospheric pressure. As the pressure was increased to 200 psig, some polymer re-adsorbed, but the total polymer loading was stiller lower than its initial value. Only after the pressure was raised to 300 psig did polymer adsorption exceed atmospheric-pressure levels. In the case of 75/25 BzMA/MAA an increase in polymer loading above 200 psig is expected due to the solubility considerations discussed above, but even 85/15 BzMA/MAA polymer exhibited a significant increase in adsorption between 200 psig and 300 psig. The trends in 85/15 BzMA/MAA polymer adsorption are plotted as a function of pressure in Figures 5-11 and 5-12; a plot of the percent change in the polymer loading with respect to the previous value is displayed in Figure 5-11, and Figure 5-12 shows the polymer loading at each pressure normalized to the initial value at atmospheric pressure.

The trend in polymer adsorption suggests that interaction between CO₂ molecules and surface groups on the carbon black particles are strong enough to replace some fraction of the adsorbed polymer molecules at low CO₂ concentrations. As the amount of CO₂ in the liquid phase increases, the concomitant reduction in polymer solubility is enough to overcome these competing interactions and cause re-adsorption. However,

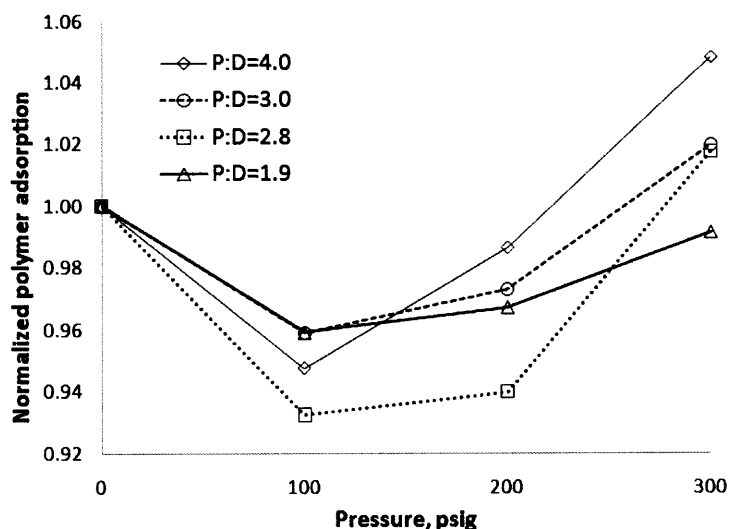


Figure 5-12: Normalized 85/15 BzMA/MAA polymer adsorption from CO₂-expanded acetone as a function of system pressure.

it should be noted that based on the data it is difficult to discern whether significant adsorption occurs before the solubility limit is reached, or if the encapsulation of particles in the model system is essentially a precipitation operation.

5.4 Conclusions

The adsorption of polymers from pure solvents and CO₂-expanded acetone onto carbon black particles was probed experimentally and analyzed using the Langmuir isotherm equation. Adsorption from common organic solvents was low for both Joncryl[®] polymers and BzMA/MAA copolymers, particularly when compared to the adsorption of Joncryl[®] 678 from water. Atmospheric-pressure isotherms offered insight into the relative strength of polymer-solvent, polymer-particle, and solvent-particle interactions present in the systems currently under investigation; these data indicate that polymer-particle interactions are not strong enough to promote adequate polymer adsorption, highlighting the potential benefits of a GAS-based process in tuning the liquid-phase solvation power.

Adsorption of 85/15 and 75/25 BzMA/MAA polymers onto carbon black from

CO₂-expanded acetone was measured at 35 °C and pressures between 0 psig and 300 psig. Pressurization with CO₂ to pressures up to 200 psig caused a decrease in the amount of polymer adsorbed on particle surfaces, but further increases in pressure resulted in higher polymer loadings. In the case of 75/25 BzMA/MAA polymer, the polymer loading increased significantly between 200 psig and 300 psig as the solubility limit was approached or exceeded. This behavior indicates that there is some degree of competitive adsorption of CO₂ onto the carbon black surfaces.

When analyzed in conjunction with the results of the phase behavior study outlined in Chapter 4, the adsorption data provide valuable insight into the interactions governing the adsorption (or precipitation) of polymer in particle coating applications. Specifically, the data indicate that most of the polymer adsorbs over a relatively narrow range of pressure, information that is directly applicable to the selection of appropriate operating conditions for a GAS-based process. Coating will only begin to occur at pressures above 200 psig for systems containing 75/25 BzMA/MAA polymer, and pressures above 300 psig are required when using 85/15 BzMA/MAA. Nearly all polymer will be present on the particle surfaces as the system pressure exceeds 400-500 psig, placing an upper limit on the pressure requirements for an industrial process.

The results of the adsorption study serve to underscore the importance of choosing a “neutral” solvent that exhibits no strong interactions with either the polymer molecules or the particle surfaces. Such interactions tend to inhibit adsorption of the polymer by either enhancing the solubility of the polymer in the liquid phase – in the case of polymer-solvent interactions – or by displacing polymer molecules at the particle surface via competitive adsorption – in the case of particle-solvent interactions.

References

- K. Bezanehtak, G. B. Combes, F. Dehghani, N. R. Foster, and D. L. Tomasko. Vapor-liquid equilibrium for binary systems of carbon dioxide + methanol, hydrogen + methanol, and hydrogen + carbon dioxide at high pressures. *Journal of Chemical and Engineering Data*, 47:161–168, 2002.
- H. P. Boehm. Some aspects of the surface-chemistry of carbon-blacks and other carbons. *Carbon*, 32(5):759–769, 1994.
- G. Brunner and M. Johannsen. New aspects on adsorption from supercritical fluid phases. *Journal of Supercritical Fluids*, 38:181200, 2006.
- D. M. Cho, Y. J. Kim, C. Erkey, and J. T. Koberstein. Deposition of block copolymer thin films onto polymeric substrates by adsorption from supercritical carbon dioxide. *Macromolecules*, 38(5):1829–1836, 2005.
- Rocco P. Ciccolini. *Carbon-Nitrogen Bond-Forming Reactions in Supercritical and Expanded-Liquid Carbon Dioxide Media*. PhD thesis, Massachusetts Institute of Technology, 2008.
- C. Y. Day, C. J. Chang, and C. Y. Chen. Correction to: Phase equilibrium of ethanol plus CO₂ and acetone plus CO₂ at elevated pressures. *Journal of Chemical and Engineering Data*, 44:365, 1999.
- J. B. Donnet and A. Voet. *Carbon Black: Physics, Chemistry, and Elastomer Reinforcement*. Marcel Dekker, Inc., New York, 2nd edition, 1993.
- A Doroszkowski. The physical chemistry of dispersion. In R Lambourne and T.A. Strivens, editors, *Paint and Surface Coatings - Theory and Practice*, pages 199–242. Woodhead Publishing, 2nd edition, 1999.
- A. Doroszkowski and R. Lambourne. Effect of molecular architecture of long-chain fatty-acids on the dispersion properties of titanium-dioxide in non-aqueous liquids. *Faraday Discussions*, (65):252–+, 1978.

- G. J. Fleen, M. A. Cohen, J. M. Stuart, and H. M. Scheutjens. *Polymers at Interfaces*. Chapman & Hall, London, 1st edition, 1993.
- K. Frey, , M. Modell, and J. Tester. Density-and-temperature-dependent volume translation for the srk eos: 1. pure fluids. *Fluid Phase Equilibria*, 279(1):56–63, 2009.
- E. R. Gilliland and E. B. Gutoff. The equilibrium adsorption of heterogeneous polymers. *JOURNAL OF PHYSICAL CHEMISTRY*, 64:407–410, 1960.
- M. Goto, M. Sasaki, S. Kawahara, T. Hirose, and S. Kawajiri. Adsorption behavior of dioxin model compounds on activated carbon in supercritical carbon dioxide. *Adsorption-Journal of the International Adsorption Society*, 11:157–161, 2005.
- M. Hafez and S. Hartland. Densities and viscosities of binary-systems toluene-acetone and 4-methyl-2-pentanone acetic acid at 20, 25, 35, and 45 degrees. *Journal of Chemical and Engineering Data*, 21(2):179–182, 1976.
- J. H. Jean and S. F. Yeh. Dispersion of glass powders in organic media. *Materials Chemistry and Physics*, 71(2):155–160, 2001.
- J. M. Kolthoff, R. G. Gutmacher, and A. Kahn. Sorption of gr-s type rubber by carbon black .2. effect of variables on the sorption by graphon. *The Journal of Physical and Colloid Chemistry*, 55(7):1240–1246, 1951.
- L. Koral, R. Ullman, and F. Eirich. The adsorption of polyvinyl acetate. *JOURNAL OF PHYSICAL CHEMISTRY*, 62(5):541–550, 1958.
- I. Langmuir. The evaporation, condensation and reflection of molecules and the mechanism of adsorption. *Physical Review*, 8(2):149–176, 1916.
- M. J. Lazzaroni, D. Bush, J. S. Brown, and C. A. Eckert. High-pressure vapor-liquid equilibria of some carbon dioxide plus organic binary systems. *Journal of Chemical and Engineering Data*, 50(1):60–65, 2005.

- Y. N. Lin, T. W. Smith, and P. Alexandridis. Adsorption of a polymeric siloxane surfactant on carbon black particles dispersed in mixtures of water with polar organic solvents. *Journal of Colloid and Interface Science*, 255(1):1–9, 2002.
- Y. S. Lipatov and L. M. Sergeeva. *Adsorption of Polymers*. John Wiley & Sons, New York, 1st edition, 1974.
- M. V. Lopez-Ramon, F. Stoeckli, C. Moreno-Castilla, and F. Carrasco-Marin. On the characterization of acidic and basic surface sites on carbons by various techniques. *Carbon*, 37(8):1215–1221, 1999.
- M. Lubbert, G. Brunner, and M. Johannsen. Adsorption equilibria of α - and δ -tocopherol from supercritical mixtures of carbon dioxide and 2-propanol onto silica by means of perturbation chromatography. *Journal of Supercritical Fluids*, 42:180–188, 2007.
- S. Lucas, M. J. Cocero, C. Zetzl, and G. Brunner. Adsorption isotherms for ethylacetate and furfural on activated carbon from supercritical carbon dioxide. *Fluid Phase Equilibria*, 219(2):171–179, 2004.
- S. J. Macnaughton and N. R. Foster. Supercritical adsorption and desorption behavior of ddt on activated carbon using carbon-dioxide. *Industrial & Engineering Chemistry Research*, 34(1):275–282, 1995.
- D. H. Napper. *Polymeric Stabilisation of Colloidal Dispersions*. Academic Press, London, 1983.
- F. Nsib, N. Ayed, and Y. Chevalier. Selection of dispersants for the dispersion of carbon black in organic medium. *Progress in Organic Coatings*, 55(4):303–310, 2006.
- G. D. Parfitt and N. H. Picton. Stability of dispersions of graphitized carbon blacks in aqueous solutions of sodium dodecyl sulphate. *Transactions of the Faraday Society*, pages 1955–1964, 1968.

- J. M. Pena, N. S. Allen, M. Edge, C. M. Liauw, S. R. Hoon, B. Valange, and R. I. Cherry. Analysis of radical content on carbon black pigments by electron spin resonance: influence of functionality, thermal treatment and adsorption of acidic and basic probes. *Polymer Degradation and Stability*, 71(1):153–170, 2000.
- R. J. Pugh and F. M. Fowkes. The dispersibility and stability of carbon-black in media of low dielectric-constant .2. sedimentation volume of concentrated dispersions, adsorption and surface calorimetry studies. *Colloids and Surfaces*, 9(1):33–46, 1984.
- H. Ridaoui, A. Jada, L. Vidal, and J. B. Donnet. Effect of cationic surfactant and block copolymer on carbon black particle surface charge and size. *Colloids and Surfaces a-Physicochemical and Engineering Aspects*, 278(1-3):149–159, 2006.
- H. Shojibara, Y. Sato, S. Takishima, and H. Masuoka. Adsorption equilibria of benzene on activated carbon in the presence of supercritical carbon-dioxide. *Journal of Chemical Engineering of Japan*, 28(3):245–249, 1995.
- C. F. Spencer and R. P. Danner. Improved equation for prediction of saturated liquid density. *Journal of Chemical and Engineering Data*, 17(2):236–241, 1972.
- H. J. Spinelli. Polymeric dispersants in ink jet technology. *Advanced Materials*, 10(15):1215–+, 1998.
- M. Stievano and N. Elvassore. High-pressure density and vapor-liquid equilibrium for the binary systems carbon dioxide-ethanol, carbon dioxide-acetone and carbon-dioxide dichloromethane. *Journal of Supercritical Fluids*, 33:7–14, 2005.
- C. S. Tan and D. C. Liou. Adsorption equilibrium of toluene from supercritical carbon-dioxide on activated carbon. *Industrial & Engineering Chemistry Research*, 29(7):1412–1415, 1990.
- Walter J. Wnek, Michael A Andreottola, Paul F. Doll, and Sean M. Kelly. Ink jet technology. In A. S. Diamond and D. S. Weiss, editors, *Handbook of Imaging Materials*, pages 531–602. Marcel Dekker, Inc., New York, 2nd edition, 2002.

- Y. Zhang and C. Erkey. Preparation of platinum-nafion-carbon black nanocomposites via a supercritical fluid route as electrocatalysts for proton exchange membrane fuel cells. *Industrial & Engineering Chemistry Research*, 44(14):5312–5317, 2005.
- Y. Zhang and C. Erkey. Preparation of supported metallic nanoparticles using supercritical fluids: A review. *Journal of Supercritical Fluids*, 38(2):252–267, 2006.
- Y. Zhang, D. F. Kang, M. Aindow, and C. Erkey. Preparation and characterization of ruthenium/carbon aerogel nanocomposites via a supercritical fluid route. *Journal of Physical Chemistry B*, 109(7):2617–2624, 2005a.
- Y. Zhang, D. F. Kang, C. Saquing, M. Aindow, and C. Erkey. Supported platinum nanoparticles by supercritical deposition. *Industrial & Engineering Chemistry Research*, 44(11):4161–4164, 2005b.
- Y. Zhang, B. Cangul, Y. Garrabos, and C. Erkey. Thermodynamics and kinetics of adsorption of bis(2,2,6,6-tetramethyl-3,5-heptanedionato)(1,5-cyclooctadiene) ruthenium (ii) on carbon aerogel from supercritical CO_2 solution. *Journal of Supercritical Fluids*, 44:71–77, 2008.

Chapter 6

Carbon black size reduction and polymer encapsulation in CO₂-expanded acetone

The previous two chapters addressed fundamental aspects of the equilibrium behavior of systems comprised of polymers and particles in CXLs. The tunability of CO₂-expanded acetone was explored with respect to changes in temperature, pressure, and composition, in order to determine the conditions under which dissolved polymer will exit the CXL phase either as a pure solid precipitate or as an adsorbate. The knowledge gained in these investigations is directly applicable to the development of a CXL-based process to produce ink jet ink precursors. The current chapter concerns the implementation and analysis of a such a process, combining GAS precipitation of polymer and traditional particle size reduction technology to produce dry, polymer-encapsulated pigment particles.

6.1 Background

6.1.1 Particle size reduction in liquid slurries

As discussed in Section 1.1.3, pigmented inks are currently produced in an aqueous process involving simultaneous particle size reduction and encapsulation with dispersant polymers. This process is typically carried out in two steps: large agglomerates are first broken apart in a high-speed disperser (HSD), and the dispersion is then fed to a final grind – most commonly in a media mill – for further particle size reduction. During each of these steps, polymer molecules adsorb onto newly exposed particle surfaces to prevent reagglomeration.

High-speed dispersers

High-speed dispersers employ shear stress and some attrition as the source of particle dispersion. The pigment mixture is placed in a tank and agitated by a disk impeller with a saw-blade edge (Cowles blade). The impeller is mounted on a shaft that is centered in the tank, and the shaft is rotated such that a laminar flow pattern is generated between the disk and the tank bottom. The shear stress, τ , is a measure of the shear forces experienced by particles within the dispersion, and is expressed in terms of the viscosity, μ , and shear rate, $\dot{\gamma}$, of the slurry as $\tau = \dot{\gamma}\mu$. Under laminar flow conditions between the HSD impeller and tank bottom, the shear rate can be approximated as $\dot{\gamma} = v/h$, where v is the velocity of the impeller, and h is the distance between the impeller and the tank bottom. The viscosity of ink dispersions is Newtonian at low pigment concentrations, and can be represented empirically by [Wnek et al., 2002]

$$\mu_D = \mu_F(1 + f(C_S)) \quad (6.1)$$

where μ_D is the viscosity of the dispersion, μ_F is the viscosity of the particle-free fluid phase, and the function f takes the form of a power series. For low pigment concentrations, a linear relationship for f provides an adequate representation of viscosity data.

Well-established heuristic guidelines generally dictate the operating conditions in an HSD. Impeller tip speed is generally in the range of 4000-5200 fpm (20-26 m/s), the impeller size is one-third the tank diameter, the liquid level at rest is 1.5 times the impeller diameter, and the distance between the impeller and the tank bottom is one-half the impeller diameter. A typical premix is conducted for 15-60 minutes.

Media milling

A media mill essentially consists of a tank with an agitator. The most common agitator designs feature multiple discs or pins positioned along the axis. A schematic of a commercially available media mill is shown in Figure 6-1. Particle size reduction is achieved through the action of grinding media within the tank, typically small ceramic, polymeric, or metallic beads. The kinetic energy imparted to the media by the agitator is transferred to pigment particles that are stressed between two colliding media beads, breaking up agglomerates or crushing primary particles. Media mills can be operated in batch or continuous modes; mills operating continuously are equipped with a screen or rotating gap in order to retain the media within the grinding vessel.

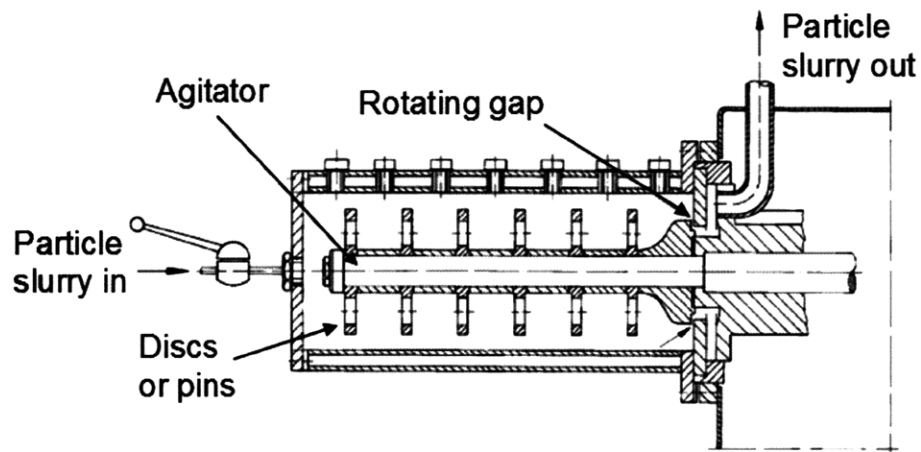


Figure 6-1: Schematic of a representative horizontal media mill for particle size reduction (adapted from Stender [2004]). Laboratory-scale mill vessels are typically between 200 ml and several liters in volume.

The mechanisms of media milling have been investigated extensively by the Schwedes

group at the Technical University at Brunswick, Germany [Becker et al., 2001, Blecher et al., 1996, Kwade, 2004, 1999b, Kwade et al., 1996, Kwade and Schwedes, 2002, Mende et al., 2004]. These studies have shown that particle size reduction primarily depends on the specific energy input, E_m , which is the total energy supplied to the mill divided by the mass of the product slurry. More precisely, the comminution process is influenced by how often each feed particle is stressed – the stress number, SN – and the intensity of each stress event – the stress intensity, SI [Kwade, 1999a]. For a batch process in which the most important milling mechanism is deagglomeration of primary particles, Kwade [1999a] has derived the following proportionality for the stress number:

$$SN \propto \frac{\phi_{GM}(1 - \varepsilon)}{(1 - \phi_{GM}(1 - \varepsilon))c_V} \frac{nt}{d_{GM}} \quad (6.2)$$

where n is the number of revolutions of the agitator per unit time, t is the milling time, d_{GM} is the diameter of the grinding media, c_V is the volume solids concentration of the particle slurry, ε is the porosity of the bulk grinding media, and ϕ_{GM} is the filling ratio of the grinding media. Expressions similar to Equation 6.2 are used as a measure of the stress number, as the actual value cannot be determined. Similarly, no expression for the actual stress intensity currently exists. However, under certain conditions the stress intensity of the grinding media, SI_{GM} , can be used as a measure of the stress intensity in the mill:

$$SI \propto SI_{GM} = d_{GM}^3 \rho_{GM} v_t^2 \quad (6.3)$$

where ρ_{GM} is the density of the grinding media, and v_t is the tip speed of the agitator discs. Other factors such as mill geometry, solids concentration, and viscosity of the suspension also influence the stress intensity, though they are not represented in Equation 6.3. Also, it is important to note that in reality, the stress intensity can only be represented by a distribution. Despite the shortcomings of Equations 6.2 and 6.3, they provide measures of the stress number and stress intensity, respectively, which are useful for analyzing the milling process. For example, the evolution of median particle size is better represented as a function of stress number than as a function of

time; a plot of median particle size versus stress number will be a straight line on a log-log diagram. Also, experiments reveal a minimum in the specific energy required to reach a certain median particle size as a function of stress intensity; once this optimum stress intensity has been determined, the stirrer speed and media size may be varied to achieve a higher stress number at constant stress intensity. Examination of Equation 6.3 indicates that a high disc tip speed and small media size will be most advantageous. Typical tip speeds in laboratory-scale media mills are between 5 and 20 m/s.

As mentioned above, the rheological properties of the particle suspension are missing in expressions for the representative stress number and stress intensity, even though they can have a significant influence on the actual values. High suspension viscosity usually indicates a high solids concentration, and hence high grinding efficiency. However, if the viscosity is too high, contact between media beads and pigment particles will be hindered, reducing the grinding efficiency. For this reason, the use of fine media is only possible with low-viscosity suspensions [Way, 1997]. With this in mind, it is important to note that due to relatively high solids loadings, rheological properties of ink dispersions are also influenced by the level of agglomeration of the product particles, with significant particle agglomeration leading to an increase in suspension viscosity [Mende et al., 2003]. With proper dispersion stabilization, suspensions of particles with a median size less than 50 nm have been produced by media milling, and no lower particle size limit has yet been reached [Mende et al., 2003].

6.1.2 Previous studies of CO₂-based particle encapsulation

The particle formation methods described in Section 1.2.3 have been applied in various configurations to the encapsulation of micro- and nano-particles. The majority of recent investigations in this field have employed some variation of the RESS process [Jung and Perrut, 2001, Matsuyama et al., 2001b, Mishima et al., 2001, Hertz et al., 2006, Dos Santos et al., 2003], although the poor solubility of most coating materials in pure scCO₂ has proven to be an important obstacle. To address this issue, Matsuyama and coworkers developed a process utilizing mixtures of CO₂ and an organic solvent

that acts as a cosolvent in high-pressure mixtures but as a non-solvent at ambient conditions [Matsuyama et al., 2003b,a, 2001a].

The PCA technique has also been employed in particle coating operations, [Young et al., 1999] but the most common use of this method for producing heterogeneous particles involves co-precipitation of composite particles [Tu et al., 2002, Falk et al., 1997, Boutin et al., 2004], most often for applications in pharmaceutical or biomedical materials. In a study with particular relevance to the current thesis, Wang et al [2004] successfully demonstrated a PCA encapsulation process to coat both hydrophobic and hydrophilic silica nanoparticles with an acrylate polymer.

Co-precipitation to form composite particles via the GAS process has been investigated for drug-delivery applications [Elvassore et al., 2001]; however, there have been few reports of GAS-based encapsulation of insoluble particles. This is due in part to the tendency of CO₂ to plasticize the coating materials and cause agglomeration of the coated particles [Young et al., 1999]. The particle encapsulation process currently under investigation minimizes this potential complication by using relatively small amounts of coating material in conjunction with vigorous agitation to break up agglomerates.

In addition to precipitation-based approaches for particle encapsulation, several researchers have applied the use of scCO₂ and CXLs to reaction-based coating methods. Pessey and coworkers [Pessey et al., 2000, 2001] implemented a technique involving the thermal decomposition of an organic precursor in scCO₂ to deposit copper onto the surface of particles. Yue et al. [Yue et al., 2004] employed *in situ* polymerization of poly(methyl methacrylate) and poly(1-vinyl-2-pyrrolidone) to encapsulate 12 μm particles of Dechlorane flame retardant, and Hertz et al [2006] encapsulated yttria stabilized zirconia nanoparticle via *in situ* polymerization of poly(methyl methacrylate). While these techniques merit further study, they often involve more demanding pressure and temperature conditions than processes based on precipitation.

6.2 Materials and methods

An experimental apparatus was designed and constructed for the purpose of encapsulating carbon black nanoparticles for use in ink jet inks. The encapsulation system combines the particle size reduction techniques described in Section 6.1.1 with the GAS process for polymer solubility reduction. The apparatus allows for particle size reduction via either HSD-type agitation or media milling. Particle encapsulation trials were carried out at pigment:dispersant (P:D) ratios of 1.25, 2.5, and 5.0 for the 85/15 BzMA/MAA and 75/25 BzMA/MAA copolymers, and at P:D ratios of 2.5 and 5.0 for the 80/20 BzMA/MAA copolymer.

6.2.1 Experimental apparatus

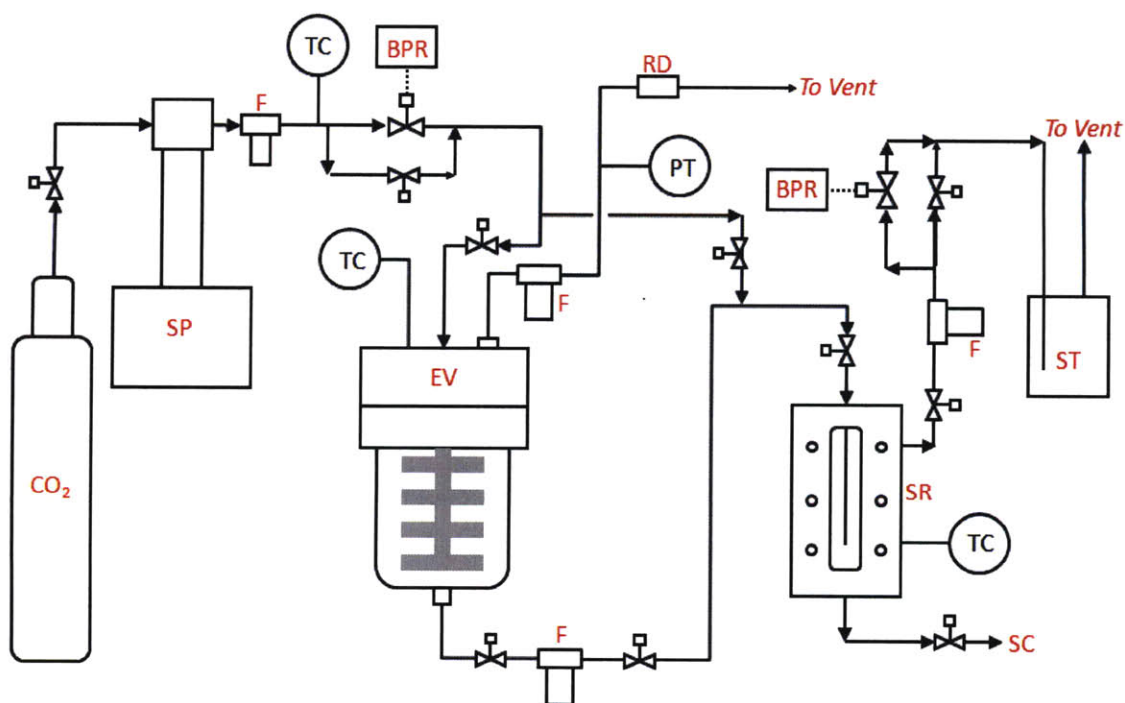


Figure 6-2: Schematic of the high-pressure particle encapsulation system. System components: carbon dioxide supply (CO₂), syringe pump (SP), back-pressure regulator (BPR), encapsulation vessel (EV), solvent recovery vessel (SR), filters (F), solvent trap (ST), rupture disk (RD), solvent collection (SC), thermocouples (TC), pressure transducer (PT).

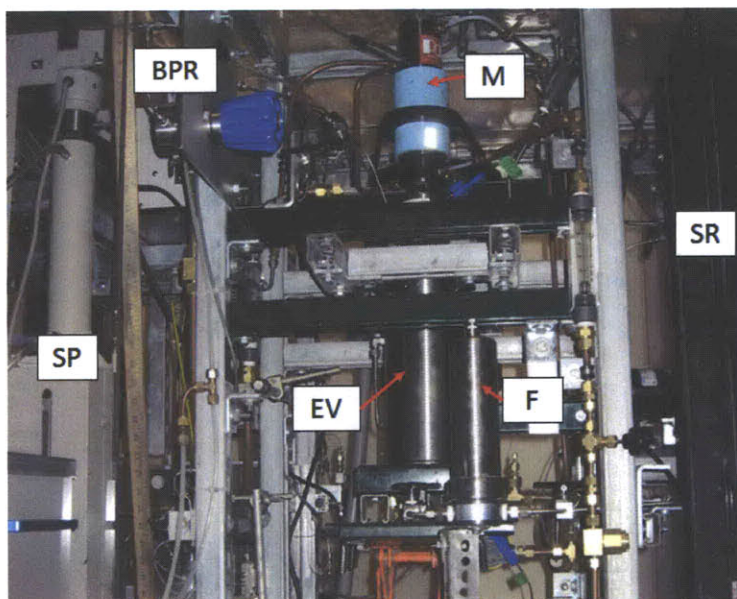


Figure 6-3: Photograph of the high-pressure particle encapsulation system. Major system components: syringe pump (SP), back-pressure regulator (BPR), encapsulation vessel (EV), solvent recovery vessel (SR), filter (F).

A schematic representation of the size reduction and encapsulation system is shown in Figure 6-2, and a photograph of the system is displayed in Figure 6-3. The encapsulation process is carried out in a stainless steel reaction vessel (Autoclave Engineers, P/N 3010-4796 [vessel] and P/N 201A-3622 [cover]) designed to operate at high pressure (1000 to 3000 psi / 70 to 200 bar) and at temperatures from 0°C to 450°C. The encapsulation vessel has a fluid volume of 1 L, with an inside diameter of 3 inches and an inside depth of 9 inches. A cooling jacket allows temperature control during the encapsulation process. The vessel cover is mounted on a steel frame within a polycarbonate enclosure, and the vessel body is raised and lowered using a laboratory jack.

Agitation within the vessel is provided by a high-pressure mixer (PDC Machines, Model P70) capable of rotating a magnetically coupled shaft at over 3400 RPM. The magnetic mixer is driven by a 5 HP motor (Reliance Electric, “Sabre” 184T) that is controlled by a variable frequency drive (Yaskawa, Model J7). A custom-fabricated adapter enabled the use of the magnetic mixer with the existing encapsulation ves-

sel, and the mixer shaft was supplied with a 3/8"-16 UNC threaded connection that extended 1" into the vessel. To allow for rotation at speeds above 3400 RPM, carbon bearings (PDC Machines, P/N A0026801) were employed in the mixer, and the bottom-most bearing was modified with grooves to accommodate two viton o-rings around the outer diameter. The o-rings prevented the bearing from spinning and reduced shaft vibration. Mixer rotational speed was monitored using a tachometer; the frequency signal from the tachometer was converted to a voltage signal by a frequency to analog converter (Red Lion, Model IFMA) before being recorded by a personal computer using LabVIEW data acquisition software. A schematic of the mixer, adapter, and shaft is shown in Figure 6-4.

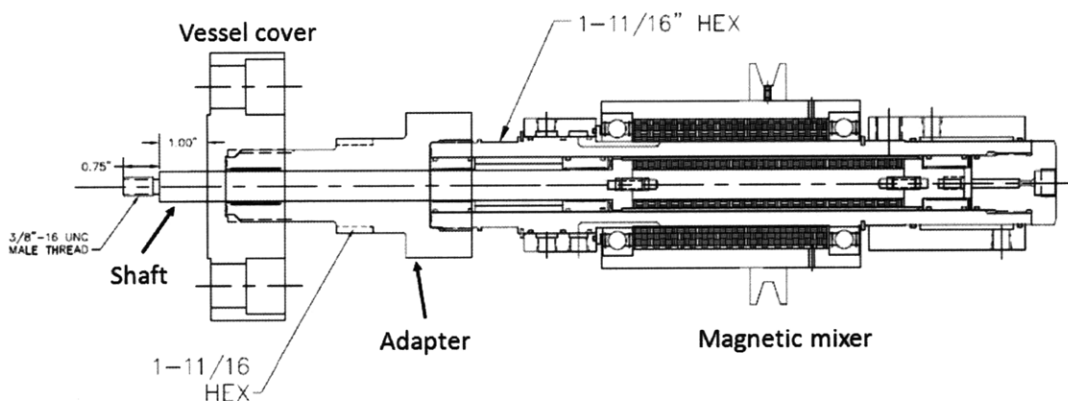


Figure 6-4: Schematic of the magnetic mixer and adapter for coupling to the encapsulation vessel cover.

The encapsulation vessel is capable of operating as an HSD or as a media mill, depending on the agitator that is coupled to the mixer shaft. A schematic of the HSD shaft is pictured in Figure 6-5; the shaft was fabricated from stainless steel by the MIT Machine Shop, and accommodates a 1" Cowles sawtooth impeller. The use of a reaction vessel as a high pressure media mill (HPMM) was first proposed by the DuPont Particle Science and Technology group for milling pharmaceutical components in supercritical fluid media [Ford et al., 2002]. The current apparatus is similar in design to that developed by DuPont. Agitation is provided by a custom-designed multi-disc

cylindrical agitator fabricated from nylon 6/6 plastic by the MIT Machine Shop. Nylon was chosen due to its light weight and resistance to swelling in high-pressure CO₂. The design of the agitator was based on commercially available agitators for laboratory-scale media mills, which generally provide a minimum gap between moving parts equal to ~5 times the diameter of the grinding media. A schematic of the HPMM agitator and stainless steel coupling adapter is shown in Figure 6-6, and pictures of both the HPMM and HSD agitators are shown in Figure 6-7. The agitator was dynamically balanced by Linskog Balancing to minimize vibrations at 3400 RPM. The hollow section at the bottom of the agitator was designed to accommodate a filter assembly which was later removed from the inside of the encapsulation vessel; however, this feature also served to reduce the weight of the unit, thereby reducing the stress experienced by the mixer bearings.

The grinding media are retained within the encapsulation vessel by a 440 μm T-type filter (Swagelok, P/N SS-4TF-440) at the vessel outlet. To prevent the media from entering the magnetic mixer through the gap between the mixer shaft and the vessel cover, a bronze thrust bearing (McMaster Carr, P/N 7814K21) with a close tolerance to the shaft diameter is held in place against the vessel cover using a shaft collar (McMaster Carr, P/N 6436K136) and wave spring (McMaster Carr, P/N 9714K36).

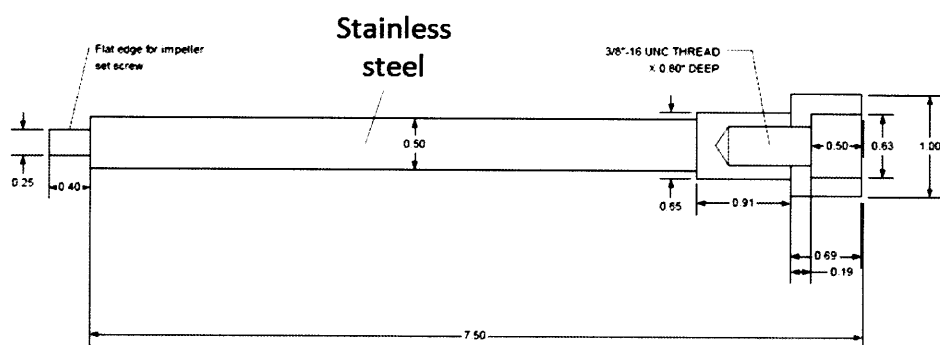


Figure 6-5: Schematic of the high-speed disperser shaft for use in high-pressure encapsulation trials.

Both the encapsulation vessel and magnetic mixer require cooling during opera-

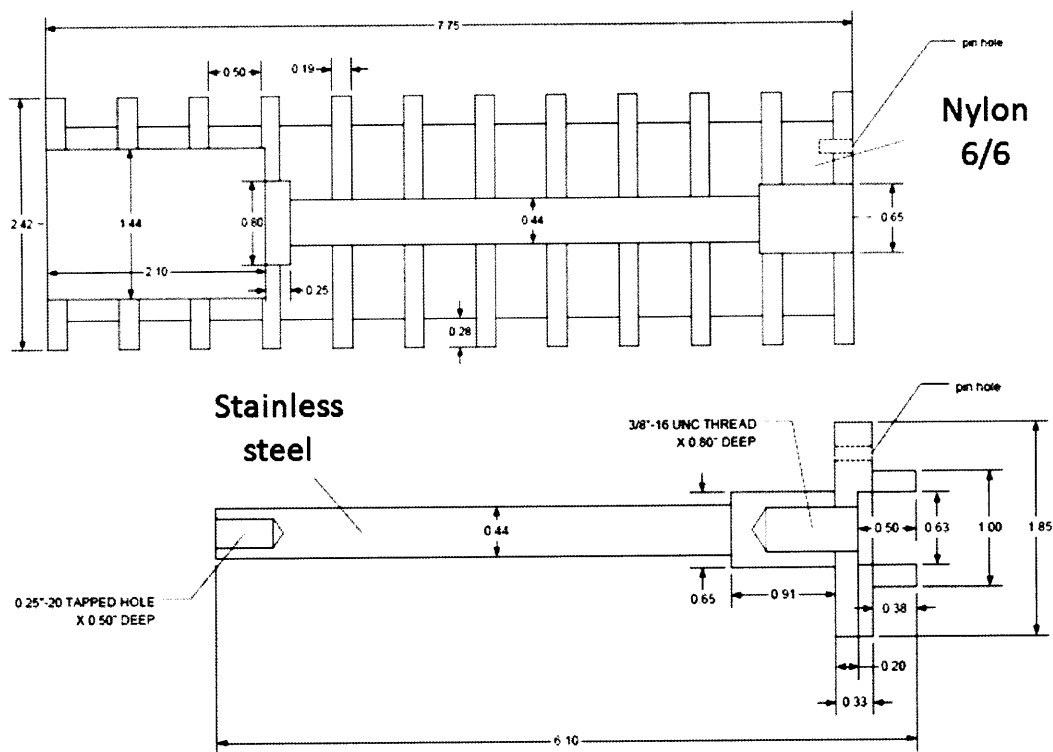


Figure 6-6: Schematic of the media milling impeller and coupling adapter for use in high-pressure encapsulation trials.

tion; chilled water is provided by a recirculating chiller (VWR, Model 1179-P) and circulated through a cooling loop, depicted schematically in Figure 6-8. The magnetic mixer requires 0.5-1.0 GPM of cooling water, monitored by a rotameter and regulated by manipulation of a needle valve. The temperature within the encapsulation vessel and at the cooling water inlet and outlet is determined using type T thermocouples (Omega Engineering, P/N GTMQSS-062U-6, tolerance $\pm 1K$) and monitored on a personal computer using LabVIEW data acquisition software. The magnetic mixer also requires 10 SCFM air cooling, provided by a house air connection and monitored via a rotameter.

Carbon dioxide is supplied to the system using two high-pressure syringe pumps (Teledyne-Isco, Models 500D and 100DM) equipped with air-actuated inlet and outlet valves (P/N 681247089) and jackets for cooling. Chilled water at 4°C – provided by a refrigerated circulator (VWR, Model 1160S) – is sent to the cooling jackets in order

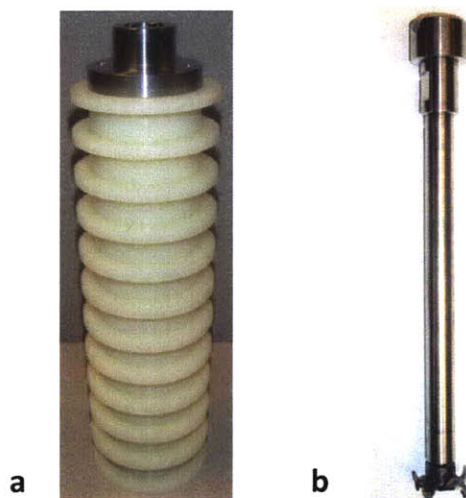


Figure 6-7: Photographs of the (a) media milling and (b) HSD agitators.

to maximize the amount of liquid CO₂ in the syringe pump cylinders during each cycle. The pumps are operated in constant flow rate mode, and the pressure within the cylinders is maintained at a constant level by a back pressure regulator (Tescom, Model 26-1763-24) modified for CO₂ service. In this manner, a constant mass flow rate of CO₂ is fed to the encapsulation vessel.

Encapsulated particles are retained in 0.1 μm bonded microfiber filter elements (Headline Filters, P/N 25-178-50K) installed in a high-pressure filter housing (Headline Filters, Model 142HP) at the outlet of the encapsulation vessel. Solvent that has passed through the filter is collected in a Jerguson sight gauge (Model 29-T-32, Max 3000 psi at 100°F), equipped with quartz windows for visual access to the filtrate. This sight gauge will be referred to henceforth as the solvent recovery vessel. A dip tube is passed through the top of the solvent recovery vessel such that the liquid CXL mixture is collected for recovery while the vapor phase is able to exit through a separate fitting at the top. Pressure is maintained within the encapsulation vessel and solvent recovery vessel by a second back-pressure regulator (Tescom, Model 26-1763-24) at the system outlet. Pressures within the encapsulation vessel and solvent recovery vessel are monitored using a pressure transducer (Omega Engineering, P/N PX303-3KG5V, accuracy ± 7.5 psi) and analog gauge (Swagelok, P/N

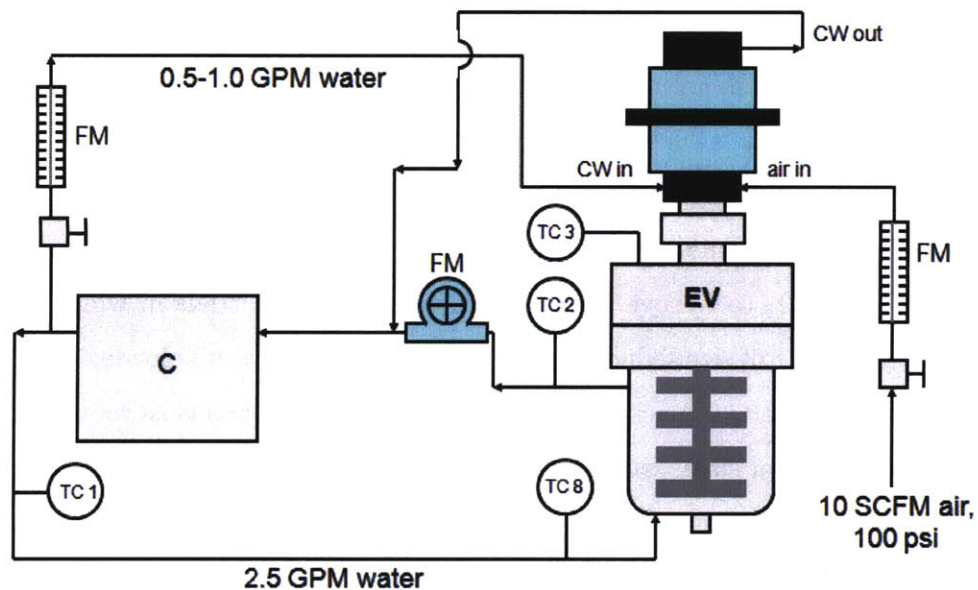


Figure 6-8: Schematic of cooling loops for the high-pressure particle encapsulation system. System components: encapsulation vessel (EV), chiller (C), flow meters (FM), thermocouples (TC), pressure transducer (PT).

PGI-63C-PG5000-LAO), respectively. The encapsulation vessel pressure was recorded by LabVIEW software on a personal computer.

6.2.2 Procedure

The process to produce encapsulated carbon black particles was operated in a semi-batch configuration, and consisted of three distinct stages: pre-mix, size reduction and encapsulation, and particle separation and recovery. In the pre-mix step, known amounts of carbon black and polymer-acetone solution were combined in a plastic jar and shaken to adequately wet the particles. The composition of the polymer solution was determined to within an uncertainty of 3% via UV spectroscopy, and the masses of carbon black and polymer solution were measured gravimetrically with an uncertainty of 0.01 g (0.2-0.02%). The resulting mixture was agitated for 30 minutes using a laboratory HSD (D.H. Melton Co., Model CM-100) with a 2" Cowles style

open sawtooth impeller. The speed of the mixer was regulated using a continuously variable controller such that a vortex formed within the jar with little splashing. The jar was suspended in an ice bath during the pre-mix in order to reduce acetone evaporation and avoid a reduction in viscosity.

Before each trial, the encapsulation vessel was cleaned thoroughly and pressure tested at 700 psig. Immediately before addition of the pigment dispersion, the system was purged with CO₂ to remove air and residual acetone. In trials in which media milling was the mode of size reduction, the encapsulation vessel was loaded with 390 g of glass grinding beads (Quackenbush Co., "Q-Bead"). The beads as received contained a distribution of sizes; sieves were employed to separate beads with diameters between 1.2 mm and 1.4 mm for use in milling trials. The density of the individual glass beads was 2.5 g/ml, and the bulk density was 1.5 g/ml.

Upon completion of the pre-mix, the dispersion was added directly to the encapsulation vessel through a funnel, and agitation was begun with either the HSD impeller or media mill agitator. Soon after the mixer reached its maximum speed, the syringe pumps were enabled at a constant flow rate of 15 ml/min until the pressure within the pumps reached ~1600 psig. At this point, the flow rate was reduced to 7 ml/min. As the pressure within the pumps reached the back pressure regulator setting of 1700 psig, CO₂ began to flow to the encapsulation vessel. The CO₂ equation of state developed by Span and Wagner [Span and Wagner, 1996] was used to calculate the mass flow rate of CO₂ based on the temperature and pressure within the syringe pumps. The valve at the vessel outlet was closed during this stage of the process, and CO₂ was added to the encapsulation and solvent recovery vessels simultaneously such that a uniform pressure was maintained throughout the system. Temperature within the encapsulation vessel was maintained at 25±2°C by manually adjusting the temperature of the recirculating chiller. As CO₂ was added to the encapsulation vessel the pressure steadily rose and the CO₂ mass fraction in the liquid phase increased, causing a reduction in polymer solubility and encapsulation of the carbon black particles. An illustration of the encapsulation process in media milling configuration is pictured in Figure 6-9.

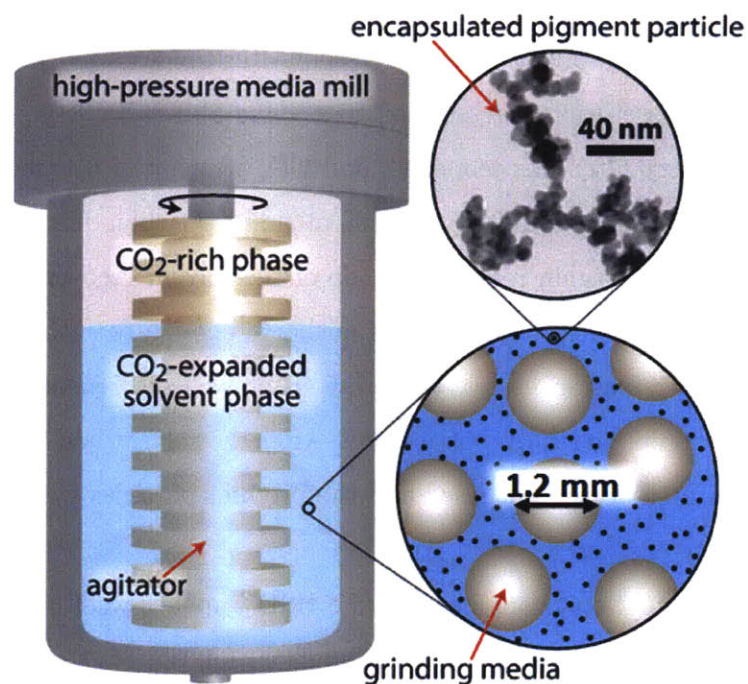


Figure 6-9: Illustration of the high-pressure media milling and encapsulation process.

The pressure within the encapsulation vessel reached 500 psig after approximately 50 minutes of CO₂ addition, and at this point the syringe pump flow rate was increased to 20 ml/min. When the system pressure reached approximately 700 psig the valve at the encapsulation vessel outlet was opened and the valve connecting the solvent recovery vessel to the CO₂ supply was closed, such that the mixture in the encapsulation vessel flowed through the high-pressure filter between the two vessels. The coated particles were retained in the filter, while the CO₂-expanded acetone entered the solvent recovery vessel. As the liquid level reached the top of the solvent recovery vessel (typically at ~850 psig), the syringe pumps and magnetic mixer were both stopped. This completed the encapsulation stage of the process.

The next step was the separation and recovery of acetone from the system. Immediately after the syringe pumps were stopped, the valve after the particle recovery filter was closed and the solvent recovery vessel was slowly let down to atmospheric pressure by opening a valve in parallel with the second back pressure regulator. Thus, the

encapsulation vessel was maintained at high pressure while the acetone was removed from the bottom of the solvent recovery vessel. After the acetone was recovered, the solvent recovery vessel was repressurized to a value above 700 psig, the valve after the particle recovery filter was reopened, and CO₂ was pumped through the system at the maximum syringe pump flowrate (100 ml/min). Carbon dioxide was fed to the system until the liquid again reached the top of the solvent recovery vessel. Because the solvent recovery vessel (~350 ml) was not large enough to accommodate all of the liquid in the encapsulation vessel, the previous steps were repeated at least eight times to ensure complete removal of acetone. After the solvent had been flushed from the system, the pressure was released and the product particles were recovered from the filter as a dry powder.

Particle encapsulation trials utilizing the HSD impeller were carried out at pigment:dispersant (P:D) ratios of 1.25, 2.5, and 5.0 for the 85/15 BzMA/MAA and 75/25 BzMA/MAA copolymers. Trials operated in media milling mode were conducted using the 80/20 BzMA/MAA copolymer at P:D=2.5 and 5.0. In addition, a trial employing the HSD was conducted in which 80/20 BzMA/MAA polymer was neutralized with dimethylaminoethanol (DMAE) before the premix stage.

6.2.3 Product characterization

The product powder obtained from the encapsulation process was redispersed in water and characterized with respect to the properties that influence ink jet performance. The particles were first added to deionized water and 60-90% of the acid functional groups neutralized with either potassium hydroxide (KOH) or sodium hydroxide (NaOH) to form mixtures containing 7.5 wt% pigment (9-14 wt% total solids). The mixtures were shaken vigorously by hand in a closed container, and then mixed overnight via a stirrer or roller to fully incorporate the particles. The resulting dispersions were sonicated at 50% amplitude for 5 minutes (2 seconds on, 2 seconds off for 10 minutes) to break up particle agglomerates. Select samples were also redispersed using the high-pressure media mill operated at ambient pressure (see Section 6.3.1).

The pigment dispersions were evaluated in ink jet inks at DuPont. Additives such

as pH buffer, de-foaming agent, and viscosity modifiers were added to the initial slurry, and the resulting inks were jetted in an actual ink jet printhead. The performance of the inks was evaluated based on “jettability”, optical density of the printed ink on the media, stability with respect to pH, and particle size. The hydrodynamic particle diameter distribution was determined via dynamic light scattering using a Nanotrak particle size analyzer.

The particles were also analysed using transmission electron microscopy (TEM). After dispersing the particles in water as described above, one or two drops of the aqueous dispersion were contacted with a lacey carbon copper TEM grid (Ted Pella, Inc., P/N 01881-F) and the water was allowed to evaporate at ambient conditions. The particles were then characterized using a 200kV Jeol 200CX TEM instrument.

6.3 Results and discussion

Carbon black particles were successfully encapsulated with both hydrophilic and hydrophobic polymers, and recovered as a dry, freely flowing powder from the high pressure filter at the encapsulation vessel outlet. The solids content of the encapsulation vessel (carbon black and polymer) was recovered at yields between 89% and 98%. The residual solids remained in the encapsulation vessel and the tubing connecting the vessel to the high-pressure filter; the filter was filled to capacity after each trial, slightly lowering the recovery of particles for larger solids loadings in the encapsulation vessel. A summary of the encapsulation trials involving BzMA/MAA copolymers is listed in Table 6.1.

The acetone initially loaded to the encapsulation vessel was collected from the solvent recovery vessel at yields between 82% and 89%; the balance of the acetone exited the process to the building ventilation system as a component of the CO₂-rich vapor phase that was used to flush the system. The filter at the encapsulation vessel outlet effectively retained the coated particles, and the recovered liquid was essentially free of solids. The acetone was analyzed for polymer content after each trial via UV spectroscopy; the total mass of polymer collected in the solvent recovery vessel was

Table 6.1: Summary of high-pressure encapsulation trials conducted using BzMA/MAA random copolymers.

Sample	BzMA/MAA mass ratio	Size reduction method	P:D	Sample mass	% yield	Neutralized before premix?
1	75/25	media milling	5.0	8.5 g	–	no
2	75/25	HSD	5.0	28.5 g	98%	no
3	75/25	HSD	2.5	33.0 g	98%	no
4	75/25	HSD	1.25	37.0 g	89%	no
5	85/15	HSD	5.0	29.5 g	98%	no
6	85/15	HSD	2.5	30.5 g	92%	no
7	85/15	HSD	1.25	38.5 g	90%	no
8	80/20	HSD	2.5	34.5 g	98%	yes
9	80/20	media milling	2.5	30.0 g	92%	no
10	80/20	media milling	5.0	25.0 g	90%	no

between 0.04 g and 0.2 g (0.9-2% of the total mass of polymer added to the initial mixtures). In addition, the mass of product powder exceeded the mass of carbon black added to the encapsulation vessel in all trials. These two facts present strong evidence that nearly all of the polymer is retained in the filter (and encapsulation vessel) as a component of the product powder. The next logical question is whether the polymer is present as a coating on the carbon black particles or as homogeneous polymer particles. A brief discussion regarding common methods for characterizing encapsulated particles is presented in the following paragraphs.

Many researchers have utilized electron microscopy techniques to characterize coatings on micro- or nanoparticles [Hertz et al., 2006, Marre et al., 2008, Wang et al., 2004]. Standard TEM or scanning electron microscopy (SEM) have been successfully employed to confirm the presence of coatings when the layer is significantly thick to alter the size or appearance of the core particles – for example, by softening sharp edges or encapsulating entire agglomerates of spherical particles. Elemental mapping microscopy/spectroscopy techniques such as TEM with electron energy loss spectroscopy (TEM-EELS) [Wang et al., 2004] and field emission SEM with energy dispersive X-ray spectroscopy (FESEM-EDX) [Reverchon and Antonacci, 2007] have been used to characterize thin coatings on nanoparticles; however, these methods are

ineffective for cases in which the particle surface and the coating material possess similar atomic compositions, and cannot be used to distinguish between polymers and carbon black surfaces composed of carbon, oxygen, and hydrogen.

The presence of thin polymer layers has also been confirmed using fluorescence labeling and analysis with confocal microscopy [Lau and Gleason, 2006], but this technique is limited to particles that are larger than the wavelength of light. Spectroscopic techniques such as X-ray photoelectron spectroscopy have been utilized to characterize powder coatings [Marre et al., 2008], but the poor spatial resolution precludes its use for analysis of individual nanoparticles. Methods of characterizing bulk powders such as Fourier transform infrared (FTIR) spectroscopy and thermogravimetric analysis (TGA) [Wang et al., 2004] are useful for confirming the presence and quantity of a coating material, but are not generally able to distinguish between material which is on particle surfaces and that which is in the form of homogeneous particles in the absence of chemical bonding.

Based on the foregoing considerations, it was determined that the presence of a polymer layer on the carbon black particles could best be confirmed by evaluating their performance in ink jet inks. Inks based on uncoated carbon black exhibits poor performance in nearly all respects: dispersion stability, printing performance, and quality of the final image. Any improvement in these areas can be attributed to the presence of a polymer coating. The particles were also characterized by standard TEM techniques to qualitatively assess the product particle morphology.

6.3.1 Performance of encapsulated particles in ink jet inks

In one of the first successful demonstrations of the high-pressure encapsulation process, carbon black particles were coated with Joncryl[®] 611 polymer at P:D=2.9 in the media milling configuration. The product was redispersed in aqueous solution according to the method outlined in Section 6.2.3, and then subjected to further dispersion in the high-pressure media mill operated at ambient pressure. The pH of the resulting aqueous dispersion was adjusted to 8.5 before and after the media milling step. The dispersion was sent to DuPont for testing, and despite a low pigment con-

centration (1.7% by mass), the ink exhibited good optical density upon jetting. This demonstration represented a major milestone for the project for two reasons: it suggested that the polymer was deposited on the particle surfaces instead of precipitating to form homogeneous polymer particles, and it also validated the feasibility of the process as a means for employing hydrophobic polymers in aqueous ink formulations.

Although the early trials employing Joncryl[®] polymers served to confirm the feasibility of the process, the prospect of milling the product particles twice to obtain an acceptable particle size is not optimal from an economic standpoint. A major goal of the thesis work is the production of encapsulated particles that are easily redispersed in water with minimal agitation. In the case of pigment dispersions, “minimal agitation” applies to the redispersion procedure outlined in Section 6.2.3. The product particles listed in Table 6.1 were redispersed in this manner at DuPont in an attempt to evaluate the ease of redispersion for use in inks. The resulting dispersions were analyzed using a Nanotrak particle size analyzer to determine the hydrodynamic particle diameter distribution; a summary of the median diameter (D50) and the 95th percentile – on a particle number basis – of the particle size distribution (D95) for each sample is presented in Table 6.2. The results indicate a trend of decreasing median particle size with increasing P:D ratio, although there is no clear trend in the D95 particle size values.

In general the measured particle size distributions for all samples were shifted to slightly higher values than would be desirable for use in commercial ink jet inks, for which D50 and D95 are approximately 100 nm and 200 nm, respectively. Nonetheless, the fact that aqueous dispersions could be obtained with particle sizes in the nanometer range at particle loadings above 7wt% is strong evidence that the process successfully encapsulated the carbon black particles, since uncoated carbon black particles processed in the same manner would quickly flocculate and settle out of suspension due to interparticle van der Waals forces.

In fact, several of the product sample dispersions were of high enough quality that they could be tested in actual ink jet inks: samples 1, 2, 6, and 8 from Table 6.2 were filtered (with a 1.2 μm filter), formulated in an ink at 3wt% pigment, and “jetted”

Table 6.2: Summary of particle size measurement results for aqueous dispersions of BzMA/MAA-encapsulated carbon black product particles. D50 = median particle size; D95 = 95th percentile (particle number basis) of the particle size distribution.

Sample	BzMA/MAA mass ratio	Size reduction method	P:D	% neutralization	D50 (nm)	D95 (nm)
1	75/25	media milling	5.0	60	168.9	398.0
2	75/25	HSD	5.0	60	156.8	239.6
3	75/25	HSD	2.5	60	162.2	354.0
4	75/25	HSD	1.25	60	174.8	326.0
5	85/15	HSD	5.0	90	137.6	299.7
6	85/15	HSD	2.5	90	156.4	273.2
7	85/15	HSD	1.25	90	172.8	298.1
8	80/20	HSD	2.5	60	162.4	282.5
9	80/20	media milling	2.5	60	188.3	447.0
10	80/20	media milling	5.0	60	166.9	378.0

in an ink jet print head. All four samples jetted as well as the control dispersion (the control used for comparison was a standard commercial ink formulation at DuPont known to jet consistently with average performance). Sample 8 exhibited poor optical density when printed, but the other three samples performed significantly better than the control, despite the fact that some of the pigment was lost during the filtration step due to the relatively large average particle size of the samples. It is important to note that the samples which exhibited the best performance in inks were produced at P:D=5.0, since conventional inks produced at this P:D ratio generally exhibit poor dispersion stability and ink performance. This too is strong evidence to support the presence of a polymer layer on the processed carbon black particles, and suggests a high efficiency in depositing the polymer evenly on the particle surfaces. The results also indicate that using more polymer does not improve the stability of the final dispersion. It is possible that at lower P:D ratios, some particle aggregates and agglomerates are held together in a matrix of precipitated polymer.

6.3.2 TEM analysis

The original goal of TEM analysis was to obtain bright field/dark field image pairs in order to confirm the presence of a polymer layer on the carbon black particles. However, this requires a crystalline carbon black in order to distinguish it from the amorphous polymer coating. The NIPex[®] 180 IQ carbon black employed in the current study is microcrystalline in nature, making this type of analysis difficult. The method is further complicated by the fact that the polymer layer on the carbon black particles is expected to be extremely thin (<5 nm).

Thus, the samples produced in the trials listed in Table 6.1 were characterized using standard bright-field TEM methods in order to qualitatively assess the structure and morphology of the particles. TEM images of each sample were obtained after depositing particles on a TEM grid as described in Section 6.2.3. Samples containing an excess of polymer were also prepared by conducting an encapsulation trial under mild agitation at P:D \approx 0.2; these samples, along with uncoated carbon black particles, served as references to which the product particles could be compared. Select micrographs of the two reference systems are pictured in Figure 6-10, and those of the products of the encapsulation trials are shown in Figure 6-11.

Particle size estimates determined from the TEM images are not accurate due to the small sample size, and also due to the possibility of particle agglomeration as the water droplets evaporate on TEM grid during sample preparation. In general, a range of particle sizes were observed in each sample, from aggregates on the order of 100 nm across to large agglomerates several microns in diameter. The encapsulated and uncoated carbon black samples were indistinguishable with regard to particle size and morphology.

Although polymer-carbon black composites were observed at very low P:D ratios (\sim 0.2), the presence of a polymer coating could not be unequivocally confirmed at the P:D ratios of interest to ink jet ink formulations due to the relatively small amounts of polymer present in these samples; however, it is important to note that neither was there any indication of homogeneous polymer particles at these higher P:D ratios.

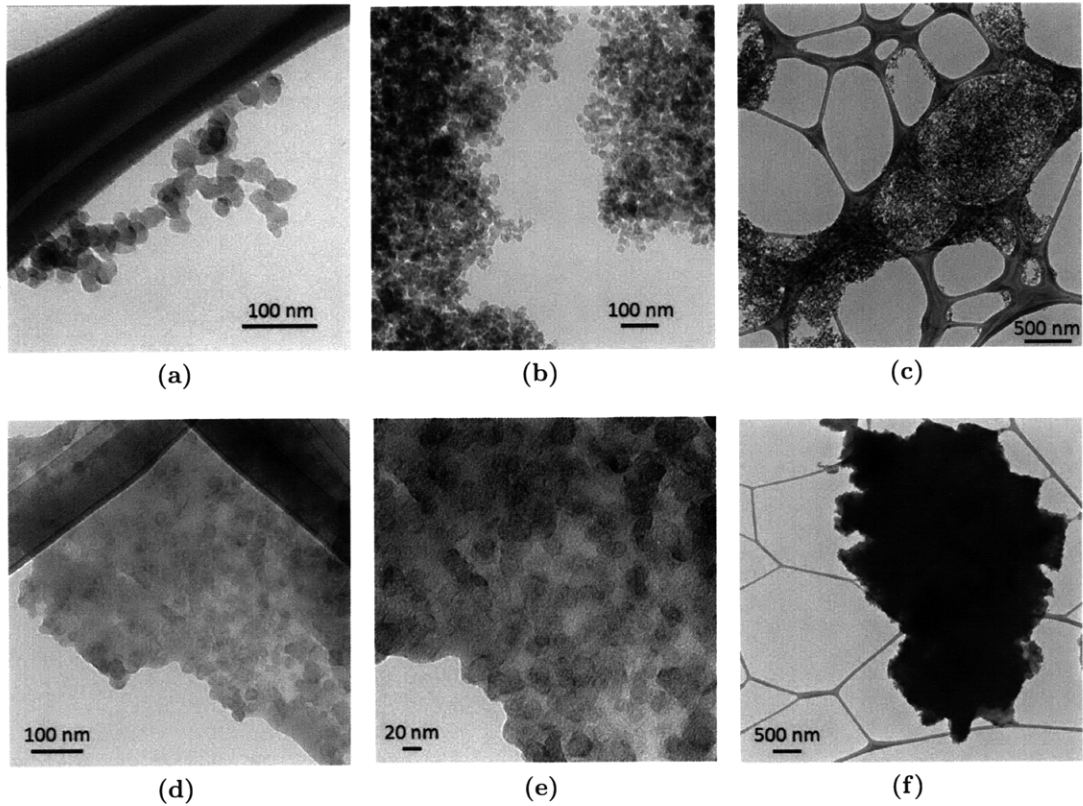


Figure 6-10: Selected TEM images of (a)-(c) uncoated carbon black and (d)-(f) carbon-polymer composites at a P:D ratio of ~ 0.2 .

6.3.3 Process considerations

Encapsulation and the evolution of system pressure

Based on the results of the product characterization in inks as well as the TEM study, it is reasonable to conclude that the CXL-based process is able to produce carbon black particles that are coated with polymer. At this point, it is instructive to analyze the encapsulation process in terms of the phase behavior and adsorption results described in Chapters 4 and 5. The evolution of temperature and pressure within the encapsulation vessel over the course of a representative experiment is plotted in Figure 6-12. The shaded region on the plot indicates the “encapsulation zone”, in which a majority of the polymer is deposited on the particle surfaces. This particular trial employed 75/25 BzMA/MAA copolymer, which is virtually insoluble

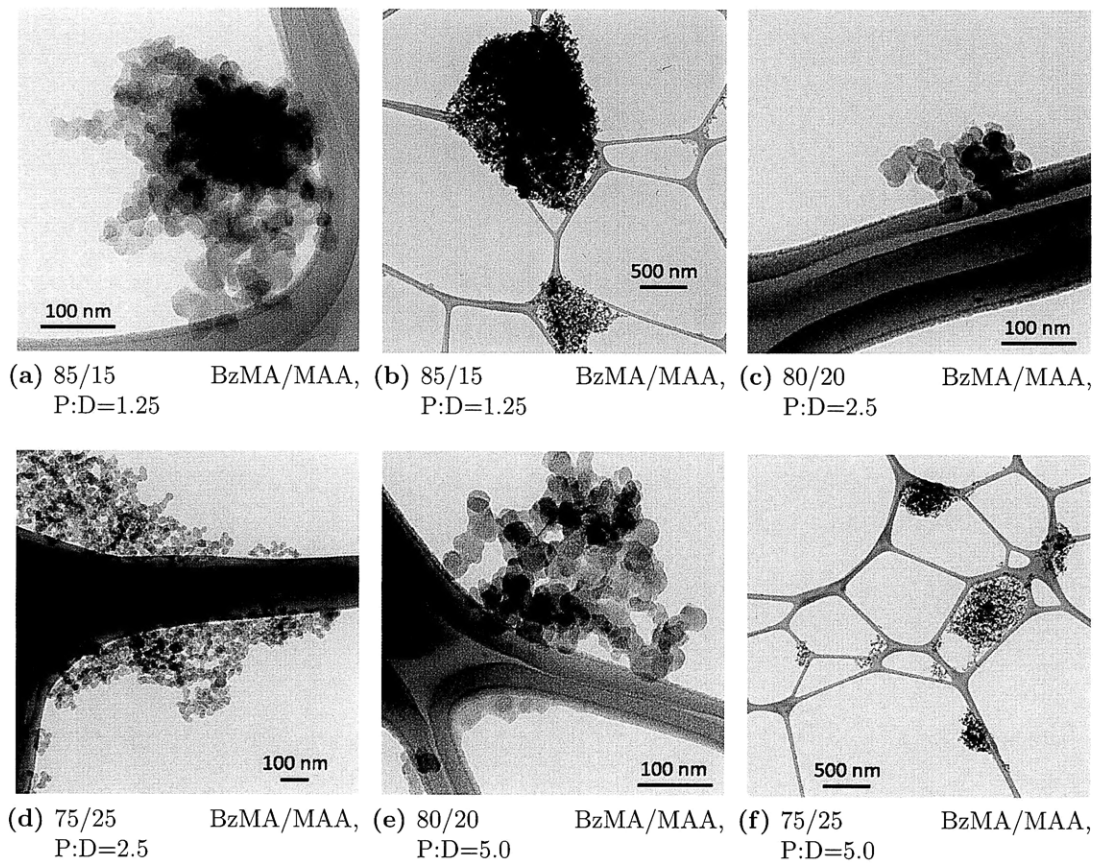


Figure 6-11: Selected TEM images of polymer-encapsulated carbon black.

in CO₂-expanded acetone at pressures above 300 psig at 25°C. The results of the high-pressure adsorption trials also indicate that the polymer loading on the carbon black particles remains largely unchanged from its value at atmospheric pressure until the pressure approaches the polymer solubility limit at the given temperature.

Thus, encapsulation is expected to occur in the relatively narrow window of pressures represented in Figure 6-12. However, the adsorption study revealed that there will be some degree of polymer adsorption even at atmospheric pressure. With the vigorous mixing conditions and break-up of agglomerates during the pre-mix stage, it can be assumed that the atmospheric-pressure dispersion has at least closely approached equilibrium with respect to polymer adsorption. If the assumption of adsorption equilibrium is valid, between 18-66% of the total polymer content would have been adsorbed on the particle surfaces before the encapsulation process was begun

for the trials listed in Table 6.1. Despite the fact that some polymer exists on the particle surface before size reduction operations commence, it is clear from inspection of Figure 6-12 that modifying the CO₂ addition profile during encapsulation trials may be beneficial; in particular, pressure should be increased rapidly to ~150 psig, then gradually raised to 300 psig in order to widen the window for encapsulation with 75/25 BzMA/MAA polymers.

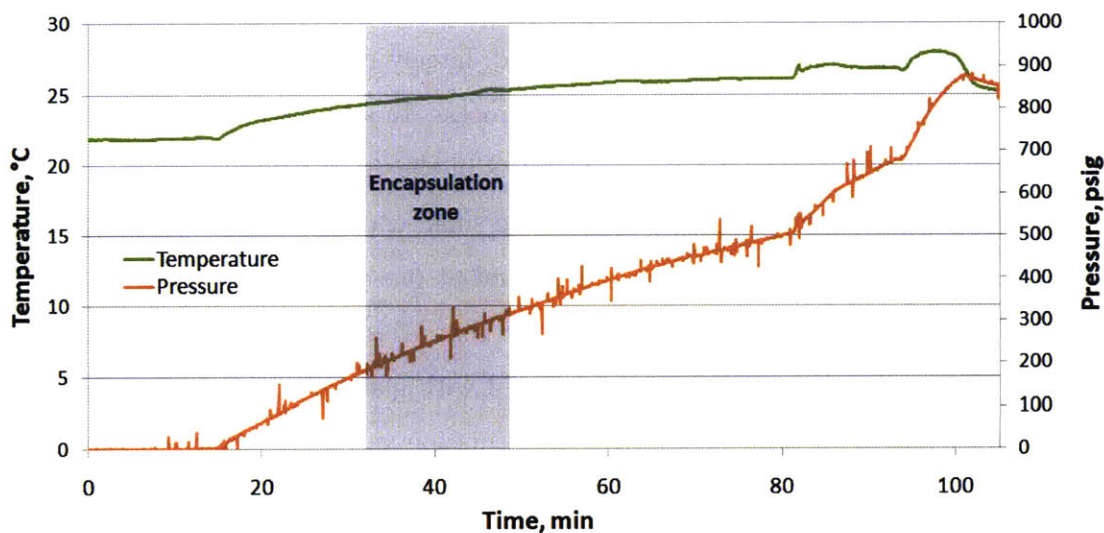


Figure 6-12: Plot of system temperature and pressure over the course of a representative high-pressure encapsulation trial.

Size reduction efficiency

The design and operation of the agitation system for the high-pressure encapsulation vessel was guided by the considerations outlined in Sections 6.1.1 and 6.1.1. Nevertheless, the system was subject to some limitations with regard to size reduction efficiency. Based on Equations 6.2 and 6.3, size reduction via media milling will be most effective when the tip speed of the agitator is maximized, and typical laboratory-scale units are operated at tip speeds of 4-20 m/s. Despite the fact that the magnetic mixer was chosen to allow the maximum rotational speed, the limiting value of 3400 RPM in conjunction with the fixed inner diameter (3") of the encapsulation vessel capped the tip speed of the high-pressure media mill at 11 m/s. The tip speed of the

HSD impeller was similarly limited to 4.5 m/s.

In addition, the vertical orientation of the mill placed constraints on the selection of grinding media for the media milling operations. Mende et al [2003] have shown the size reduction to the nanometer range is enhanced via the use of high-density, small-diameter grinding media. Thus, yttria-stabilized zirconia grinding media (Quackenbush, YTZ[®]) with a density of 6.0 g/ml and bead diameter of 300 μm to 500 μm were initially chosen for use in media milling trials. After initial testing, it was apparent that the grinding media were poorly fluidized, largely remaining near the bottom of the encapsulation vessel during the milling process. In addition, the small media size resulted in high retention of product particles in the voids between beads, reducing product recovery yields. The beads were also small enough to pass through the gap between the mixer shaft and vessel cover, and at one point caused serious damage to the shaft and mixer. Upon the advice of Tom Weiss at Quackenbush Company, the YTZ[®] media were subsequently replaced with glass grinding beads in order to increase media fluidization within the encapsulation vessel. A larger bead diameter (1.2 mm) was chosen in order to improve product recovery, aid in cleaning the vessel, and prevent damage to the mixer.

Dispersion stabilization in CXLs

The particles produced in the current process are not expected to be stable in scCO₂ or CXL dispersions due to the poor solubility of these polymers in CO₂ (see Chapter 4) and the unsuitability of random copolymers for steric stabilization. Although researchers have developed surfactants and polymers for steric stabilization of colloids in scCO₂ [Sirard et al., 2004, Cooper et al., 1997], the polymers employed in the current study have been chosen based on their expected performance in the final aqueous inks. This may influence the efficiency of the milling process, since Stenger et al [2003] have demonstrated that effective stabilization of milled particles results in a lower energy requirement to reach the desired particle size.

Despite limitations with respect to the efficiency of size reduction, the encapsulation process was successfully implemented to produce carbon black particles coated

with both hydrophilic and hydrophobic polymers. Further optimization of size reduction conditions can be expected to yield product particles with smaller average diameters for use in high-performance inks.

6.4 Conclusions

A particle encapsulation process combining traditional particle size reduction methods with a high-pressure CO₂-based polymer processing technique has been successfully demonstrated. Polymer-encapsulated carbon black nanoparticles were produced in CO₂-expanded acetone and recovered as a dry, freely-flowing powder at yields between 89% and 98%. Particles were coated with commercially available Joncryl[®] polymers as well as BzMA/MAA random copolymers at pigment:dispersant (P:D) ratios between 1.25 and 5.0. Encapsulation was achieved using both hydrophilic and hydrophobic polymers, and the resulting powders were redispersed in aqueous solution and employed in ink jet inks. Average hydrodynamic particle diameters of coated particles redispersed in water via ultrasonication were between 135 nm and 190 nm. Samples produced at P:D=5.0 exhibited the best performance in inks, with optical densities significantly better than that of a control ink jetted under the same conditions.

The high-pressure encapsulation process represents a means of depositing a wide variety of polymers on the surface of pigment particles in the nanometer size range. This greatly increases the selection of polymeric dispersants that are available for use in aqueous inks, as the current process requires resins which exhibit a certain degree of solubility in water. In addition, the ability to deposit hydrophobic polymers with negligible solubility in water onto the surface of pigment particles for use in aqueous inks enables the elimination of “free” polymer dissolved in the final ink dispersion, increasing flexibility with regard to the final ink formulation.

The process under investigation is not limited to the encapsulation of pigment particles, and is broadly applicable to coating operations in a variety of fields. In general, the technique can be applied to any system in which the core particles are

insoluble in both scCO₂ and the given solvent, and in which the coating material is soluble in the solvent but not in scCO₂. Of course, the solvent choice offers additional flexibility, and can be selected to optimize the performance of a given system.

References

- M. Becker, A. Kwade, and J. Schwedes. Stress intensity in stirred media mills and its effect on specific energy requirement. *International Journal of Mineral Processing*, 61(3):189–208, 2001.
- L. Blecher, A. Kwade, and J. Schwedes. Motion and stress intensity of grinding beads in a stirred media mill, Part 1: Energy density distribution and motion of single grinding beads. *Powder Technology*, 86:59–68, 1996.
- O. Boutin, E. Badens, E. Carretier, and G. Charbit. Co-precipitation of a herbicide and biodegradable materials by the supercritical anti-solvent technique. *Journal of Supercritical Fluids*, 31(1):89–99, 2004.
- A. I. Cooper, J. D. Londono, G. Wignall, J. B. McClain, E. T. Samulski, J. S. Lin, A. Dobrynin, M. Rubinstein, A. L. C. Burke, J. M. J. Frechet, and J. M. DeSimone. Extraction of a hydrophilic compound from water into liquid CO₂ using dendritic surfactants. *Nature*, 389(6649):368–371, 1997.
- I. R. Dos Santos, J. Richard, C. Thies, B. Pech, and J. P. Benoit. A supercritical fluid-based coating technology. 3: Preparation and characterization of bovine serum albumin particles coated with lipids. *Journal of Microencapsulation*, 20(1):110–128, 2003.
- N. Elvassore, A. Bertucco, and P. Caliceti. Production of insulin-loaded poly(ethylene glycol)/poly(L-lactide) (PEG/PLA) nanoparticles by gas antisolvent techniques. *Journal of Pharmaceutical Sciences*, 90(10):1628–1636, 2001.
- R. Falk, T. W. Randolph, J. D. Meyer, R. M. Kelly, and M. C. Manning. Controlled release of ionic compounds from poly (L-lactide) microspheres produced by precipitation with a compressed antisolvent. *Journal of Controlled Release*, 44(1):77–85, 1997.
- W. N. Ford, E. H. J. C. Gommeren, and Q. Q. Zhao. *High pressure media mill*. International Patent WO 02/094443 A2, 2002.

- A. Hertz, S. Sarrade, C. Guizard, and A. Julbe. Synthesis and encapsulation of yttria stabilized zirconia particles in supercritical carbon dioxide. *Journal of the European Ceramic Society*, 26:1195–1203, 2006.
- J. Jung and M. Perrut. Particle design using supercritical fluids: Literature and patent survey. *Journal of Supercritical Fluids*, 20(3):179–219, 2001.
- A. Kwade. Determination of the most important grinding mechanism in stirred media mills by calculating stress intensity and stress number. *Powder Technology*, 105(1-3):382–388, 1999a.
- A. Kwade. Wet comminution in stirred media mills - research and its practical application. *Powder Technology*, 105(1-3):14–20, 1999b.
- A. Kwade. Mill selection and process optimization using a physical grinding model. *International Journal of Mineral Processing*, 74:S93–S101, 2004.
- A. Kwade and J. Schwedes. Breaking characteristics of different materials and their effect on stress intensity and stress number in stirred media mills. *Powder Technology*, 122(2-3):109–121, 2002.
- A. Kwade, L. Blecher, and J. Schwedes. Motion and stress intensity of grinding beads in a stirred media mill, Part II: Stress intensity and its effect on comminution. *Powder Technology*, 86:69–76, 1996.
- K. K. S. Lau and K. K. Gleason. Particle surface design using an all-dry encapsulation method. *Advanced Materials*, 18(15):1972–1977, 2006.
- S. Marre, F. Cansell, and C. Aymonier. Tailor-made surface properties of particles with a hydrophilic or hydrophobic polymer shell mediated by supercritical CO₂. *Langmuir*, 24:252–258, 2008.
- K. Matsuyama, K. Mishima, H. Umemoto, and S. Yamaguchi. Environmentally benign formation of polymeric microspheres by rapid expansion of supercritical carbon

- dioxide solution with a nonsolvent. *Environmental Science & Technology*, 35(20): 4149–4155, 2001a.
- K. Matsuyama, S. Yamauchi, T. Hirabaru, K. Hayashi, S. Hattori, and K. Mishima. Microencapsulation of proteins with polymer-blend by rapid expansion of supercritical carbon dioxide. *Kagaku Kogaku Ronbunshu*, 27(6):707–713, 2001b.
- K. Matsuyama, K. Mishima, K. Hayashi, and R. Ohdate. Preparation of composite polymer-SiO₂ particles by rapid expansion of supercritical solution with a nonsolvent. *Journal of Chemical Engineering of Japan*, 36(10):1216–1221, 2003a.
- K. Matsuyama, K. Mishima, K. I. Hayashi, H. Ishikawa, H. Matsuyama, and T. Harada. Formation of microcapsules of medicines by the rapid expansion of a supercritical solution with a nonsolvent. *Journal of Applied Polymer Science*, 89(3):742–752, 2003b.
- S. Mende, F. Stenger, W. Peukert, and J. Schwedes. Mechanical production and stabilization of submicron particles in stirred media mills. *Powder Technology*, 132(1):64–73, 2003.
- S. Mende, F. Stenger, W. Peukert, and J. Schwedes. Production of sub-micron particles by wet comminution in stirred media mills. *Journal of Materials Science*, 39(16-17):5223–5226, 2004.
- K. Mishima, K. Matsuyama, A. Furukawa, T. Fujii, J. Shida, N. Nojiri, H. Kubo, and N. Katada. Control of polymer coating thickness of microcapsules containing inorganic microparticles using cosolvency of supercritical carbon dioxide. *Kagaku Kogaku Ronbunshu*, 27(6):700–706, 2001.
- V. Pessey, R. Garriga, F. Weill, B. Chevalier, J. Etourneau, and F. Cansell. Core-shell materials elaboration in supercritical mixture CO₂/ethanol. *Industrial & Engineering Chemistry Research*, 39(12):4714, 2000.
- V. Pessey, D. Mateos, F. Weill, F. Cansell, J. Etourneau, and B. Chevalier. SmCo₅/Cu

- particles elaboration using a supercritical fluid process. *Journal of Alloys and Compounds*, 323:412–416, 2001.
- E. Reverchon and A. Antonacci. Drug-polymer microparticles produced by supercritical assisted atomization. *Biotechnology and Bioengineering*, 97(6):1626–1637, 2007.
- S. M. Sirard, H. J. Castellanos, H. S. Hwang, K. T. Lim, and K. P. Johnston. Steric stabilization of silica colloids in supercritical carbon dioxide. *Industrial & Engineering Chemistry Research*, 43(2):525–534, 2004.
- R. Span and W. Wagner. A new equation of state for carbon dioxide covering the fluid region from the triple-point temperature to 1100 K at pressures up to 800 MPa. *Journal of Physical and Chemical Reference Data*, 25(6):1509–1596, 1996.
- H. H. Stender, A. Kwade, and J. Schwedes. Stress energy distribution in different stirred media mill geometries. *International Journal of Mineral Processing*, 74: S103–S117, 2004.
- F. Stenger and W. Peukert. The role of particle interactions on suspension rheology - application to submicron grinding in stirred ball mills. *Chemical Engineering & Technology*, 26(2):177–183, 2003.
- L. S. Tu, F. Dehghani, and N. R. Foster. Micronisation and micro encapsulation of pharmaceuticals using a carbon dioxide antisolvent. *Powder Technology*, 126(2): 134–149, 2002.
- Y. L. Wang, R. N. Dave, and R. Pfeffer. Polymer coating/encapsulation of nanoparticles using a supercritical anti-solvent process. *Journal of Supercritical Fluids*, 28 (1):85–99, 2004.
- H. Way. Particle size reduction of ceramic powders using a small media mill. Corporate report, Netzsch, Inc, 1997.

- W. J. Wnek, M. A. Andreottola, P. F. Doll, and S. M. Kelly. Ink jet technology. In A. S. Diamond and D. S. Weiss, editors, *Handbook of Imaging Materials*, pages 531–602. Marcel Dekker, Inc., New York, 2nd edition, 2002.
- T. J. Young, K. P. Johnston, K. Mishima, and H. Tanaka. Encapsulation of lysozyme in a biodegradable polymer by precipitation with a vapor-over-liquid antisolvent. *Journal of Pharmaceutical Sciences*, 88(6):640–650, 1999.
- B. Yue, J. Yang, Y. L. Wang, C. Y. Huang, R. Dave, and R. Pfeffer. Particle encapsulation with polymers via in situ polymerization in supercritical CO₂. *Powder Technology*, 146(1-2):32–45, 2004.

Chapter 7

Conclusions and Recommendations

The main thesis objective – as stated in Chapter 2 – is the demonstration and analysis of a particle size reduction and encapsulation process which takes place in CO₂-expanded acetone and produces colloidal carbon black particles. These particles should be uniformly coated with functionalized hydrophobic resins, such that they are easily redispersed in water or solvent to form stable nanoparticle dispersions suitable for use in ink jet inks.

The proposed high-pressure process has been developed and tested, and a two-part investigation of the interactions between system components has been conducted in order gain a deeper understanding of the fundamental processes that govern the process behavior. In the first component of this analysis, the phase behavior of the polymer-solvent-CO₂ ternary system was probed experimentally and modeled with the PC-SAFT equation of state; in the second component, the adsorption of polymers from pure solvents and CO₂-expanded acetone onto carbon black particles was measured and subsequently analyzed using the Langmuir isotherm equation. The conclusions drawn from these investigations – as well as from the particle encapsulation study – are presented below, and recommendations for future investigations are given.

7.1 Phase behavior study

Conclusions

The selection of process conditions for encapsulation is guided by knowledge of the phase behavior of the polymer-solvent-CO₂ ternary systems which comprise the fluid phase. Solid-liquid-vapor equilibrium curves for these ternary systems were measured using an apparatus incorporating the detection of scattered laser light to determine the onset of polymer precipitation. Measurements were made at various values of the polymer weight fraction at three fixed temperatures; the equilibrium data gathered were then correlated using the PC-SAFT equation of state.

Precipitation of BzMA/MAA copolymers generally required a larger overall CO₂ mole fraction – and thus a higher system pressure – for more dilute polymer solutions; however, a minimum in the precipitation pressure was observed for all polymer compositions and temperatures near a CO₂-free polymer mass fraction of 0.03. The ternary systems were characterized by a rapid reduction in polymer solubility over a relatively narrow range of pressure (between 200 psig and 400 psig, depending on the polymer and system temperature); the precipitation pressure increased with increasing temperature and BzMA mass fraction (per polymer mass unit).

The PC-SAFT EOS was successfully employed to correlate the phase behavior data by adjusting only two binary interaction parameters. Both qualitative and quantitative agreement between the experimental and calculated values of the precipitation pressure was achieved. The average relative error associated with the predictions of precipitation pressure for each polymer was 3.7% over the range of temperature and composition explored in the experimental study, demonstrating that accurate correlations of phase behavior data over a wide range of conditions relevant to GAS processing can be obtained with a relatively small amount of data.

The information obtained from the phase behavior study is directly applicable to the optimization of the GAS-based particle encapsulation process. The experimentally-determined solubility limits effectively define the upper boundaries of the operating pressures required in the coating procedure to completely remove the polymer from

solution and deposit it onto the particle surfaces.

Recommendations

The experimental apparatus developed for the current phase behavior investigation was well-suited for the collection of phase behavior data relevant to the GAS-based particle encapsulation process under investigation. Nevertheless, several modifications could be made in order to improve the speed and accuracy of data collection.

The rate of data collection could be increased most dramatically by enabling accurate addition of polymer solutions and/or pure solvent during the course of a phase behavior experiment. This would allow a series of isothermal experiments to be conducted rapidly without depressurization of the system: after polymer precipitation occurs, additional solvent could be added to the system until the solid phase disappears. A solvent delivery system was implemented for this purpose, with an HPLC pump providing solvent to the system and an electronic balance in place to measure the mass of solvent added. However, the relatively small size of the view cell made it difficult to add an appropriate amount of solvent between precipitation events, and limited the number of times that solvent could be added before the liquid level reached the top of the vessel. If such a system is to be implemented in future studies, a larger view cell and/or a mass flow meter for accurate addition of solvent should be employed to maintain the accuracy of the measurements.

The addition of a coriolis-type mass flow meter in the CO₂ delivery system would allow a more accurate determination of the amount of CO₂ added to the view cell. This value is currently calculated based on the initial and final conditions within the syringe pump using an accurate equation of state for CO₂; however, the syringe pump specifications note that a slow leak at the pump seals is unavoidable. During a representative phase behavior trial, the leak rate was found to be 0.1-0.3 ml/min (0.005-0.02 g/min).

The limits of the laser light scattering device for the detection of precipitated polymer in dilute systems were not reached during the phase behavior trials; however, if the system was to be used for extremely dilute solutions, the sensitivity of the

detection system could be improved by lengthening the path of the laser light through the liquid phase (e.g., by using a longer view cell) or by using a more powerful laser. Fractionation of the BzMA/MAA polymers to reduce the polydispersity of the samples would allow more accurate determination of precipitation pressure, and would also potentially facilitate correlation of the data with the PC-SAFT EOS. At the opposite end of the composition range, more concentrated systems could be investigated by employing stronger agitation within the precipitation vessel. A CSTR-type vessel equipped with a magnetically coupled mixer and windows for visual access would be appropriate for this purpose.

With regard to the correlation of experimental data using the PC-SAFT EOS, an investigation of the phase behavior of pure poly(BzMA) polymer in CO₂-expanded acetone would enable regression of more accurate pure-component parameters (parameters were calculated using a group contributions method in the current study). Beyond adjustments to the pure component and binary interaction parameters, another possible route to improving the correlations is via the introduction of additional perturbation terms to the PC-SAFT EOS. The implementation of the association term \tilde{a}^{assoc} – neglected for the current study – would enable more accurate modeling of the associations among and between acetone molecules and MAA polymer segments, and the incorporation of a term proposed by Karakatsani and Economou [2006] would take into account the quadrupolar interactions exhibited by CO₂ molecules. The incorporation of these terms also introduces additional adjustable binary interaction parameters.

7.2 Investigation of polymer adsorption onto carbon black from CXLs

Conclusions

The conventional process to produce inks is governed by the adsorption equilibrium of the dispersing resin on the surface of the pigment particles. The high-pressure process

under investigation can also be analyzed in terms of the adsorption equilibrium conditions; however, pressure is introduced as an additional parameter. An apparatus was designed and constructed for the experimental investigation of CO₂-solvent-polymer-particle interactions via high-pressure adsorption isotherms, and isotherm data was gathered for 75/25 BzMA/MAA and 85/15 BzMA/MAA polymers. The atmospheric-pressure adsorption behavior of the BzMA/MAA and Joncryl[®] polymers was also investigated, and all data were correlated with the Langmuir equation.

Adsorption from several common organic solvents was low for both the Joncryl[®] polymers and BzMA/MAA copolymers, particularly when compared to the adsorption of Joncryl[®] 678 from water. Atmospheric-pressure isotherms offer insight into the relative strength of polymer-solvent, polymer-particle, and solvent-particle interactions present in the systems currently under investigation; these data indicate that polymer-particle interactions are not strong enough to promote adequate polymer adsorption, highlighting the potential benefits of a GAS-based process in tuning the liquid-phase solvation power.

Adsorption of 85/15 and 75/25 BzMA/MAA polymers onto carbon black from CO₂-expanded acetone was measured at 35°C and pressures between 0 psig and 300 psig. Pressurization with CO₂ to pressures up to 200 psig caused a decrease in the amount of polymer adsorbed on particle surfaces, but further increases in pressure resulted in higher polymer loadings. In the case of 75/25 BzMA/MAA polymer, the polymer loading increased significantly between 200 psig and 300 psig as the solubility limit was approached or exceeded. This behavior indicates that there is some degree of competitive adsorption of CO₂ onto the carbon black surfaces.

Whereas the phase behavior study yielded upper limits for system pressures during particle encapsulation, the adsorption data offer insight into the minimum pressures required to cause the polymers of interest to be deposited on carbon black particle surfaces. Specifically, the data indicate that most of the polymer adsorbs over a relatively narrow range of pressure: coating will only begin to occur at pressures above 200 psig for systems containing 75/25 BzMA/MAA polymer at 35°C, and pressures above 300 psig are required when using 85/15 BzMA/MAA. Nearly all polymer will

be present on the particle surfaces as the system pressure exceeds 400-500 psig.

The results of the adsorption study serve to underscore the importance of choosing a “neutral” solvent that exhibits no strong interactions with either the polymer molecules or the particle surfaces. Such interactions tend to inhibit adsorption of the polymer by either enhancing the solubility of the polymer in the liquid phase – in the case of polymer-solvent interactions – or by displacing polymer molecules at the particle surface via competitive adsorption – in the case of particle-solvent interactions.

Recommendations

The separation and removal of particle-free supernatant samples from the adsorption apparatus at elevated pressures presented a challenging experimental task. Although useful information was obtained using the existing apparatus, several strategies to improve the accuracy and precision of the measurements should be implemented if further investigations are to be undertaken.

Sufficient recirculation of the particle-free supernatant is critical in order to achieve reproducible results. Improvements to the adsorption apparatus should be focused on ensuring temperature uniformity within the system and improving recirculation through the sample loop. Temperature control of the adsorption apparatus could be improved by placing the entire system in an air bath or oven. If temperature uniformity can be ensured, a larger vessel with strong agitation would be preferable to the sight gauge used in the current study; a possible alternative would be a CSTR-type vessel equipped with a magnetically coupled mixer and sapphire windows for visual access. A larger vessel of this type would minimize the effect of removing a 2 ml sample from the system, and allow the use of a larger filter (in terms of surface area) before the HPLC switching valve. The 40 μm filter used in the adsorption trials was chosen to maximize the recirculation rate of the supernatant while protecting the gear pump and HPLC from large carbon black agglomerates, but allowed smaller carbon black aggregates to enter the sample loop. By employing a larger filter with a smaller pore size, the recirculation rate could be maintained while excluding most

of the carbon black from the sample loop.

If the accuracy of the adsorption measurements were to be improved, the apparatus could be used to collect more data in the vicinity of the polymer solubility limit in order to determine whether encapsulation is more accurately described in terms of adsorption or precipitation. In either case, the pressure dependence of the empirical constants K and n_m in the Langmuir Equation can be determined via the collection of adsorption isotherm data over a range of mixture compositions; the pressure-dependent Langmuir isotherm could then be combined with the PC-SAFT EOS correlations based on fluid phase behavior data to model the equilibrium state of high-pressure systems.

The collection of atmospheric pressure adsorption data at 35°C would provide useful insight regarding the effect of temperature on the adsorption of BzMA/MAA polymers onto carbon black. An estimate of the enthalpy of adsorption of the polymer segments could then be calculated from Equation 5.1. A more meaningful estimate of the enthalpy of adsorption could be obtained by collecting adsorption data at 25°C and 35°C for small-molecule probes representing the BzMA and MAA functional groups. Acetic acid benzyl ester and propionic acid could be used as probes for BzMA and MAA segments, respectively. Micro-flow calorimetry studies have been previously employed in the literature to investigate the strength of adsorbate-particle interactions [Fowkes et al., 1989]; however, the use of carbon black in such studies would be difficult due to its small particle size and tendency to form tightly-packed structures with a small void fraction.

By extending the study to other solvents, the model system could be optimized to enhance the adsorption of polymer at atmospheric pressure. The desired solvent would exhibit relatively weak solvating power with respect to the polymer, and would not possess any strong interactions with the polymer anchor groups or with the particle surfaces adsorption sites. The introduction of a second organic solvent would allow further tunability in the system, and possibly enable the encapsulation of particles at a significantly reduced pressure upon the addition of CO₂.

7.3 Particle size reduction and encapsulation in CXLs

Conclusions

A prototype high-pressure process was designed, constructed, and demonstrated for both size reduction and polymer encapsulation of pigment particles in gas-expanded solvent media. The process is based on the Gas-Antisolvent (GAS) process for solvent power reduction, and incorporates high-pressure milling techniques developed at DuPont. The results of the supporting tasks described above informed the selection of process operating conditions; the resulting product powders were characterized via TEM, and were also submitted to DuPont for evaluation in actual inks.

The GAS-based process was successfully employed to produce polymer-encapsulated carbon black nanoparticles which were recovered as a dry, freely-flowing powder at yields between 89% and 98%. Particles were coated with commercially available Joncryl[®] polymers as well as BzMA/MAA random copolymers at pigment:dispersant (P:D) ratios between 1.25 and 5.0. Encapsulation was achieved using both hydrophilic and hydrophobic polymers, and the resulting powders were redispersed in aqueous solution and employed in ink jet inks. Average hydrodynamic particle diameters of coated particles redispersed in water via ultrasonication were between 135 nm and 190 nm.

The high-pressure encapsulation process represents a means of depositing a wide variety of polymers on the surface of pigment particles in the nanometer size range. This greatly increases the selection of polymeric dispersants that are available for use in aqueous inks, as the current process requires resins which exhibit a certain degree of solubility in water. In addition, the ability to deposit hydrophobic polymers with negligible solubility in water onto the surface of pigment particles for use in aqueous inks enables the elimination of “free” polymer dissolved in the final ink dispersion, increasing flexibility with regard to the final ink formulation.

Recommendations: Particle size reduction apparatus

The prototype apparatus was able to produce encapsulated carbon black particles which were easily redispersed in water as aggregates in the nanometer size range. While this represents an important demonstration of the feasibility of the high-pressure process for simultaneous size reduction and particle encapsulation, the final hydrodynamic particle size in water was slightly higher than that of most commercial ink jet inks. Research efforts in the current thesis were largely focused on the phenomena that affect the encapsulation of carbon black particles; any further investigations should include attempts to optimize the size reduction process.

Optimization of the carbon black size reduction operations should begin with a redesign of the apparatus for high-pressure media milling. A shorter, wider vessel would allow a higher tip speed at the maximum RPM of the magnetic mixer, and also require a shorter agitator that would be more amenable to dynamic balancing. The agitator used in the current study was difficult to balance due to its length, and also due to the fact that the threaded connection at the end of mixer shaft did not provide a completely reproducible coupling. A mixer shaft that extends farther into the vessel would facilitate balancing of agitator attachments and extend bearing life; in this configuration, the shaft could be passed through the length of the impeller to achieved a firm, reproducible connection. Mounting the milling vessel cover and motor on a fixed frame securely bolted to the floor would also reduce system vibrations and extend bearing life.

If possible, the milling vessel should be mounted in a horizontal configuration to allow the use of smaller, high-density grinding media such as yttrium-stabilized zirconia (these beads were poorly fluidized within the existing vertical milling vessel). Based on the conclusions of Mende et al [2003], this would enhance the size reduction of carbon black particles to the nanometer range. If finer media are to be used, the opening in the vessel cover should be machined such that the gap between the cover and the rotating shaft is less than approximately half the diameter of the smallest media.

The incorporation of an external recirculation loop would greatly enhance mixing within the milling vessel, and promote a more uniform distribution of stress events among the pigment particles. A recirculation loop would also allow for larger batch sizes with the existing apparatus. A high-pressure gear pump would be appropriate for this application, provided that the dimensions within the pump are large in comparison to the carbon black agglomerates present in the system. The gear pump employed in the adsorption study was tested in a recirculation loop for the current encapsulation system; however, the carbon black agglomerates quickly formed a blockage within the gear pump head, even when filters were placed in the recirculation loop immediately upstream from the pump.

If a recirculation loop can be successfully implemented in the milling apparatus, it may be possible to monitor the milling progress in real time via ultrasonic spectroscopy [Dukhin and Goetz, 2001]. This is one of the few techniques by which the particle size distribution of concentrated dispersions at high pressure could be directly measured. A sample loop would allow the removal of high-pressure samples during the course of an encapsulation trial, but the recovery of samples which are representative of the state of the particles within the system would present a challenging task.

Recommendations: Particle size reduction process considerations

The effectiveness of size reduction operations also depends on the rheological properties of the suspension as well as the stabilization of the particles against re-agglomeration. The stabilization of BzMA/MAA polymer-coated particles in gas-expanded acetone is relatively poor, due to the low dielectric constant of the medium and the lack of steric repulsive forces. A solvent with a higher dielectric constant (e.g., methanol) may provide some electrostatic stabilization if the polymers were neutralized before the encapsulation process. Another possibility for improving dispersion stability during the size reduction process is the use of “ambidextrous” polymers that are capable of dispersing particles in both CXLs and water, such as those developed by Yates et al [1999]. However, the use of these polymers would significantly reduce flexibility

in the selection of dispersant polymers, which represents an important benefit of the high-pressure process.

The viscosity of the particle dispersions should be investigated more thoroughly in order to optimize size reduction operations. In general, the viscosity of the dispersions should be high in the initial stages of the milling process; however, the viscosity of particle suspensions increases rapidly after a certain solids volume fraction is exceeded, to the point that the mixture behaves as a solid under shear conditions. To avoid this viscosity regime, pigment content of the dispersions in the pre-mix step of the current study was held relatively constant at approximately 8wt%. A systematic exploration of the viscosity of these systems over a range of compositions would enable the use of more concentrated dispersions in encapsulation trials. In addition to facilitating the break-up of particle agglomerates during the pre-mix and initial milling phase, more concentrated pigment dispersions would allow the production of more product particles within the same encapsulation apparatus.

Another potential means of improving particle size reduction efficiency is via optimization of the CO₂ addition profile during the encapsulation process. In the current study, CO₂ was added to the encapsulation vessel at a constant mass flow rate; however, it is apparent from the results of the adsorption study that much of the polymer adsorption occurs over a relatively narrow pressure range, indicating that a gradual increase in pressure from atmospheric to some value near the vapor pressure of CO₂ may not be the most favorable for producing an even polymer coating. It may be advantageous to quickly increase the pressure to a value at which adsorption is thought to increase – based on adsorption experiments – and then either hold the pressure constant or increase it very slowly over the encapsulation “window” during milling operations.

Recommendations: Product characterization

The product particles produced using the high-pressure encapsulation process were mainly characterized based on their performance in aqueous dispersions. While this method of evaluation is appropriate for the pigment particles targeted for use in ink

dispersions, it may be desirable to conduct a direct characterization of the polymer layer surrounding the particles. Although the polymer layer was not detected using TEM at the P:D ratios employed during the current investigation, it may be informative to carry out encapsulation trials at a series of lower P:D ratios in order to determine when the polymer is first observed in TEM micrographs. In a parallel study, GAS precipitation trials could be carried out in particle-free acetone solutions to form pure polymer particles – these could then be characterized using TEM and compared to previous images in order to search for signs of polymer particles among the carbon black aggregates.

In the event that the use of TEM was not able to provide satisfactory confirmation of a polymer coating, other particles could be used as a model that may be more easily analyzed. Several examples of possible model particles are titanium dioxide (TiO_2), polymer latexes, and silica. In particular, silica particles such as Evonik's Aerosil are similar in size and structure to carbon black, and have more uniform surface chemistry. As an example of the potential advantages of using such a model system, Wang et al [2004] have coated silica nanoparticles with polymer and successfully confirmed the presence of a polymer layer on the particle surfaces using TEM-EELS. Energy-dispersive X-ray spectroscopy (EDXS) in conjunction with SEM analysis is another possible technique to detect polymer layers on silica particles.

Recommendations: Overall process design and applications

By carrying out the investigations outlined in the previous sections, a reduction in the final particle size of encapsulated carbon black particles in aqueous dispersions should be possible. However, due to the poor stabilization of the encapsulated particle dispersions in CXLs, it may not be possible to achieve the desired particle size without significant energy input to the aqueous dispersions. If this is the case, the high-pressure process could be investigated strictly as an encapsulation method that could be used in place of the current pre-mix step. By choosing the solvent and operating temperature carefully, modest pressures could be used to induce polymer adsorption under HSD-type agitation, and the product could then be milled in a conventional

media mill.

Regardless of the method of size reduction employed in the encapsulation process, spray-drying techniques could be investigated for particle recovery instead of filtration. Such a configuration would be more amenable to continuous operation, and the reduction of system pressure across an orifice could also aid in agglomerate break-up by rapidly expanding CO₂ within the tertiary structure of carbon black.

If the recommendations described above were to be implemented, it is reasonable to expect that the proposed high-pressure milling and encapsulation process could be optimized to produce uniformly coated particles suitable for ink jet applications. The current thesis work also serves as a foundation upon which further investigations of other model systems may be based; a framework has been developed for analysis of the interactions between the CO₂, solvent, coating material, and particle surfaces which is broadly applicable to high-pressure coating operations for a variety of applications. By selecting an appropriate solvent – or solvent mixture – it is possible in principle to encapsulate nearly any solid material with a wide range of organic or polymeric molecules, as long as neither the particle nor the coating material exhibits significant solubility in high-pressure CO₂.

References

- A. S. Dukhin and P. J. Goetz. New developments in acoustic and electroacoustic spectroscopy for characterizing concentrated dispersions. *Colloids and Surfaces A - Physicochemical and Engineering Aspects*, 192(1-3):267–306, 2001.
- F. M. Fowkes, K. L. Jones, G. Z. Li, and T. B. Lloyd. Surface-chemistry of coal by flow microcalorimetry. *Energy Fuels*, 3(1):97–105, 1989.
- E. K. Karakatsani and I. G. Economou. Perturbed chain-statistical associating fluid theory extended to dipolar and quadrupolar molecular fluids. *Journal of Physical Chemistry B*, 110(18):9252–9261, 2006.
- S. Mende, F. Stenger, W. Peukert, and J. Schwedes. Mechanical production and stabilization of submicron particles in stirred media mills. *Powder Technology*, 132(1):64–73, 2003.
- Y. L. Wang, R. N. Dave, and R. Pfeffer. Polymer coating/encapsulation of nanoparticles using a supercritical anti-solvent process. *Journal of Supercritical Fluids*, 28(1):85–99, 2004.
- M. Z. Yates, G. Li, J. J. Shim, S. Maniar, and K. P. Johnston. Ambidextrous surfactants for water-dispersible polymer powders from dispersion polymerization in supercritical CO₂. *Macromolecules*, 32(4):1018–1026, 1999.